Year : 2020

Developmental origin of central memory CD8+ T cells

Pais Ferreira Daniela

UNIL | Université de Lausanne

Faculté de biologie
et de médecine

Département d'Oncologie

Developmental origin of central memory CD8$^+$ T cells

Thèse de doctorat ès sciences de la vie (PhD)

présentée à la

Faculté de biologie et de médecine
de l'Université de Lausanne

par

Daniela PAIS FERREIRA

Master de Biomédicine de l'Université de Aveiro, Portugal

Jury

Prof. Fabienne Tacchini-Cottier, Présidente
Prof. Werner Held, Directeur de thèse
Prof. Martin Bachmann, Expert
Prof. Joerg Huelsken, Expert

Lausanne
(2020)

Ecole Doctorale

Doctorat ès sciences de la vie

Imprimatur

Vu le rapport présenté par le jury d'examen, composé de

Président·e	Madame	Prof.	Fabienne	**Tacchini-Cottier**
Directeur·trice de thèse	Monsieur	Prof.	Werner	**Held**
Expert·e·s	Monsieur	Prof.	Martin	**Bachmann**
	Monsieur	Prof.	Joerg	**Huelsken**

le Conseil de Faculté autorise l'impression de la thèse de

Madame Daniela Pais Ferreira

Master de Biomédecine, Université de Aveiro, Portugal

intitulée

Developmental origin of central memory CD8$^+$ T cells

Lausanne, le 23 octobre 2020

pour le Doyen
de la Faculté de biologie et de médecine

Prof.   Fabienne Tacchini-Cottier

Acknowledgements

Foremost I would like to thank my thesis director, Prof. Werner Held. During the time I've spent in his lab I had the opportunity to perform a wide range of techniques that allowed me to acquire consistent knowledge in the field of T cell Immunology. I'm also grateful for the immense knowledge that he shared with me over the years, allowing my personal scientific growth. I'll be forever grateful for his kind support and motivation, ideas and feedback, and enthusiasm throughout the research phase but also for the writing of this thesis.

I would also like to express my gratitude to my thesis committee representative, Prof. Fabienne Tacchini-Cottier, as well as the remaining members of the thesis committee, for the useful comments and remarks.

During these years I was lucky to have the support of a friendly and cheerful group of fellow colleagues, for which I'm also thankful. Particularly I would like to thank Mélanie, Beena, Joana, Maxime, Catherine, Julia, Imran and Vijay for all the laughs shared in the lab and morning coffees, but also for their scientific expertise and insights, as well as their support. I would especially like to thank Joana for her friendship and for bringing at little bit of home to the lab. Another special thanks to Catherine for her precious help in the translation of my thesis summaries to French.

I would also like to thank Tania for all the bioinformatic analyses, Leonardo and Roeltje for the immunohistochemistry experiments and analyses, Patrick for sharing his expertise with cloning/molecular biology, as well as all other collaborators that made this project possible.

I'm equally grateful to Catherine Fumey and Aline Decultot for mouse management, as well as the UNIL Genomic Technology Facility for RNA-seq and ATAC-seq experiments. I would also like to thank the members of the UNIL Flow Cytometry Facility, Romain, Francisco and Kevin for the joyful environment in all the immense hours we've spend sorting.

All the people in the scientific community of Epalinges also made my PhD experience somehow easier and happier, with a really special thanks to Amélie for her precious friendship, immense support and all the good times at the gym and coffee times.

I also would like to express my deepest gratitude to all my loved ones, for their kind support and encouragement, without which the completion of this thesis would not be possible. Therefore I would like to thank my parents for their unconditional love, education, unceasing encouragement and for supporting me throughout all my studies at the University; my boyfriend for the equally encouragement, support and patience during these years, and for always stand by my side since 2008; my beloved sister for the continuous support and motivation, although separated by distance she is always in my heart; and my uncles, aunt and cousins resident in Switzerland for all the Saturday night dinners, all the laughs and the getaways. I would also like to thank my grandparents for their love and advices, as well as the rest of my family members, without exception.

Last, but not least, I would like to thank my best friend Cláudia for her enormous friendship since 2009, a friendship that not even time and distance can end. Thank you for all the Skype conversations and for always cheering me up.

This thesis was only possible with help and support of many others. Therefore I would like to extend my sincere thanks to all of them.

Origine développementale des lymphocytes T CD8⁺ mémoires

Le système immunitaire protège l'hôte contre une infection. L'éradication des agents pathogènes intracellulaires, tels que les virus, est principalement médiée par les lymphocytes T CD8⁺ cytotoxiques. Ces cellules immunitaires peuvent tuer les cellules infectées par des agents pathogènes via la libération de molécules cytotoxiques.

Après l'élimination initiale du pathogène, certaines cellules T CD8⁺ spécifiques du pathogène peuvent persister pendant de longues périodes. Ces cellules constituent une mémoire de l'exposition à cet agent pathogène et permettent ainsi une réponse immunitaire plus rapide et plus robuste lors d'une réinfection ultérieure. Cette propriété, caractéristique de la réponse des lymphocytes T CD8⁺, est appelée mémoire immunologique. La protection efficace contre la réinfection conférée par les cellules mémoires est en partie due à leurs propriétés de cellules souches, c'est-à-dire leur capacité à proliférer efficacement, se différencier en cellules cytotoxiques et se renouveler automatiquement lors d'une nouvelle réexposition.

La capacité à former une mémoire est la base de l'induction d'une protection immunitaire par la vaccination, c'est-à-dire l'inoculation de matériel dérivé d'un agent pathogène pour induire une protection immunitaire contre l'infection. Cependant, les approches de vaccination induisent une mémoire faible comparativement à une infection naturelle, ce qui indique que nos connaissances actuelles concernant la formation de cellules T mémoire sont encore insuffisantes.

De l'avis général, les cellules T CD8⁺ mémoires dérivent de cellules effectrices cytotoxiques, après l'élimination du pathogène. Un scénario alternatif est que les cellules T mémoires sont générées tôt pendant l'infection et produisent des cellules différenciées cytotoxiques qui peuvent tuer les cellules infectées par des agents pathogènes.

Pour identifier le mécanisme responsable de la formation des cellules T CD8⁺ mémoires, nous avons suivi l'expression du facteur 1 des cellules T (Tcf1), un facteur de transcription connu pour être important pour la formation de la mémoire, lors d'une infection virale primaire chez la souris. Cela nous a permis d'identifier une petite sous-population de cellules T CD8⁺ répondant à une infection virale qui n'avait pas la capacité de tuer les cellules infectées mais qui avait des propriétés de cellules souches. Surtout, ces cellules Tcf1⁺ ont permis la mise en place d'une mémoire immunologique. Nous avons en outre constaté que Tcf1 était essentiel pour la fonction de ces cellules précoces en préservant leurs propriétés de cellules souches.

Nos résultats résolvent la question de longue date concernant l'origine développementale des cellules mémoires aux propriétés de cellules souches. Ces cellules sont générées tôt pendant l'infection et sont à l'origine des cellules différenciées qui peuvent tuer les cellules infectées par des agents pathogènes.

De plus, nous avons observé une population de cellules T CD8⁺ Tcf1⁺ similaires rapidement après vaccination. Ainsi, l'utilisation de Tcf1 comme marqueur clé des cellules T CD8⁺ aux propriétés de cellules souches devrait grandement faciliter la conception et l'optimisation de nouvelles immunothérapies visant à générer des cellules T CD8⁺ mémoires multifonctionnelles.

Origine développementale des lymphocytes T CD8⁺ mémoires

Les lymphocytes T CD8⁺ de la mémoire centrale (T$_{CM}$) assurent un contrôle soutenu des infections secondaires systémiques ou prolongées ainsi qu'une puissante protection immunitaire contre le cancer dans des modèles expérimentaux de transfert de lymphocytes T. L'efficacité des T$_{CM}$ s'explique par leurs propriétés semblables à celles des cellules souches, c'est-à-dire que lors d'une restimulation, ils peuvent se multiplier/proliférer, s'auto-renouveler et se différencier en cellules effectrices et produire d'autres sous-types de mémoire. Cependant, malgré leur importance, l'origine développementale des T$_{CM}$, et par conséquent le fondement de leurs propriétés de cellules souches, sont restées floues.

L'hypothèse la plus répandue concernant la différenciation des T$_{CM}$ est qu'ils dérivent de lymphocytes T CD8⁺ cytolytiques effecteurs qui, suite à l'éradication du pathogène, perdent la fonction cytolytique et acquièrent des propriétés d'expansion, différenciation et auto-renouvellement. Inversement, il a été suggéré que les cellules T CD8⁺ naïves se différencient directement en cellules avec fonction mémoire et qu'elle se différencient en cellules effectrices lors d'une stimulation ultérieure. Cependant de telles cellules n'ont jamais été isolées. Afin d'identifier l'origine développementale des T$_{CM}$, nous avons suivi l'expression de Tcf1 (codé par le gène *Tcf7*), un facteur de transcription requis pour la formation et la fonction des T$_{CM}$, lors d'une réponse immunitaire primaire à une infection virale aiguë.

En utilisant des souris rapportrices pour le gène *Tcf7*, nous avons identifié une petite population de cellules T CD8⁺ *Tcf7*ʰⁱ présentes lors de la phase effectrice de la réponse immune à l'infection virale. Ces cellules T CD8⁺ *Tcf7*ʰⁱ étaient dépourvues d'activité cytotoxique et très similaires phénotypiquement, transcriptionnellement et épigénétiquement aux cellules T$_{CM}$. Fonctionnellement, ces cellules avaient une capacité d'expansion, de différenciation multipotente et d'auto-renouvellement, c'est-à-dire les propriétés des cellules souches qui sont également une caractéristique des T$_{CM}$. De plus, la déplétion *in vivo* des cellules *Tcf7*ʰⁱ en phase effectrice a gravement altéré la génération d'une mémoire centrale. D'un point de vue mécanistique, Tcf1 a permis l'expression du caractère souche des cellules *Tcf7*ʰⁱ en phase effectrice. Tcf1 a supprimé la différenciation effectrice et a maintenu l'expression d'un ensemble de gènes associés aux cellules souches adultes. Enfin, la diminution individuelle de l'expression de plusieurs de ces gènes dépendants de Tcf1 a révélé leur importance dans la protection des propriétés d'expansion, différenciation et auto-renouvellemnt des cellules T CD8⁺ *Tcf7*ʰⁱ au stade effecteur.

Dans l'ensemble, nos données suggèrent que les cellules T$_{CM}$ ne dérivent pas de cellules effectrices cytolytiques qui subissent une dé-différenciation et acquièrent des propriétés des cellules souches suite de l'élimination du pathogène. Les cellules T$_{CM}$ dérivent plutôt d'une petite sous-population de cellules non cytolytiques présentes lors de la réponse aiguë à une infection virale et possédant des propriétés de cellules souches. L'identification des cellules T CD8⁺ de type souche au cours des premiers stades de l'infection aiguë ainsi que lors d'une vaccination devraient faciliter la conception et l'optimisation des schémas vaccinaux et d'immunothérapies anticancéreuses qui visent à générer ou à maintenir des cellules T CD8⁺ T$_{CM}$ ayant des propriétés de cellules souches.

Developmental origin of central memory CD8+ T cells

Central memory CD8+ T cells (T_{CM}) mediate sustained control of systemic or protracted secondary infections as well as potent immune protection against cancer in experimental adoptive T cell transfer settings. The potency of T_{CM} is explained by their stem cell-like properties, i.e. following re-stimulation they can expand, self-renew and differentiate into effector cells and yield other memory subtypes. However, despite their importance, the developmental origin of T_{CM} cells, and consequently the underpinning of CD8+ T cell stemness, have remained unclear.

A prevalent view of T_{CM} differentiation is that they derive from cytolytic effector CD8+ T cells that lose cytolytic function and re-acquire stemness subsequent to pathogen clearance. Conversely, it was suggested that naive CD8+ T cells directly differentiate into cells with T_{CM} function and these yield effector cells based on further stimulation. However, such cells have not been isolated. To discriminate between these two possibilities, we monitored the expression of Tcf1 (encoded by the *Tcf7* gene), a transcription factor required for the formation and function of T_{CM}, during a primary immune response to acute viral infection.

Using *Tcf7* reporter mice we identified a small but discrete population of *Tcf7*hi CD8+ T cells present during the effector phase of the immune response to viral infection. These effector-phase *Tcf7*hi CD8+ T cells lacked cytotoxic activity and were phenotypically, transcriptionally, and epigenetically very similar to T_{CM} cells. Functionally, these cells had recall expansion, multipotent differentiation and self-renewal capacity, i.e. the stem cell properties that are a hallmark feature of T_{CM}. Further, *in vivo* depletion of *Tcf7*hi effector-phase cells severely impaired the generation of central memory. Mechanistically, Tcf1 ensured the stemness of *Tcf7*hi effector-phase cells. Tcf1 suppressed effector differentiation and maintained the expression of a set of genes associated with adult stem cells. Finally, individual knockdown of several of these Tcf1-dependent adult stem genes revealed their importance in guarding the stemness of effector-stage *Tcf7*hi CD8+ T cells.

Overall, our data suggest that T_{CM} do not derive from cytolytic effector cells that undergo de-differentiation and acquire stemness following the elimination of pathogen. Rather T_{CM} derive from a small subset of non-cytolytic cells present during the acute response to viral infection that display stemness. The identification of stem-like CD8+ T cells during early stages of acute infection as well as vaccination should facilitate the design and optimization of vaccine regimens and cancer immunotherapies that aim at generating or maintaining T_{CM} CD8+ T cells with stem cell properties.

List of Abbreviations

7-AAD: 7-aminoactinomycin D

Ab: Antibody

ACK: Ammonium-Chloride-Potassium buffer

ACT: Adoptive T cell transfer

APC: Adenomatous polyposis coli

APC: Antigen presenting cell

Arm: Armstrong

Armcx2: Armadillo Repeat Containing X-Linked 2

ATACseq: Assay for Transposase Accessible Chromatin with high-throughput sequencing

AXIN1/2: Axis inhibition protein 1/2

B6: C57BL/6

BAC: Bacterial artificial chromosome

Bcl2: B-cell lymphoma 2 protein

Bcl6: B-cell lymphoma 6 protein

Blimp1: B lymphocyte-induced maturation protein-1

BM: Bone marrow

BMP: Bone morphogenetic protein

BZ: B cell zone

CCL19/21: Chemokine (C-C motif) ligand 19/21

CCR7: C-C chemokine receptor type 7

CD: Cluster of Differentiation

CFSE: Carboxyfluorescein succinimidyl ester

ChIPseq: Chromatin immunoprecipitation sequencing

CK1: Casein kinase 1

CpG: CpG dinucleotides

Cpq: Carboxypeptidase Q

Ctrl: Control

CTV: Cell Trace Violet

Cx3cr1: C-X3-C Motif Chemokine Receptor 1

Cxcr 3/5: C-X-C Motif Chemokine Receptor 3/5

Cyp4v3: Cytochrome P450, family 4, subfamily v, polypeptide 3

DAR: Differentially accessible regions

DEG: Differently expressed gene

DP: Double positive

DT: Diphtheria Toxin

DTR: Diphtheria toxin receptor

Elovl6: Elongation of very long chain fatty acids protein 6

Eomes: Eomesodermin

Ezh2: Enhancer Of Zeste 2

FasL: Fas ligand

FC: Fold change

FDR: False discovery rate

FloKA: Flow cytometry-based killing assay

Foxo1: Forkhead Box O1

FOXP3: Forkhead box P3

FRC: Fibroblast reticular cell

Gata3: GATA binding protein 3

GRG/TLE: Groucho-related gene / transducin-like enhancer

GSEA: Gene set enrichment analysis

GSK3β: Glycogen synthase kinase 3β

GVHD: Graft-versus-host disease

GzmA/B: Granzyme A/B

HDAC: Histone deacetylase

HIV: Human immunodeficiency virus

HMG: High-mobility group

HSC: Hematopoietic stem cell

i.p.: intraperitoneally

i.v.: intravenously

Id-2/3: Inhibitor Of DNA Binding 2/3

IEL: Intraepithelial Lymphocyte

IFN: Interferon

IL: Interleukin

IL12rβ2: IL-12 receptor β2 chain

IL2rβ: IL-2 receptor β chain

IL2rα: IL-2 receptor α chain

IL7rα: IL-7 receptor α chain

Kit: Mast/stem cell growth factor receptor Kit

Klf4: Kruppel Like Factor 4

KLRG-1: Killer cell lectin-like receptor G1

Ko: Knock out

LAMP-1: Lysosomal Associated Membrane Protein 1

LCMV: Lymphocytic choriomeningitis virus

Lef1: Lymphoid Enhancer Binding Factor 1

LFA-1: Lymphocyte function-associated antigen 1

LN: Lymph node

LRP5/6: Low density lipoprotein receptor-related protein 5/6

LV: Lentivirus

MHC: Major Histocompatibility Complex

MP: Memory precursor effector cell

mTORC2: Mammalian target of rapamycin Complex 2

NES: Normalized ES

NK: Natural killer cell

Oct4: Octamer-binding transcription factor 4

Ova: Ovalbumin

p.i.: post-infection

PBMC: Peripheral blood mononuclear cell

PCA: Principal component analysis

PD-1: Programmed cell death protein 1

PEDF: Pigment Epithelium-Derived Factor

PFU: Plaque forming units

PKCz: Protein Kinase C Zeta

Plxdc2: Plexin domain-containing protein 2

PRC: Polycomb repressive complex

Rag2: Recombination activation gene 2

ROI: Region of interest

RORC: RAR Related Orphan Receptor C

RP: Red pulp

RT: Room Temperature

RV: Retrovirus

s.c.: sub-cutaneously

Sca-1: Stem cell antigen-1

SD: Standard deviation

shRNA: short-hairpin RNA

Smad1: Mothers against decapentaplegic homolog 1

Sox2: Sex determining region Y-box 2

STAT: Signal Transducer And Activator Of Transcription

Suv39h1: Suppressor Of Variegation 3-9 Homolog 1

T-bet: T-box transcription factor 21

Tcf1: T cell factor 1

T_{CM}: Central memory CD8$^+$ T cell

TCR: T cell receptor

TE: Terminally differentiated effector cell

T_{Eff}: Cytotoxic effector CD8$^+$ T cell

T_{EM}: Effector memory CD8$^+$ T cell

TF: Transcription factor

T_{FH}: Follicular helper T cell

T_H: Helper T cell

ThPOK: T-helper-inducing POZ/Krueppel-like factor

TIL: Tumour infiltrating lymphocyte

TLR1/2: Toll-like receptor 1/2

T_{ML}: Memory-like CD8$^+$ T cell

T_N: Naive CD8$^+$ T cell

TNF: Tumor necrosis factor

T_{PM}: Peripheral memory CD8$^+$ T cell

TRAIL: TNF-related apoptosis-inducing ligand

T_{RM}: Tissue-resident memory CD8$^+$ T cell

T_{SCM}: Stem cell memory CD8$^+$ T cell

TSS: Transcriptional start site

TZ: T cell zone

Wnt: Wingless/Integration 1

WRE: Wnt responsive element

Wt: Wild type

Zeb2: Zinc Finger E-Box Binding Homeobox 2

βBD: β-catenin binding domain

βTRCP: β-transducin-repeat-containing protein

Table of contents

List of Figures

Introduction

The immune system protects the host from infection. Innate immune cells, such as macrophages, neutrophils or dendritic cells, and soluble mediators constitute a first line of defence against infection [1]. The innate immune system recognizes molecular patterns shared by many pathogens, which can lead to their elimination by phagocytosis and induce an inflammatory response [2]. An innate immune response is often not sufficient for complete pathogen clearance and the induction of an adaptive immune response, which is exquisitely pathogen specific, is required for pathogen control. In addition, the adaptive immune system has the ability to remember prior pathogen exposure and to mount a more rapid and robust response upon re-infection with the same pathogen [3]. This hallmark property of the adaptive immune response is referred to as immunological memory. Vaccination, i.e. the induction of protective immunity by inoculating with pathogen-derived material, is entirely based on the induction of immunological memory [4].

The adaptive immune system comprises B and T lymphocytes. The activation and differentiation of pathogen-specific B lymphocytes into plasma cells leads to the production of soluble pathogen receptors, so-called antibodies. These can bind pathogens and components thereof, which leads to neutralization, direct killing (via the complement system) and enhanced phagocytosis of extracellular pathogens [3]. However, when pathogens infect host cells, antibodies are not well suited to eliminate the pathogens. In such cases T cell immunity mediated by cytotoxic CD8+ T lymphocytes, is normally required to clear pathogen infected cells [3]. Although CD8+ T cells cannot recognize free pathogens, they can recognize infected cells and mediate their elimination via the release of cytotoxic molecules, such as perforin and granzymes [5]. Thus, the development of CD8+ T cell responses is crucial for the immune protection against intracellular pathogens, such as viruses, fungi, certain bacteria and parasites. Additionally, CD8+ T cells can also recognize and eliminate cancer cells when they display tumor-specific antigens on their surface [6, 7].

After the initial clearance of intracellular pathogens, antigen-specific CD8+ T cells can persist for long periods of time, providing the cellular basis for immunological memory [8]. During a second exposure to the same pathogen memory CD8+ T cells can more rapidly generate secondary cytotoxic cells to control infection [9]. Memory CD8+ T cells are particularly important for the protection against systemic, high dose and protracted re-infections [9].

Certain infections, such as human immunodeficiency virus (HIV), cannot be controlled by the immune system. Notwithstanding CD8+ T cells play an important role in these so-called persistent (or chronic) infections. Indeed CD8+ T cells mediate some degree of protection and their presence is required to keep infection in check, while not sufficient to control it [10]. Similar effects are observed in cancer, where CD8+ T cells provide a certain degree of protection [7, 11].

Immunotherapy aims at boosting the function of CD8^{+} T cells to improve viral clearance or tumor control.

Vaccination, i.e. the administration of antigenic material to help the immune system develop protection, is effective for the induction of antibodies. However, to protect against certain infectious diseases or cancer the elicitation of potent and durable CD8^{+} T cell responses may be needed [12, 13]. Still, the efficacy of T cell vaccines is comparably poor. The efficiency of T cell vaccination is usually measured by the magnitude of the response elicited. However, it has become clear that long-term protection depends both on the quantity and quality of the memory CD8^{+} T cells generated [12, 13]. In fact, the generation of multifunctional memory cells is associated with enhanced protection [4, 12]. Nevertheless, the factors and mechanisms that regulate the generation of such cells are still incompletely understood.

1. CD8^{+} T cell response to acute infection

Naive CD8^{+} T cells (T_N) recirculate and are attracted to secondary lymph organs due to a gradient of the homeostatic chemokines CCL19 and CCL21 [14]. If T_N encounter cognate antigen in the context of properly activated antigen presenting dendritic cells they are activated, expand and differentiate. It is estimated that the mouse naive CD8^{+} T cell repertoire comprises 100 to 1000 cells specific for a given antigen [15]. Following infection this number can increase up to 500'000-fold [16]. Efficient activation, expansion and differentiation of T_N cells requires 3 signals [17]: (1) interaction of their T cell receptor (TCR) with the specific antigenic peptide complexed with MHC (Major Histocompatibility Complex) class I molecules present on the surface of antigen presenting cells (APC); (2) co-stimulation, e.g. binding of the co-receptor CD28 on T cells to B7.1 (CD80) or B7.2 (CD86) expressed on mature APC's; and (3) inflammatory cytokines, such as interleukin-12 (IL-12) and type I interferon (IFN). The latter are required for full clonal expansion and differentiation to acquire effector functions, in particular the ability to kill antigen expressing cells [15]. These so-called effector cells can migrate to infected tissues where they can secrete cytokines, such as IFN-γ and tumor necrosis factor (TNF)-α, or kill infected cells through the release of perforin and granzymes, contributing to the control of intracellular pathogens [5, 18, 19]. After pathogen clearance, the majority of these cells (90-95%) die by apoptosis, leaving behind a population of long-lived antigen-specific memory CD8^{+} T cells (**Fig. 1**) [8, 13, 20]. By classical definition memory cells are cells that can persist/exist in the absence of antigen [9].
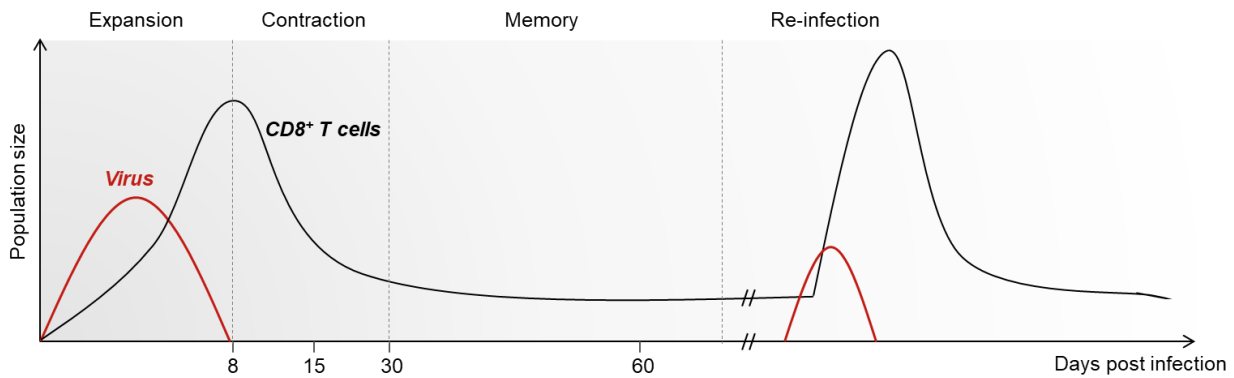
FIGURE 1: Primary and secondary CD8+ T cell responses to acute viral infection.
Antigen presentation and other stimuli leads to the activation of rare antigen-specific naïve CD8+ T cells, which expand and differentiate into effector cells. Usually the expansion peak of CD8+ T cells occurs at day 8 post-infection and coincides with viral clearance. Once virus is cleared there is a contraction phase, in which most effector cells die. Nonetheless, 5-10% of CD8+ T cells survive allowing formation of functional memory CD8+ T cells. In case of a second exposure to the same pathogen the memory CD8+ T cells allow a more rapid and efficient viral control.

A hallmark of immunological memory is the ability to provide enhanced protection against re-infection. This protection is due to several memory-specific attributes, including an increased number of antigen-specific T cells as compared to a naive T cell repertoire [9]; long-term persistence in the absence of antigen due to cytokine-driven (IL-7 and IL-15) homeostatic turnover [21, 22, 23, 24, 25, 26]; and the capacity of memory cells to respond more rapidly to antigen encounter as compared to naive cells [27].

1.1. Subsets of memory CD8+ T cells

The memory CD8+ T cell compartment is heterogeneous, comprising multiple subsets of cells present at distinct anatomical locations, with distinct recirculation patterns and functions [28, 29]. Sallusto and colleagues [28] were the first to report the diversity of the memory compartment. They described two subsets of recirculating memory cells, which they have termed central memory (T_{CM}) and effector memory (T_{EM}) T cells. T_{CM} express high levels of the lymph node (LN) homing receptors CD62L and CCR7, allowing them to migrate through secondary lymphoid organs. T_{EM} lack these receptors and are present in lymphoid and non-lymphoid tissues, but not in secondary lymphoid organs (**Fig. 2**) [28, 29]. Subsequent studies have identified tissue-resident memory (T_{RM}) T cells, that lack the capacity to re-circulate [30, 31, 32]. This population is restricted to non-lymphoid tissues, due to their low/absent expression of CD62L/CCR7 and high expression of CD69, CD103 and tissue-specific chemokine receptors and integrins [33, 34, 35].

	Central Memory	Effector Memory	Tissue-Resident Memory
Phenotype	CD62L^{high} CCR7^{high} CD69$^-$CD103$^-$	CD62L^{low} CCR7^{low} CD69$^-$CD103$^-$	CD62L^{low} CCR7^{low} CD69$^+$CD103$^+$
Location	LN, spleen, blood	Spleen, blood, liver	Skin, lung, gut, brain
Functional properties			
Stemness / Multipotency	+++	+/-	-
Proliferative capacity	+++	+	+/-
IL-2 production	+++	+	+/-
Migration	+++	++	+/-
Effector functions (IFNγ, TNFα, Killing)	+	+++	+++

FIGURE 2: Phenotype, location and functional properties of memory CD8$^+$ T cells.
The three main subsets of memory CD8$^+$ T cells have distinct expression of surface receptors / markers which influences their anatomical location. Additionally, these memory subsets also differ in their function, as summarized above, allowing division of labour. For example, while the T$_{CM}$ are responsible for maintaining the memory pool, due to self-renewal and multipotency, the T$_{EM}$ and T$_{RM}$ can directly mediate effector functions. (*This figure was created using Servier Medical Art templates*).

The above memory subsets differ in their function (**Fig. 2**). T$_{CM}$ display an increased capacity to persist *in vivo,* to produce IL-2 and to proliferative/re-expand upon antigen reencounter [36, 37]. *In vivo* clonogenic studies performed by Graef and colleagues showed that single T$_{CM}$ cells have the ability to self-renew (i.e. the ability to divide while maintaining an undifferentiated state) and are multipotent, i.e. can generate diverse differentiated progeny, including T$_{EM}$ and effector cells [38]. This study formally established that T$_{CM}$ cells have stem cell properties. Incidentally we define and use "stemness" as the capacity of relatively undifferentiated cells to self-renew (reproduce) and to yield more differentiated progeny upon cell division.

In contrast to T$_{CM}$, T$_{EM}$ have limited multipotency and self-renewal capacity [38]. However upon re-stimulation, T$_{EM}$ and T$_{RM}$ exert immediate effector functions, in particular lytic activity, thanks to granzyme B and perforin expression [39]. Hence, during a second encounter with antigen, T$_{EM}$ and T$_{RM}$ cells provide immediate antigen-specific defense in lymphoid and non-lymphoid tissues. T$_{EM}$ and T$_{RM}$ are thus essential for immune protection against local challenges, such as influenza virus [34, 35, 40]. In contrast, T$_{CM}$ cells can generate more secondary antigen-specific effector cells, due to their greater expansion/differentiation capacity, and they maintain the memory T cell compartment by self-renewal [38, 41, 42]. T$_{CM}$ are thus essential for protection

against high dose, protracted and/or systemic re-infections, such as Lymphocytic choriomeningitis virus (LCMV) infections [29].

Additional memory subsets have been described. For example an expanded population of mouse CD8$^+$ T cells with a naive-like phenotype (CD44^{lo} CD62L^{hi}) was identified in graft-versus-host disease (GVHD) [43]. These so-called stem cell memory T cells (T$_{SCM}$) reconstituted the entire memory T cell compartment upon re-stimulation [43, 44, 45]. These cells, comprising 2-3% of circulating T lymphocytes, are clonally expanded and defined by a naive-like phenotype in combination with memory markers, including Sca-1, Cxcr3, IL2rβ (CD122), Bcl2 and CD95 [43, 45, 46]. T$_{SCM}$ cells share the re-circulation and tissue distribution patterns of naïve cells [47], but they also display properties of memory cells, such as the capacity to rapidly re-expand upon antigen re-exposure and IL-15/IL-7 dependent homeostatic maintenance [45, 48]. Indeed, human antigen-specific cells with a T$_{SCM}$ phenotype are stably maintained for > 25 years after vaccination [49]. Additionally, *in vitro* generated T$_{SCM}$ cells were shown to differentiate into T$_{CM}$ and T$_{EM}$ subsets while self-renewing the T$_{SCM}$ pool in response to IL-15 signals [44, 45] or antigenic stimulation [48]. Even though T$_{SCM}$ cells are well-defined in human and non-human primates [45, 46], pathogen-specific T$_{SCM}$ cells are not detected in mice [50]. In mice, T$_{CM}$ cells are, so far, the only memory subset with stem cell properties [38, 51].

The CD8$^+$ T cell memory compartment may be even more complex. Based on the expression of Cx3cr1, Gerlach and colleagues described peripheral memory T cells (T$_{PM}$) [52]. These cells express intermediate levels of the effector-marker Cx3cr1, recirculate and survey non-hematopoietic tissues. In addition, these cells undergo homeostatic proliferation and self-renewal [52].

The differentiation state of memory cells correlates with their protective capacity. Using the adoptive transfer of Pmel-1 CD8$^+$ T cells (specific for the tumor antigen gp100), Klebanoff and Gattinoni showed that *in vitro* generated T$_{SCM}$ cells exert the highest capacity to eradicate established solid tumors, followed by T$_{CM}$ and lastly T$_{EM}$ [44, 53]. The transfer of fully differentiated effector cells had minimal anti-tumor effect in these settings [54]. Additionally, adoptive transfer of LCMV-primed T$_{CM}$ cells also provides a more rapid control of chronic viral infection compared to T$_{EM}$ [37]. Thus, increased stemness and recall expansion capacity of adoptively transferred cells correlates with improved anti-tumor efficacy (**Fig. 3**) or enhanced viral control.
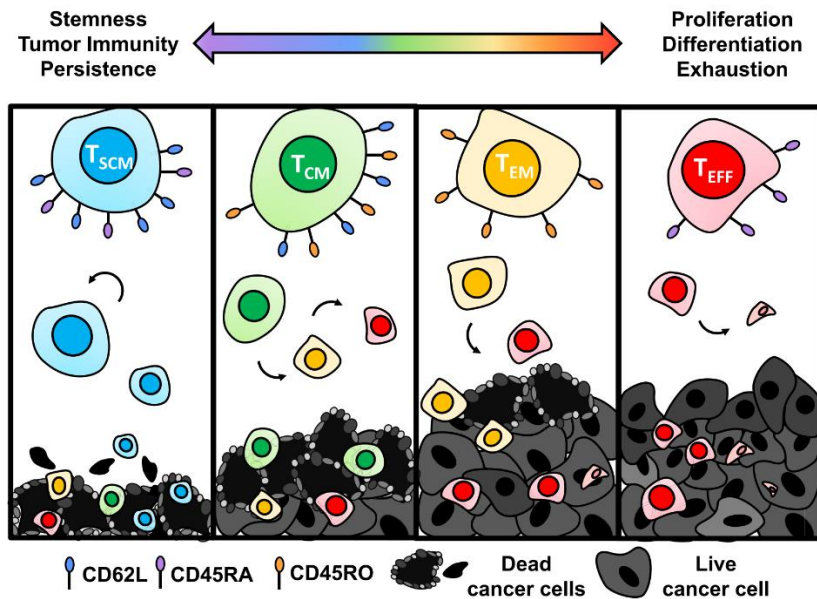
FIGURE 3: Antitumor therapeutic potential of memory CD8^{+} T cell subsets.
Antitumor efficiency correlates with increased stemness and persistence of the memory CD8^{+} T cell subsets, thus T$_{SCM}$ have the best therapeutic potential. Conversely, cells with an increased differentiation state lose the ability to self-renew and become exhausted, leading to poor antitumor immunity. (From Knochelmann *et al.*, *Frontiers in Immunology*, 2018 [55]).

1.2. Developmental origin of memory T cells

The ontogeny of memory T cells and their relationship to effector T cells is still incompletely understood [56, 57]. The strength and duration of antigenic stimulation has been shown to influence effector vs memory diversification [58, 59, 60]. While very high or repetitive TCR stimulation favors terminal effector differentiation, intermediate TCR signals are required for the development of functional long-lived memory cells [61, 62, 63]. One possible explanation was that distinct naive T cells give rise to distinct fates ('one cell, one fate' concept), dependent on intrinsic and extrinsic signals [64]. Elegant studies using the transfer of single T$_N$ cells demonstrated that an individual T$_N$ cell can give rise to both effector and memory cells [65, 66, 67]. This discovery led to the establishment of the single-cell-derived subset diversification concept, since effector and memory cells do not arise from different T$_N$. At least 3 models can account for effector versus memory CD8^{+} T differentiation from single T$_N$ [56].

1.2.1. Linear differentiation model

Seminal work based on LCMV-specific mouse CD8^{+} T cell responses has suggested that effector cells, present at the peak of the primary response, lack the hallmark qualities of memory T cells, such as homeostatic maintenance and high proliferative potential in response to re-stimulation. Rather, memory functions gradually appeared following antigen clearance (around day 22 p.i.) [68]. These observations supported the so-called linear differentiation

model, which proposes that memory cells derive from the cytolytic effector T cell population (naive → effector → memory) after pathogen clearance (**Fig. 4**) [29, 68, 69, 70, 71, 72, 73].
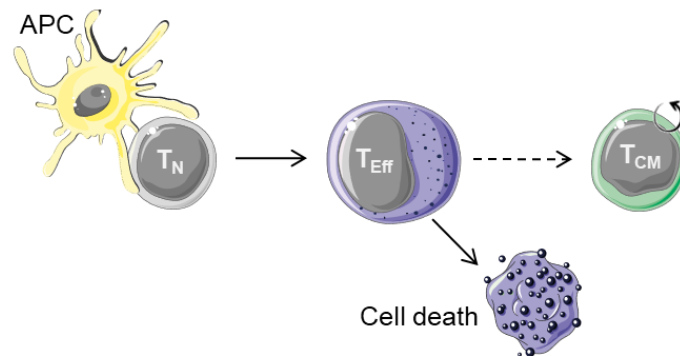
FIGURE 4: Linear model for CD8+ T cell differentiation.
Activation of naive (T_N) CD8+ T cells leads exclusively to the development of cytolytic effector cells (T_{Eff}). Once pathogen is cleared, effector cells can either become terminally differentiated and die or differentiate into central memory cells (T_{CM}), which persist for long periods of time. APC, antigen presenting cell. (*This figure was created using Servier Medical Art templates*).

Bannard and colleagues provided further support for this model using a transgenic mouse line that allowed the irreversible marking of CD8+ T cells that expressed Granzyme B (GzmB), an essential component of the lytic machinery [74]. They proposed that memory cells that had previously expressed GzmB (i.e. were cytolytic) displayed robust recall expansion, suggesting that memory cells pass through a cytolytic effector phase [74]. Similar observations were made for memory CD8+ and CD4+ T cells that had previously expressed IFN-γ [75]. Thus, it was concluded that long-lived memory T cells with recall expansion potential derived from cytolytic effector cells [74, 75, 76].

Genome-wide chromatin accessibility studies have uncovered that effector and memory CD8+ T cells have distinct epigenetic landscapes [77, 78, 79]. Thus, in the past years, there was an increased interest in understanding of the epigenetic mechanisms, such as DNA methylation and histone modifications, in the regulation of memory versus effector differentiation [72, 79, 80, 81, 82]. A recent study proposed that naive cells acquire repressive DNA methylation marks at genes associated with T_{CM} cells, some of which are shared with naive cells, such as *Sell* (CD62L), during effector differentiation [81]. It was further proposed that these repressive CpG methylation marks at the *Sell* promoter are later erasure in memory cells and that this allows the re-expression of CD62L during memory differentiation. Therefore, it was suggested that cytolytic effector cells silence and memory cells re-acquire a T_{CM}-associated gene expression program upon pathogen clearance [80, 81]. In agreement with the linear differentiation model, long-lived memory cells are thus thought to "de-differentiate" from a subset of cytolytic effector cells [81] while maintaining an epigenetic imprint from their effector phenotype past, given that

key effector genes remain demethylated [79, 80, 81]. It is noteworthy that the linear differentiation model implies that CD8^{+} T cell stemness follows an On-Off-On pattern (**Fig. 5**), which would be unique in stem cell driven tissues, except perhaps cancer.
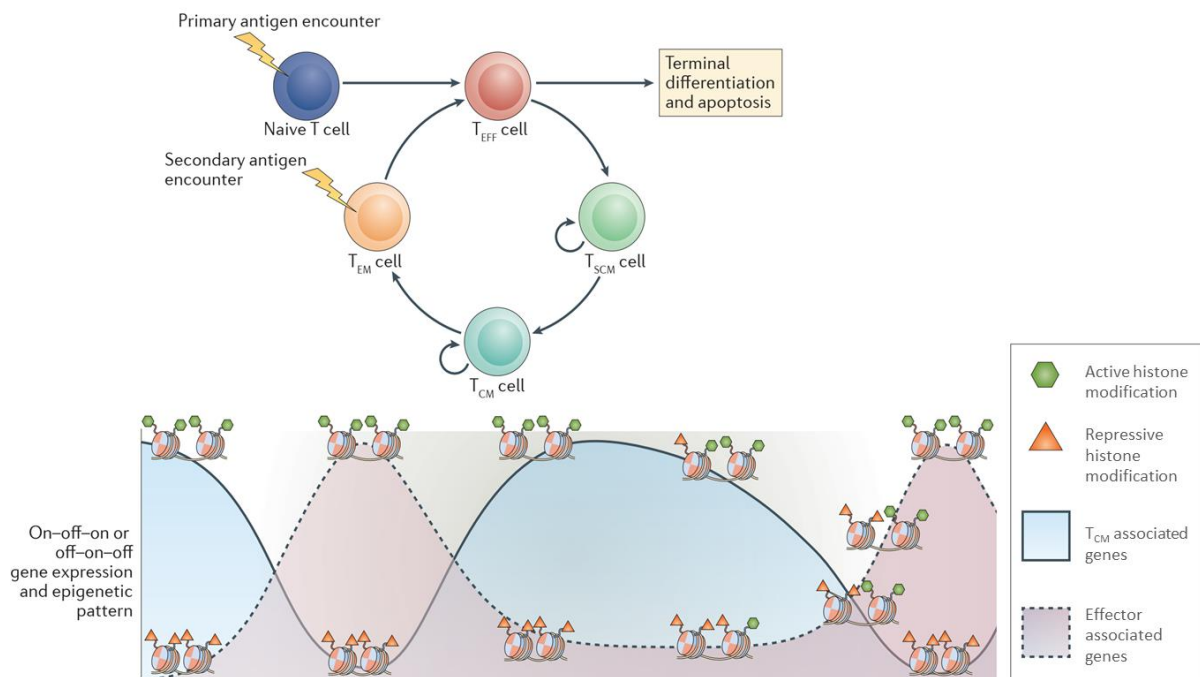
FIGURE 5: Transcriptional and epigenetic patterns of the linear differentiation model. According to the linear model for CD8^{+} T cell differentiation, terminal differentiated effector cells de-differentiate into memory cells following pathogen withdrawal. This would indicate an off-on-off pattern of effector-associated transcriptional and epigenetic changes over time (or on–off–on pattern of T_{CM}-associated changes). (Adapted from Henning *et al.*, *Nat Rev Immunol*, 2018 [83]).

Inconsistent with this model, the length of telomeres is reduced in effector cells as compared to memory cells [84, 85], indicating that memory cells undergo fewer cell divisions than effector cells. Additionally, memory cells have been shown to develop without transitioning through a cytolytic effector phase [86], indicating that effector differentiation is not an obligatory step for memory differentiation.

1.2.2. Bifurcative differentiation model

The observation of heterogeneity amongst effector T cells lead to the development of a second model of CD8^{+} T cell differentiation, known as the bifurcative differentiation model (**Fig. 6**). This model is based on the identification of a subset of effector cells present at the peak of the immune response (termed memory precursor cells (MP)) that has an increased potential to form memory T cells [46, 87]. MP cells are characterized by low expression of KLRG-1 and high expression of IL7rα (CD127), while the opposite phenotype (KLRG-1^{hi} CD127^{lo}) defines a

population of terminally differentiated effector cells (TE) that is more prone to undergo cell death following antigen clearance. Likewise, CD8$^+$ T cells expressing high levels of the IL-2 receptor α chain (IL2rα^{hi}) are more prone to yield TE cells [88, 89]. It is thus possible to identify cells that are more likely to survive and differentiate into memory cells (MP) versus cells that are programmed to undergo apoptosis (TE), before clearance of the pathogen [69, 90]. However, cells with a MP phenotype still contract and some cells with a TE phenotype can survive long-term [91]. Therefore, classically defined MP cells do not yield memory quantitatively. Further, MP cells express GzmB and have lytic activity [87, 88, 90], and thus require further differentiation upon antigen clearance to form memory, similar to the linear differentiation model.
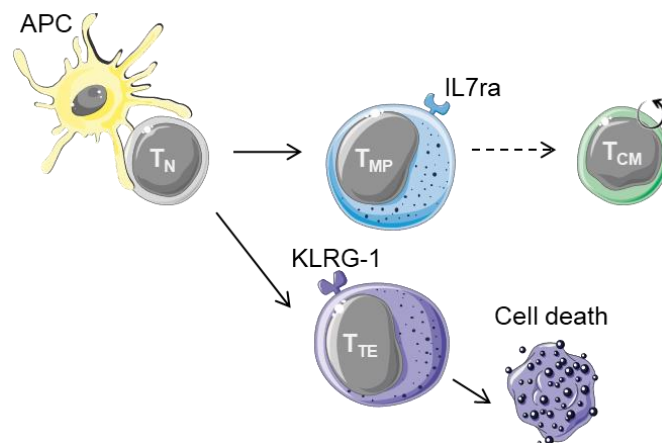
FIGURE 6: Bifurcative model for CD8$^+$ T cell differentiation.
Activation of naive (T$_N$) CD8$^+$ T cells leads the generation of both memory precursor (T$_{MP}$, IL7rα^+) and terminally differentiated effector (T$_{TE}$, KLRG-1$^+$) cells that have distinct lineage potential. While both have cytolytic activity, T$_{TE}$ die after elimination of pathogen and T$_{MP}$ survive and differentiate into long-lived central memory cells (T$_{CM}$). APC, antigen presenting cell. (*This figure was created using Servier Medical Art templates*).

There is some debate when during the primary response the bifurcation to effector versus memory fated cells occurs. Reiner and colleagues [92], suggested that these T cell fates diverge during the very first cell division, based on an unequal inheritance of cellular components (asymmetric division). Relevant components include CD8 and the adhesion molecule LFA-1 [92], PKCz [92]; the effector transcription factor T-bet and proteasome proteins [93]. A prolonged contact between a T cell and an APC promoted by high-affinity TCR binding was required for asymmetric division [94]. The daughter cell proximal to the APC, which formed an immunological synapse and received more TCR and cytokine signals, inherited more CD8, LFA-1, PKCz and T-bet and adopted a short-lived effector fate. In contrast, the daughter cell distal to the synapse retained memory potential. Therefore, asymmetric partitioning during the first division resulted in the generation of a "memory-fated" distal daughter cell and an "effector-fated" proximal daughter cell, whose progeny undergo apoptosis following pathogen clearance [56, 92, 93, 94].

Single-cell gene expression analyses supported an early bias to memory or effector CD8^{+} T cell fates [95, 96]. Using single-cell RNA sequencing, Kakaradov and colleagues have demonstrated the existence of two CD8^{+} T cell populations with distinct transcriptomes among cells that have divided exactly once. One population, termed "Div1$_{TE}$ cells", showed increased expression of *Il2ra*, *Stat5a* and *Tbx21* (T-bet), factors known to be involved in effector differentiation [88, 89, 90, 97, 98]. The other population, "Div1$_{MEM}$ cells", was transcriptionally more similar to memory cells [96]. In addition, there was an increased expression of Ezh2 among "Div1$_{TE}$" daughter cells, suggesting a role for epigenetic regulation of CD8^{+} T cell fate. The methyltransferase Ezh2, which is the catalytic subunit of Polycomb repressive complex (PRC) 2, mediates gene repression via trimethylation of histone H3 at Lys27 (H3K27me3) [99]. In effector CD8^{+} T cells, Ezh2 is required for efficient secretion of inflammatory cytokines as well as for restraining apoptosis [96, 100, 101]. In KLRG-1^{+} cells, Ezh2 mediates silencing of memory associated loci, thus enforcing the differentiation of TE cells [100]. It is thus conceivable that increased Ezh2 expression by "Div1$_{TE}$ cells" epigenetically marks them to adopt an effector fate, supporting the view that CD8^{+} T cell lineages diverge as early as the first cell division. Nonetheless, while memory fate may be programmed very early during the primary response, memory functions are still thought to emerge following pathogen clearance.

1.2.3. Developmental differentiation model

Finally, the developmental differentiation model (**Fig. 7**) states that the activation of T$_N$ directly yields cells with central memory function and these are the source for the cytolytic effector population [58, 102, 103]. As such, this model proposes a progressive differentiation of naive cells into memory and finally terminally differentiated effector cells. This hypothesis is supported by the gene expression profile of memory cells, which is more related to naive than to effector cells [104].
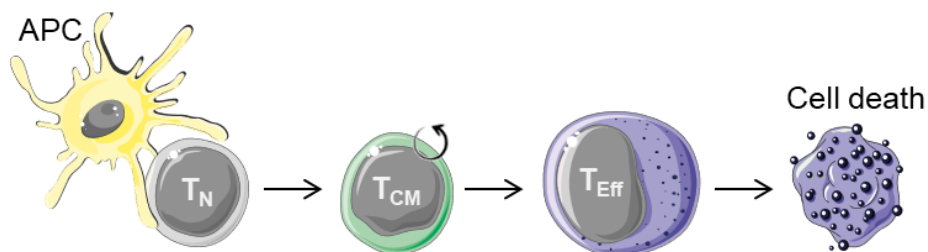
FIGURE 7: Developmental model for CD8^{+} T cell differentiation.
Activation of naive (T$_N$) CD8^{+} T cells leads the development of long-lived central memory cells (T$_{CM}$) before pathogen clearance. In such model, cytolytic effector cells (T$_{Eff}$) are thought to derive from the less differentiated T$_{CM}$ cells upon further signaling. APC, antigen presenting cell. (*This figure was created using Servier Medical Art templates*).

Studies using *in vivo* fate mapping of mouse T cells by Gerlach *et al.* and Buchholz *et al.* have recently provided additional support for the developmental differentiation model [67, 105]. The authors followed individual T_N CD8$^+$ T cells (either DNA-barcoded [67] or differentially expressing CD45.1/2 and CD90.1/2) [105], responding to *Listeria monocytogenes* infection. In both studies individual T_N cells yielded very variable numbers of progeny. Importantly, the large clones showed reduced fraction of CD62L$^+$ and IL-2$^+$ cells, suggesting an inverse relation between expansion and memory precursor phenotype [67, 105]. Buchholz and colleagues further used computational analysis to model the possible differentiation pathway of a single T_N into T_{CM} or T_{EM} precursors (pT_{CM} or pT_{EM}, respectively) and effector cells. Out of the 304 possible pathways of diversification only 2 fitted the experimental data, both of which predicted a developmental differentiation pathway ($T_N \rightarrow pT_{CM} \rightarrow pT_{EM} \rightarrow T_{EFF}$). The proliferation rates of T_{CM} precursors were lower compared to pT_{EM} or effector cells [105]. Thus, this study proposes that T_N differentiate into slow-cycling memory precursors, which self-renew and initially give rise to fast-cycling and later to non-cycling effector cells [105]. These data suggest a differentiation process in which cells progressively lose proliferative capacity and multipotency, dependent on the strength of the signaling input [39, 58].

The existence of additional memory subtypes, such as T_{SCM}, T_{EM} and intermediate subsets of memory T cells (T_{PM}), is also more easily explained by the strength of the signaling input and thus the developmental differentiation model. The least differentiated T_{SCM} cells, which may be exposed to very weak stimulation signals, were shown to directly differentiate form naive precursors in hematopoietic stem cell transplantation settings [106, 107]. Indeed, the transcriptome of T_{SCM} is the closest to that of T_N [45, 108], suggesting that T_{SCM} cells precede T_{CM} cells in the developmental differentiation.

In further agreement with this model, genome-wide histone modifications in T_N, T_{SCM}, T_{CM} and T_{EM} CD8$^+$ T cells revealed a progressive loss of accessibility in T_{CM} associated genes, which was accompanied by gene expression differences [109]. It was further suggested that effector differentiation is dependent on the irreversible Ezh2 or Suv39h1-mediated epigenetic silencing of T_{CM} associated genes [82, 100]. Indeed, absence of Ezh2 or Suv39h1 reduced the abundance and differentiation of TE cells, but the number of memory cells remained constant [82, 100]. This is inconsistent with a model in which effector cells precede the generation of memory cells. Rather, memory cells are epigenetically more related to naive cells and silencing of T_{CM} associated genes is a feature associated with effector cell differentiation. Collectively this model implies that CD8$^+$ T cell stemness follows an On-On-Off pattern, i.e. is lost during effector differentiation (**Fig. 8**).
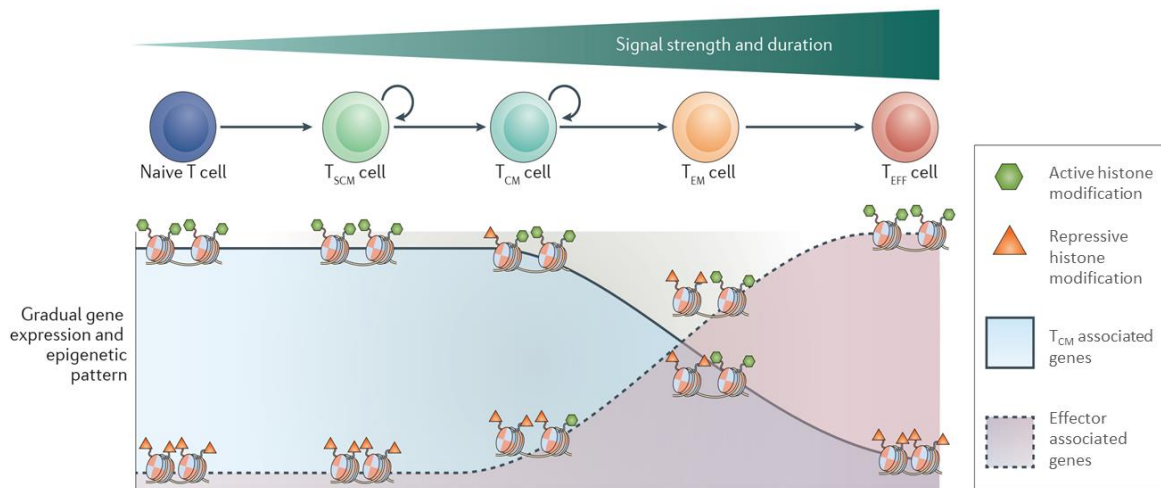
FIGURE 8: Transcriptional and epigenetic patterns of the developmental differentiation model. The developmental model for CD8^{+} T cell differentiation is based on a progressive acquisition of effector functions, dependent of the antigenic signal strength and duration. As such, these changes would be accompanied by a gradual loss of T_{CM} associated transcriptional and epigenetic patterns (or gradual gain of effector-associated patterns). (Adapted from Henning *et al.*, *Nat Rev Immunol*, 2018 [83]).

Finally, while the developmental differentiation model predicts the presence of CD8^{+} T cells with central memory function during the acute phase / peak of the immune response to viral infection, such cells have not been described.

1.3 Transcriptional control of effector vs memory CD8^{+} T cell differentiation

Multiple extrinsic factors act simultaneously to regulate the differentiation of CD8^{+} T cells, including TCR signal strength, co-stimulation (CD28, CD27, etc), cytokine signals (IL-12, type I IFN, etc) and the availability of nutrients (**Fig. 9a**) [110]. Additionally, differentiation of CD8^{+} T cells also depends on help from CD4^{+} T cells. CD8^{+} T cells primed in the absence of CD4^{+} T cells ('helpless' cells), are capable of primary expansion and effector differentiation, but memory cells respond poorly to re-challenge [111, 112]. The upregulation of TNF-related apoptosis-inducing ligand (TRAIL) upon re-stimulation and consequently activation-induced cell death is the known mechanism behind the impaired re-expansion capacity of 'helpless' CD8^{+} T cells [113, 114].

Extrinsic factors regulate the expression and function of transcription factors (TFs) that play key roles in the fate determination of CD8^{+} T cells. Generally, the dichotomic differentiation into effector vs memory cells is controlled by the expression of competing sets of TFs. While T-bet (*Tbx21*), Id-2, Blimp1 (*Prdm1*) and STAT4 have been shown to promote effector cell

differentiation [98, 115, 116, 117, 118], Id-3, Bcl6, STAT3, Foxo1 and Tcf1 are known to play important roles for memory formation and/or function [119, 120, 121, 122, 123, 124, 125, 126, 127] (**Fig. 9b**).
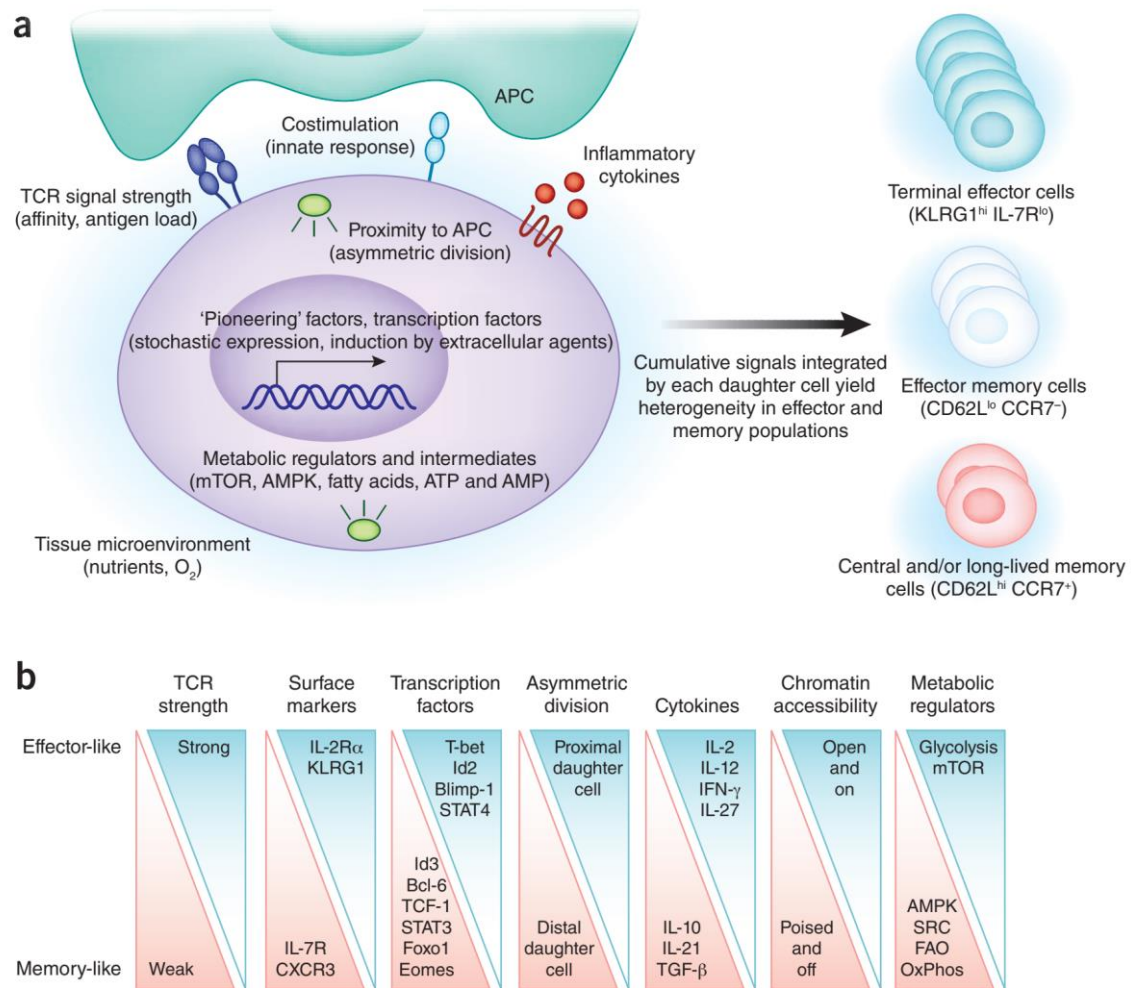
FIGURE 9: Extrinsic and intrinsic factors that determine effector vs memory CD8$^+$ T cell fate. (**a**) Upon antigen stimulation, a naive T cell is subjected to multiple extrinsic and intrinsic signals, such as TCR signal strength, co-stimulation, inflammatory cytokines, tissue microenvironment, metabolic regulators, transcription factors and the mode of cellular division. Integration of all signals by the T_N cell regulates its lineage specification. (**b**) Factors known to favor effector (top, blue) or memory differentiation (bottom, pink). APC, antigen-presenting cell; FAO, fatty acid oxidation; SRC, spare respiratory capacity; OxPhos, oxidative phosphorylation. (From Chang *et al.*, *Nat Immunol Rev*, 2014 [110]).

This lab and others have found that the transcription factor T cell factor 1 (Tcf1, encoded by *Tcf7*) is dispensable for the development of a normal CD8$^+$ T cell primary immune response, but selectively required for the formation and function of T_{CM} cells in response to acute viral infection [125, 126, 127, 128, 129]. Likewise, the transcription factor Foxo1 is essential for the recall expansion capacity of memory cells upon re-infection. Foxo1 suppresses T-bet and induces Eomes to support T_{CM} development. Moreover Foxo1 reduces cell cycle progression [124, 130,

[131, 132, 133]. Foxo1 itself is regulated by the expression of the nutrient sensor mTORC2. Indeed, absence of mTORC2 stabilizes Foxo1 in the nucleus of CD8$^+$ T cells, promoting memory differentiation [134, 135, 136, 137].

Interestingly, Tcf1 expression in memory cells seems to be supported by Foxo1, which directly binds to an intergenic region of the *Tcf7* gene [131]. In a recent study, Foxo1 was dispensable for the expression of Tcf1 in naive cells, but was essential for the emergence of a small subset of cells expressing *Tcf7* shortly after primary infection [138]. This Foxo1-dependent population exhibited higher memory-associated genes (Bcl2 and Eomes) and decreased hallmarks of effector cells (GzmB and T-bet) [138]. In turn, Tcf1 directly represses cytotoxic effector molecules, such as Granzymes [139], Blimp1 [140, 141], CD25 (IL2rα) [142] and Fas ligand [140]. In addition, Blimp1 deficient CD8$^+$ T effector cells upregulate Tcf1 [117], suggesting that this pair of TFs have mutually antagonistic actions in antigen-activated CD8$^+$ T cells. On the other hand, Tcf1 can positively regulate the expression of Eomes, which in turn is responsible for the upregulation of IL2rβ [127], allowing better maintenance of memory cells. Finally, Tcf1 also mediates the activation of the memory-associated transcription factor Bcl6 [142, 143, 144, 145].

Recently, c-Myb was also described to promote T$_{CM}$ functions [146]. The frequency of CD62L$^+$ T$_{CM}$ cells was reduced among c-Myb deficient antigen-specific CD8$^+$ T cells, which correlated with reduced re-expansion potential. Conversely, overexpression of this TF enhanced recall expansion capacity and conferred long-lasting antitumor immunity. It was thus concluded that c-Myb plays a key role in the generation and function of T$_{CM}$ cells. Mechanistically, c-Myb promoted pro-memory and survival programs (*Tcf7* and *Bcl2)* while limiting effector differentiation through the repression of *Zeb2* [146].

2. Tcf1 and Wnt signaling pathway

Tcf1, together with Tcf3 (*Tcf7L1*), Tcf4 (*Tcf7L2*), and Lef1, form a small subfamily of high-mobility group (HMG) DNA-binding transcription factors [147, 148]. These factors are best-known as nuclear effectors of the canonical Wingless/Integration 1 (Wnt) signaling pathway, which depends on the nuclear β-catenin accumulation [149]. The Wnt pathway controls multiple key developmental processes and adult tissue homeostasis, via the regulation of cell polarity, stem cell function and progenitor-cell proliferation [150, 151]. As a result, this pathway is often exploited by malignant cells, where uncontrolled Wnt signaling has been associated with excessive proliferation and renewal of cancer stem cells, especially in colon carcinoma [152] but also in hematological malignancies [151].

Alternative splicing and differential promoter usage produce multiple Tcf1 isoforms [147, 149]. The long isoforms (p45 and p42) contain a NH2-terminal β-catenin binding domain, while the short isoforms (p33 and p30) lack this domain. The latter cannot bind β-catenin and may function as negative regulators of the canonical Wnt pathway. In contrast, the COOH-terminal HMG DNA-binding domain, which recognizes a consensus binding motif known as Wnt responsive element (WRE) [151], is present in all isoforms [147]. Binding of HMG domain to DNA leads to DNA bending, which may impact gene expression via an architectural role, i.e. to bring adjacent TFs into proximity. Further, the HMG domain and neighboring central region of Tcf1 can interact with Groucho-related gene / transducin-like enhancer (GRG/TLE) co-repressor proteins [153]. GRG/TLE proteins can recruit histone deacetylases, such as Rpd3 [154], mediating chromatin remodeling and transcriptional silence. Finally all Tcf1 isoforms contain a histone deacetylase (HDAC) domain [140]. This domain is located between the β-catenin and the HMG domains (**Fig. 10**) and endows Tcf1 with intrinsic HDAC activity to modify chromatin structure [140]. This domain overlaps with the GRG/TLE binding domain and thus might allow the repression of Wnt target genes even when co-repressors are not recruited.
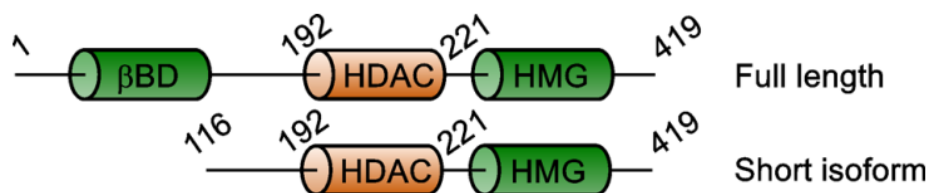
FIGURE 10: Functional structure of Tcf1 isoforms.
Long or full length Tcf1 isoforms (p45 and p42) contain a β-catenin binding domain (βBD), which is absent in short isoforms (p33 and p30). All isoforms have a histone deacetylase (HDAC) activity domain and a high mobility group (HMG) DNA binding domain. The numbers denote boundaries of the indicated domains based on the full length Tcf1 protein. (From Gullicksrud *et al.*, *Front. Biol. Rev*, 2017 [155]).

2.1. Canonical Wnt pathway

The canonical Wnt pathway, also known as Wnt - β-catenin pathway, depends on the stabilization and intracellular accumulation of non-phosphorylated β-catenin [149, 156]. In the absence of Wnt signals, β-catenin is targeted for degradation by the proteasome. This is achieved via a destruction complex, which is composed of anchor proteins (axis inhibition protein 1 (AXIN1) and adenomatous polyposis coli (APC)) and serine/threonine kinases (casein kinase 1 (CK1) and glycogen synthase kinase 3β (GSK3β)). Phosphorylation of β-catenin, first by CK1 and then by GSK3β, is recognized by the E3 ubiquitin ligase βTRCP, which leads to ubiquitylation and proteasomal breakdown of β-catenin [157] (**Fig. 11a**). In the absence of nuclear β-catenin, the Tcf1 HMG DNA binding domain is bound to GRG/TLE co-

repressors [158]. The binding of the Tcf1 – GRG/TLE complex to WREs promotes histone deacetylation and chromatin compaction, leading to the suppression of Wnt target genes [153].
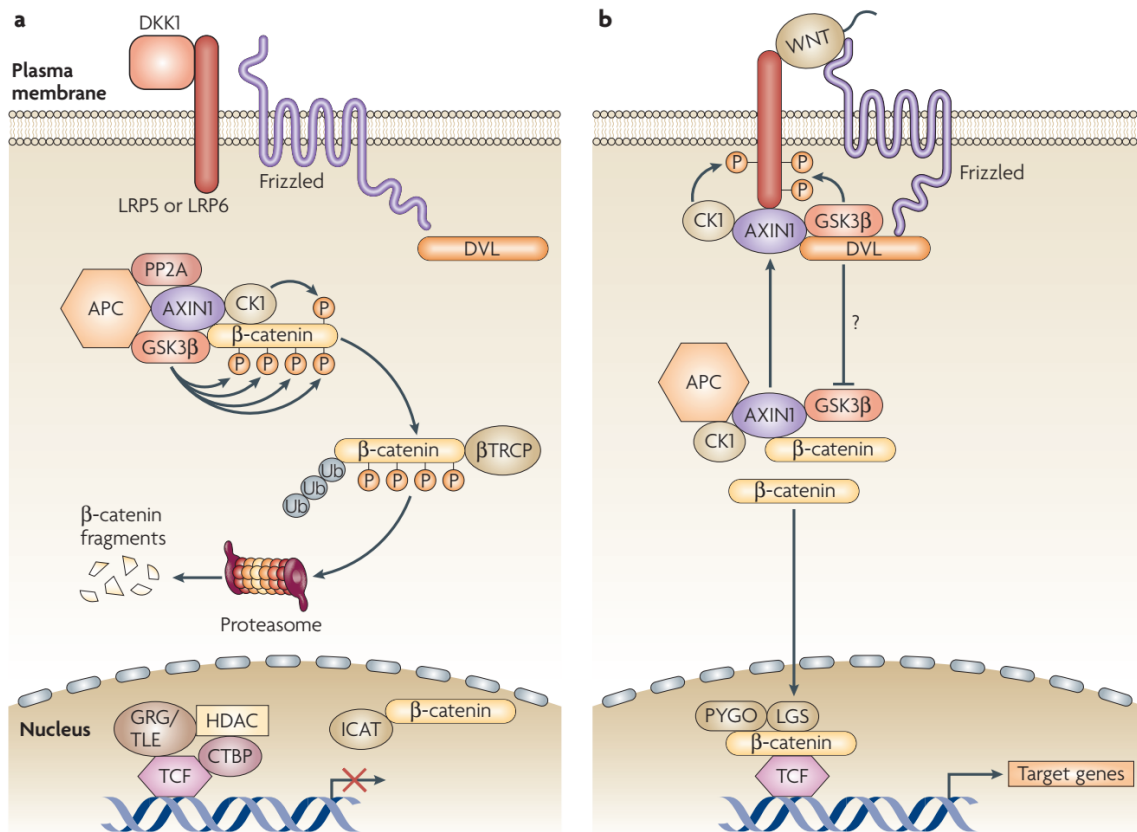
FIGURE 11: Canonical Wnt signaling pathway.
(**a**) In the absence of Wnt signaling, cytoplasmic β-catenin is continuously degraded by the proteasome due to targeted phosphorylation by the destruction complex (CK1, GSK3β, AXIN1, APC). As a result, in the nucleus Tcf1 is bound to GRG/TLE co-repressors preventing the expression of Wnt target genes. (**b**) Binding of Wnt proteins to the Wnt receptor complex (Frizzled receptor and LRP5 or LRP6) recruits proteins from the destruction complex to the plasma membrane (CK1, GSK3β and AXIN1). Consequently, β-catenin can accumulate and translocate to the nucleus where it will bind to Tcf1 and allow the transcription of Wnt target genes. (From Staal *et al.*, *Nat. Rev. Immunol.*, 2008 [151]).

The binding of some of the 19 Wnt ligands to one of the receptor complexes (Frizzled receptor with low density lipoprotein receptor-related protein 5 (LRP5) or LRP6 co-receptors) induces stabilization of β-catenin (**Fig. 11b**). Formation of the Frizzled–LRP5/LRP6 complex leads to the phosphorylation of LRP5 or LRP6 by CK1 and GSK3β [159]. Subsequently AXIN1 is recruited to this complex at the membrane and is no longer available to form the β-catenin destruction complex [160]. Finally, this allows accumulation of cytoplasmatic β-catenin and its translocation to the nucleus. Here, β-catenin functions as co-activator of Tcf1, and other transcription factors of the Tcf family, by disrupting the Tcf1 – GRG/TLE complex [153, 161]. Tcf1-β-catenin complexes

recruit additional co-activators to induce the expression of Wnt target genes, including *Tcf7*, *c-myc* or *cyclin D1* [162]. In T cells, *Tcf7* targets are still comparably poorly defined.

2.2. Role of Tcf1 in T cell development

Tcf1 is essential for normal T cell development and thymocyte maturation [163, 164, 165, 166, 167]. During the earliest phase of T cell development, Tcf1 is directly activated by Notch signals in early thymic progenitors, initiating the T-cell lineage specification program [166, 167]. Interestingly, ectopic expression of Tcf1 in fibroblasts is sufficient to generate *de novo* chromatin accessibility at sites associated with T cell-restricted genes [168], establishing a key role for this TF in the control of T cell fate. In addition, Tcf1 ensures the survival of CD4$^+$CD8$^+$ double-positive (DP) thymocytes [163, 164]. Decreased survival of Tcf1-deficient DP thymocytes was rescued by the long Tcf1 isoform but not with the short isoform, suggesting that thymocyte survival depends on Wnt/β-catenin signaling [164]. Finally, Tcf1 is also involved in the control of CD4$^+$ and CD8$^+$ T cell-lineage choice [140, 169]. In DP thymocytes, Tcf1 (and Lef1) directly induces the expression of ThPOK, a transcription factor essential for CD4$^+$ T cell lineage specification [169]. Additionally, Tcf1 intrinsic HDAC activity reduces the expression of CD4, RORC, and FOXP3 in CD8$^+$ T cells [140]. Thus, Tcf1 establishes CD8$^+$ T cell identity by repressing CD4$^+$ lineage-associated genes.

2.3. Role of Tcf1 in T cell responses to acute infection

Besides its role in T cell development, Tcf1 is also critical for peripheral T cell differentiation. Upon infection, CD4$^+$ T cells can differentiate into several lineages, including IFN-γ secreting T$_H$1 cells (regulated by T-bet expression) [170], IL-4 secreting T$_H$2 cells (controlled by Gata3) [171] and Cxcr5$^+$ T follicular helper (T$_{FH}$) cells (directed by Bcl6 and antagonized by Blimp1) [172]. In the absence of Tcf1, activated CD4$^+$ T cells show increased production of IFN-γ and reduced expression of Gata3 [173]. Direct binding of Tcf1 upstream of the *Gata3* locus was shown to positively regulate Gata3 expression [173]. Thus, Tcf1 drives the T$_H$2 fate and limits IFN-γ production, i.e. restrains T$_H$1 differentiation [173].

Moreover, T$_{FH}$ cells deficient for Tcf1 display decreased levels of Bcl6 expression and aberrant Blimp1 upregulation [143]. Tcf1 was then shown to directly promote the expression of Bcl6 and repress Il2rα and Blimp1 expression [141, 143], thus controlling T$_{FH}$ differentiation. Conversely, in T$_H$1 cells Blimp1 binds to and represses *Tcf7* expression [142], forming a negative feedback loop (**Fig. 12**). A recent study found that long Tcf1 isoforms (including a β-catenin domain) were needed for proper T$_{FH}$ differentiation, but were dispensable for T$_H$1 differentiation [174]. Even

though short Tcf1 isoforms were sufficient for the induction of Bcl6 expression, they failed to supress Blimp1 and other T$_H$1 associated genes [174].
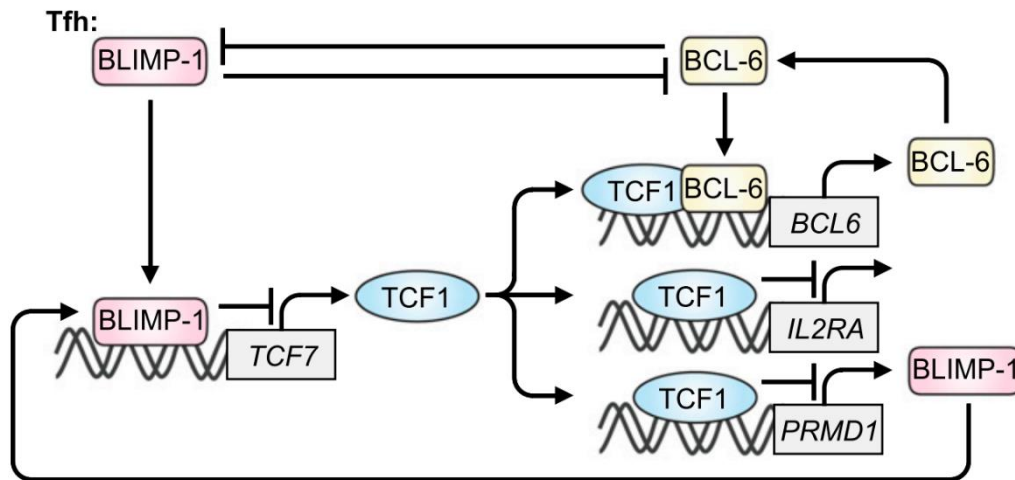
FIGURE 12: Molecular mechanism of the regulation of T$_{FH}$ differentiation by Tcf1.
Tcf1 promotes T$_{FH}$ differentiation by directly increasing the expression of Bcl6 and repressing the transcription of *Il2ra* and *Prdm1* (that promote T$_H$1 differentiation). Blimp1 itself can also repress the transcription of *Tcf7*. (From van Loosdregt and Coffer, *J Immunol*, 2018 [175]).

Furthermore, Tcf1 plays a prominent role in CD8$^+$ T cell differentiation [125, 126, 127, 128, 129]. Tcf1 is highly expressed by naive CD8$^+$ T cells, downregulated in most effector cells during a primary immune response to infection and expressed in memory cells [126, 127, 128, 176, 177, 178]. Following activation of CD8$^+$ T cells in response to infection, Tcf1 expression remains high during at least 3 cell divisions [179, 180]. Therefore, unlike T-bet [93], Tcf1 does not asymmetrically distribute during the 1st division. After 3 symmetric divisions, Tcf1$^+$ cells produced Tcf1$^-$ effector-fated daughter cells, as well as Tcf1$^+$ memory-fated cells, and this reportedly occurred through asymmetric Tcf1 partitioning [179, 180]. Similar observations were described upon the TCR-stimulation of human naive TCF1$^+$ CD8$^+$ T cells *in vitro* [181].

Even though Tcf1 deficient CD8$^+$ T cells can mount a normal primary immune response and form antigen-specific memory cells, the generation and persistence of T$_{CM}$ is diminished [125, 127]. Moreover, upon re-challenge Tcf1 deficient memory cells have impaired re-expansion capacity. While long Tcf1 isoforms were dispensable for maintaining the size of the memory CD8$^+$ T cell compartment [174], they were essential for optimal maturation of T$_{CM}$ cells and their recall expansion [125, 174], indicating that Wnt / β-catenin signalling plays a role in this regulation. Consistent with this possibility, effector CD8$^+$ T cells with higher Wnt signalling (i.e. higher expression of the Wnt target Axin2) had superior capacity to form central memory [128].

Moreover, in a recent study from this lab, Danilo and colleagues showed that IL-12 mediated inflammatory signals, via IL12rβ2 and STAT4, downregulated Tcf1 in primed CD8+ T cells [182]. Primed cells lacking Tcf1 underwent effector differentiation even in the absence of systemic inflammation, showing that Tcf1 counteracts effector differentiation. Indeed, during a response to infection, absence of Tcf1 increases effector differentiation and the expression of TNF-α, IFN-γ and KLRG-1 [176]. Tcf1 downregulation in primed CD8+ T cells was transcriptionally regulated, depended on cell cycling and could be prevented in part by inhibiting *de novo* DNA methylation (**Fig. 13**) [182], indicating that *Tcf7* expression was silenced via epigenetic mechanisms.
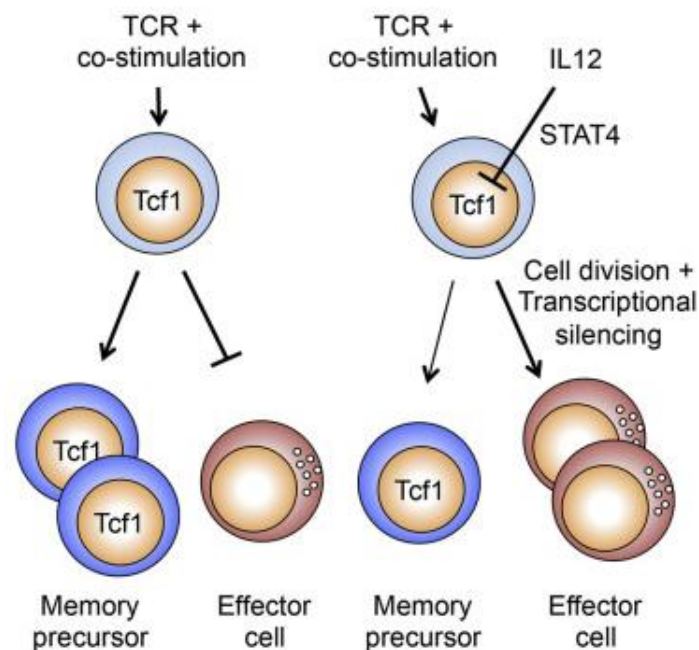
FIGURE 13: Role of the inflammatory cytokine IL-12 in Tcf1 expression and CD8+ T cell fate determination.
In the absence of inflammation (left) levels of Tcf1 expression remain high, favouring the generation of memory precursor cells over effector cells. When all 3 signals are present, TCR signal, co-stimulation and inflammation (right), Tcf1 is downregulated and differentiation is skewed towards an effector cell fate. IL-12 is the cytokine responsible for the suppression of Tcf1 via IL12r/STAT4 signaling. In addition, Tcf1 downregulation requires cell cycling and is explained by reduced transcription. (From Danilo *et al.*, *Cell Reports*, 2018 [182]).

2.4. Role of Tcf1 in T cell responses to chronic infection and cancer

Compared to acute resolved infection, antigen persistence in chronic infections or in the tumor microenvironment drives the exhaustion of CD8+ T cells. This so-called exhausted state is characterized by terminal differentiation, including the progressive loss of lytic activity, expansion and cytokine production capacity and increased expression of inhibitory receptors,

such as PD-1 (programmed cell death protein 1) [183, 184, 185]. These changes are accompanied by epigenetic, transcriptional and metabolic alterations, which were previously thought to prevent the formation of functional memory T cells [185, 186, 187]. However, exhausted CD8+ T cells persist for long periods of time and they can expand in response to PD-1 checkpoint blockade [188].

This lab and others have recently found that Tcf1 expression identifies a subpopulation of CD8+ T cells that sustains the immune response to chronic viral infection [145, 189, 190]. These Tcf1+ cells co-expressed the inhibitory receptor PD-1, and thus had hallmarks of exhausted cells, but they also displayed central memory markers (CD62L, CD127, etc). Since these cells existed in the presence of antigen we termed them memory-like T cells (T$_{ML}$) [189]. Functionally, the Tcf1+ PD-1+ T$_{ML}$ cells had stem-like properties, i.e. they had the capacity to expand in response to re-challenge, self-renew and differentiate into Tcf1- PD-1+ GzmB+ cells (**Fig. 14**). The latter expressed an effector gene expression program (*Klrg1*, *Gzma*, *Gzmb*, *Tbx21*, *Prdm1*, etc) [145, 189]. Additionally, Tcf1+ PD-1+ T$_{ML}$ cells also mediated the proliferative burst in response to inhibitory receptor blockade [189, 190].
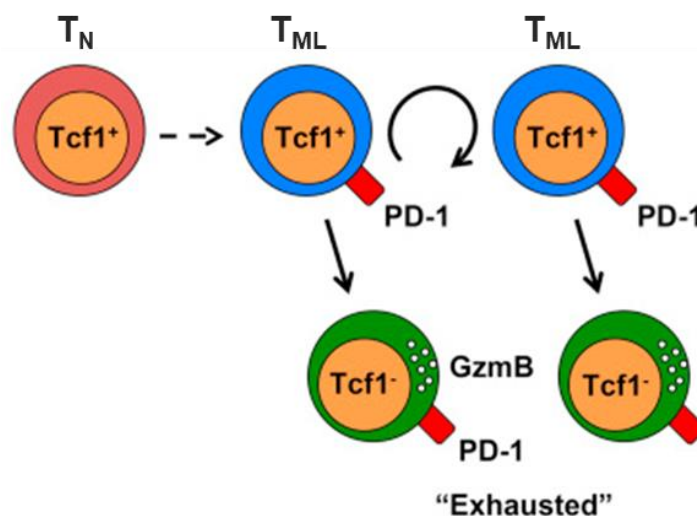
FIGURE 14: Antigen-specific Tcf1+ PD-1+ CD8+ T cells can sustain the immune response to chronic viral infections and cancer.
Tcf1+ PD-1+ CD8+ T cells identified during chronic infection where termed memory-like T cells (T$_{ML}$) since they showed hallmarks of exhausted (PD-1) and central memory cells (CD62L). T$_{ML}$ lack effector function, but retain proliferative capacity, regenerate, and produce differentiated cells (GzmB+ "exhausted" cells). (From Utzschneider *et al.*, *Immunity*, 2016 [189]).

Mechanistically, Tcf1 expression was essential for the formation of memory-like CD8+ T cells in chronic infection [145, 189, 191]. Tcf1 induced the expression of Bcl6 in CD8+ T cells, to promote the formation of the memory-like subpopulation [145], similar to the role of Tcf1 in CD4+ T cells. In a recent study, Tcf1 was shown to govern the early commitment towards the T$_{ML}$ lineage in

chronic infection [191]. Tcf1 positively regulated the expression of c-Myb and Bcl2, and this favored the survival of early Tcf1$^+$ PD-1$^+$ T_{ML} cells [191].

This lab and others further identified a similar Tcf1$^+$ PD-1$^+$ T_{ML} population among tumor infiltrating lymphocytes (TILs) [192, 193]. Interestingly the tumor-resident Tcf1$^+$ PD-1$^+$ cells were transcriptionally similar to the Tcf1$^+$ PD-1$^+$ cells identified during chronic infection. Other similarities included their ability to produce IL-2 and their stem cell-like properties [192]. Selective depletion of tumor-resident Tcf1$^+$ cells, while preventing the influx of new T cells, reduced the capacity of TILs to control tumor growth in response to immunotherapy [192]. These results suggested that tumor-resident Tcf1$^+$ PD-1$^+$ T_{ML} cells were essential for tumor control. In agreement with these data, the abundance of CD8$^+$ T cells expressing *TCF7* in human tumors correlated with positive clinical outcome in melanoma patients treated with immune checkpoint inhibitors [194]. Unlike in chronic infection, the generation of Tcf1$^+$ PD-1$^+$ TILs is normal in the absence of Tcf1 protein expression [195]. However, Tcf1 was required to maintain the TIL's memory-like population upon re-stimulation [195]. These data suggested that stemness of T_{ML} TILs is impaired in the absence of Tcf1.

Collectively, the available evidence suggests that Tcf1 plays a unique positive regulatory role for the formation and function of CD8$^+$ T cells that have stem cell-like properties.

Aim of the Project

Infection activates very rare antigen-specific naive CD8$^+$ T cells (T$_N$), which expand and differentiate into cytotoxic effector cells (T$_{Eff}$) that are normally able to clear pathogen-infected cells. Acute resolved infection further leads to the emergence of long-lived memory cells that are crucial for the protection against secondary infections. Central memory CD8$^+$ T cells (T$_{CM}$) are essential for the protection against systemic and/or protracted reinfection, due to their stem cell-like properties, i.e. to efficiently expand, differentiate into effector cells and self-renew upon re-challenge. Since T$_{CM}$ have the potential to control chronic infection and cancer based on experimental T cell transfers [53, 189, 196, 197], the generation of such cells is a central goal of vaccination. However, T cell vaccination approaches still induce central memory poorly compared to natural infection, indicating that our current knowledge regarding the generation of central memory is still poor.

Despite their first description in 1999, the molecular programs that regulate the formation and maintenance of these stem-like T cells are still not fully understood. This is in part due to the fact that the developmental origin of T$_{CM}$ is unclear and, consequently, it has remained uncertain whether CD8$^+$ T cells acquire stemness or whether they need to maintain stemness during a primary immune response. This is related to the fact that effector-stage CD8$^+$ T cells that have stem cell properties, or that quantitatively acquire stemness subsequent to antigen clearance, have not been identified.

The aim of this thesis was to address these issues by following the expression of the transcription factor Tcf1, which plays a critical role for central memory formation and function.

Materials and Methods

Mouse strain information

C57BL/6 (B6) (CD45.2) mice were obtained from Charles River (L'Arbresle Cedex, France), CD45.1 congenic B6 mice were bred locally. P14 TCR transgenic mice, expressing a TCR specific for the LCMV gp33–41 epitope (gp33) in the context of H-2D^b [P14 T cells], were provided by H.P. Pircher (Freiburg, Germany) (CD45.2$^+$) [198], *Tcf7$^{-/-}$* (Ko) mice [163] provided by H. Clevers (Utrecht, The Netherlands), Vβ5 TCR transgenic mice [199] provided by P. Fink (Seattle, USA). *Tcf7^{GFP}* [189] and *Tcf7$^{DTR-GFP}$* [192] mice have been described.

Rag2$^{-/-}$ γc$^{-/-}$ mice were obtained from the SPF animal facility of the University of Lausanne. P14 *Tcf7^{GFP}*, P14 *Tcf7$^{-/-}$* (Ko) *Tcf7^{GFP}* and P14 *Tcf7$^{DTR-GFP}$* mice were obtained by breeding (all CD45.2$^+$).

Mouse strains were maintained in the SPF animal facility of the University of Lausanne. Experiments used both male and female mice between 6 and 12 weeks of age whereby donors and recipients of adoptive T cell transfers were sex matched. Animal experiments were conducted in accordance with protocols approved by the veterinary authorities of the Canton de Vaud.

LCMV infections and viral titers

Mice were infected intraperitoneally (i.p.) with 2×10^5 plaque forming units (PFU) LCMV 53b Armstrong (Arm) or intravenously (i.v.) with 200 PFU of LCMV WE strain. For recall responses mice were infected with 2×10^5 PFU LCMV Arm (i.p.) (knockdown experiments) or 2'000 PFU of LCMV WE (i.v.) (all other experiments).

To determine viral titers, spleen suspensions from LCMV-infected mice were 'shock frozen'. Diluted samples were used for infection of Vero cells, and viral titers were determined by an LCMV focus-forming assay as described elsewhere [200]. LCMV Plaque Forming Units (PFU) were calculated per gram of spleen.

Adoptive T cell transfer

P14 CD8$^+$ T cells were obtained by mashing the spleen through a 40 µm nylon cell strainer (BD Falcon). Red blood cells were lysed with a hypotonic Ammonium-Chloride-Potassium (ACK) buffer. CD8$^+$ T cells were purified using mouse CD8$^+$ T cell enrichment kit (StemCell Technologies). Purified P14 cells (CD45.2) (usually >95% pure) were adoptively transferred i.v. into naive B6 (CD45.1 or CD45.1/2) one day prior to infection (d-1). For primary responses, 10^4 naïve P14 cells were usually transferred, except for the early time point analysis (d2-4), in which mice received 2x10^6 P14 cells. For experiments using Ko *Tcf7^{GFP}* cells, CD62L$^+$ *Tcf7^{GFPhi}*

P14 cells were sorted from the spleen of naïve mice and transferred (10^4) into B6 recipient. For secondary transfer experiments, 10^4 flow sorted $Tcf7^{GFPhi}$ or $Tcf7^{GFP-}$ P14 cells were transferred. For tertiary transfers 2'000 cells were injected i.v.. Finally, to test the recall response of d8 $Tcf7^{GFP+}$ in knockdown experiments, 500 to 1'000 flow sorted cells were transferred. For all experiments involving flow sorted cells, cell transfer and infection and was done on the same day (d0).

Diphtheria toxin (DT) treatment

A Diphtheria Toxin (DT) (D0564, Sigma) stock solution (2 mg/mL in H_2O) was diluted in PBS to 5 µg/mL. Mice were injected i.p with 50µg/kg of body weight (around 1 µg of DT in 200 µL per mouse of 20g). Control mice were injected with PBS.

Vaccination

$Tcf7^{GFP}$ mice were injected sub-cutaneously (s.c.) at the base of tail with a modified synthetic long peptide (KKKKKLEQLEAAYSIINFEKL, termed KL-SLP) (15.86nmole) (GenScript, Piscataway, New Jersey, USA) mixed with Pam3CSK4 (2 nmole) (InvivoGen, San Diego, California, USA) in Montanide (25 µL, SEPPIC, Paris, France)), or Pam3CSK4 only in Montanide. The immune response in the peripheral blood or spleen was analyzed using H-$2K^b$ Ovalbumin (SIINFEKL) tetramers (K^bOva) (TCMetrix) one week or 3 weeks post the boost.

Plasmids, virus production and T cell transduction

Retroviral (RV) constructs, as well as the RV packaging construct (pCL-Eco), were obtained from Addgene, as shown in the Recombinant DNA List. pMSCV-pBabeMCS-mIL-2Ra-IRES-RFP (IL2rα RV) construct was generated by restriction enzyme cloning with BamHI + XhoI between pMSCV-pBabeMCS-IRES-RFP (Ctrl RV) and pScalps_puro_mIL-2Rα. Lentivirus (LV) U6-shRNA hPGK-mCherry knockdown constructs were synthesized by Cyagen and 2nd generation packaging constructs (pCMV-dR8.74 and pMD2.G) were obtained from D. Trono (EPFL).

For RV production, 293T cells (passage number <10) were transiently transfected with IL2rα RV or Ctrl RV and pCL-Eco packaging plasmid using TurboFect™ Transfection Reagent (ThermoFisher). Alternatively, for LV production, 293T cells were transiently transfected with knockdown and 2nd generation packaging plasmids (pCMV-dR8.74 and pMD2.G) using lipofectamine 2000 (ThermoFisher) in the absence of antibiotics. RV and LV culture supernatants were collected 48h after transfection, filtered through a 0.45µM filter (Millex) and either used directly to transduce activated CD8+ T cells or stored frozen.

For T cell activation and transduction, CD8^{+} T cells were purified from the spleen of naïve P14 *Tcf7*[GFP] or *Tcf7*[DTR-GFP] mice, as described above. The *Tcf7*[DTR-GFP] reporter was used for the shRNA knockdown experiments since the original *Tcf7*[GFP] reporter expresses Cherry in addition to GFP. Purified cells were activated with Dynabeads Mouse T-Activator CD3/CD28 (ThermoFisher) (in a 1:1 cells:beads ratio) in the presence of recombinant human IL-2 (50ng/mL) (a gift from N. Rufer, CHUV) *in vitro* for 24h before the addition of viral supernatant. RV transduction of activated cells was performed in the presence of polybrene (10 µg/mL) (Sigma) during spin infection (1800rpm for 100min at 35°C). P14 cells were further cultured for 3h at 32°C before being transferred i.v. (10^5 cells/mouse) to B6 (CD45.1) mice that had been infected with LCMV WE one day before. Transduction with LV was performed in the presence of 4 µg/mL of polybrene during spin infection (1800rpm for 90min at 30°C). The cells were further cultured overnight at 37°C. The next morning, transduced P14 cells (10^5) were injected i.v. into B6 (CD45.1) mice that had been infected with LCMV Arm one day before. Alternatively, P14 cells were kept in culture for 48h and analyzed for the transduction efficiency.

Recombinant DNA List

Plasmid name	Source	Identifier / Target sequence
pMSCV-pBabeMCS-IRES-RFP	Addgene	Addgene: 33337
pScalps_puro_mIL-2Rα	Addgene	Addgene: 59917
pMSCV-pBabeMCS-mIL-2Ra-IRES-RFP	In house	Cloning BamHI + XhoI between Addgene 33337 & 59917
pCL-Eco	Addgene	Addgene: 12371
pCMV-dR8.74	D. Trono, EPFL	Addgene: 22036
pMD2.G	D. Trono, EPFL	Addgene: 12259
pLV[shRNA]-mCherry-U6>Scramble_shRNA	Cyagen	CCTAAGGTTAAGTCGCCCTCG
pLV[shRNA]-mCherry-U6>mTcf7[shRNA#1]	Cyagen	GCCACAAGTCTAAACAATAAT
pLV[shRNA]-mCherry-U6>mTcf7[shRNA#2]	Cyagen	TTCTCCACTCTACGAACATTT
pLV[shRNA]-mCherry-U6>mTcf7[shRNA#3]	Cyagen	AGAAGCCAGTCATCAAGAAAC
pLV[shRNA]-mCherry-U6>mArmcx2[shRNA#1]	Cyagen	CCTGGTACTGTGTCTACAAAT
pLV[shRNA]-mCherry-U6>mArmcx2[shRNA#3]	Cyagen	CCAGCTTTAAGCTGAACCATT
pLV[shRNA]-mCherry-U6>mElovl6[shRNA#1]	Cyagen	CCCATGTAGATCAAGTCATAA
pLV[shRNA]-mCherry-U6>mElovl6[shRNA#2]	Cyagen	GTCAGCAAATTCTGGGCTTAT
pLV[shRNA]-mCherry-U6>mKlf4[shRNA#1]	Cyagen	CATGTTCTAACAGCCTAAATG
pLV[shRNA]-mCherry-U6>mKlf4[shRNA#2]	Cyagen	AGTTGGACCCAGTATACATTC
pLV[shRNA]-mCherry-U6>mKit[shRNA#1]	Cyagen	ACTTCGCCTGACCAGATTAAA
pLV[shRNA]-mCherry-U6>mKit[shRNA#2]	Cyagen	CCCTGGTCATTACAGAATATT
pLV[shRNA]-mCherry-U6>mPlxdc2[shRNA#1]	Cyagen	GTTCGAAGAAGAACAATTTAT
pLV[shRNA]-mCherry-U6>mPlxdc2[shRNA#3]	Cyagen	GTACTGGCTTACAGGTGTTAA
pLV[shRNA]-mCherry-U6>mSmad1[shRNA#1]	Cyagen	GGACTACCTCATGTCATTTAT
pLV[shRNA]-mCherry-U6>mSmad1[shRNA#2]	Cyagen	GACGAAGGAGCCACGATAATA

In vitro killing assay

RMA mouse tumor cells were pulsed with gp33-41 peptide (KAVYNFATM) (1μM) for 1h at 37°C, labelled with CTV (Cell Trace Violet) (2 μM) for 8 min at 37°C and washed 3x. Gp33-pulsed RMA target cells were co-cultured with sorted $Tcf7^{GFPhi}$ or $Tcf7^{GFP-}$ effector cells, at the indicated effector:target cell (E:T) ratios, for 4h at 37°C. In parallel, target cells were cultured alone to measure basal apoptosis. Following incubation, cells were stained with 7-AAD 5 min before acquisition. Target cell apoptosis was determined by the incorporation of 7-AAD among CTV$^+$ cells. The percentage of specific lysis for a given E:T ratio was calculated as 100*(%lysis-%spontaneous lysis)/(100-%spontaneous lysis) whereby spontaneous lysis corresponded to the % of apoptotic target cells in the absence of effector cells.

Tissue preparation and cell suspensions

For the analysis of T$_{RM}$, mice were injected i.v. with 3 μg of APC-eF780 labeled anti-CD8α mAb (clone 53-6.7) 4 min prior to sacrifice. CD8α^- cells were considered to be resident in non-lymphoid tissues.

For the isolation of Intraepithelial Lymphocytes (IELs) the mouse's small intestine was collected and the Peyer's patches were excise. The intestine was flushed with HBSS 2% FCS and cut in small pieces before being cut longitudinally (to open the intestine), followed by incubation with 1mM of Dithiothreitol (DTT) (Applichem, A3668) in HBSS 10% FCS and 2mM EDTA for 30min at 37°C while stirring. After digestion, the cell suspension (containing the IELs) was filtered using a 100μM strainer (Falcon) and centrifuged to obtain a pellet. The cells were then resuspended in FACS buffer and stained immediately. Alternatively, the resulting pellet was enriched for CD8 T cells using MACS positive selection (Miltenyi Biotec kit 130-116-478).

Liver and Lung were cut in small pieces and digested enzymatically with Tumor Dissociation kit (Miltenyi Biotec: 130-096-730) for 30min at 37°C. Following digestion, the tissues were further dissociated using a 40μM strainer. Hematopoietic cells were then isolated using a 40/80% discontinuous Percoll density gradient (GE Healthcare). Cells at the interface were harvested, washed 2x and red blood cells were lysed with ACK buffer.

For the analysis of bone marrow (BM) the femur was collected and flushed with RPMI 10% FCS using a 10mL syringe and a 26G needle. The BM cells were then pipeted up and down to obtain a single cell suspension and passed through a 40μM cell strainer. Finally, red blood cells were lysed using ACK buffer.

Cell suspensions from spleen and lymph nodes (LN) were obtained by mashing through a 40µM nylon cell strainer, followed by red blood cells lysis using ACK buffer.

Peripheral blood was collected into 1.5mL Eppendorf containing 15 µL of 0.5M EDTA. Peripheral blood mononuclear cells (PBMCs) were obtained by lysing the red blood cells with ACK buffer and subsequent wash with FACS buffer.

Flow cytometry and cell sorting

Surface staining was performed with mAbs for 20 min at 4°C in PBS supplemented with 2% FCS (FACS buffer) using the reagents shown in the Antibody List. For tetramer staining, cell suspensions were incubated with anti-CD16/32 (2.4G2) hybridoma supernatant before staining for 90min at 4°C with APC-conjugated MHC-I tetramers. Zombie Aqua Fixable Viability kit (Biolegend) was used to exclude dead cells.

For intranuclear staining, cells were surface stained before fixation and permeabilization using the Foxp3 transcription factor staining kit (eBioscience: Cat. No. 00-5523) followed by intranuclear staining in Permeabilization buffer 1x (Perm buffer).

For the detection of cytokine production, splenocytes were re-stimulated *in vitro* with LCMV gp33-41 (gp33) (1µM) or OVA$_{257-264}$ (SIINFEKL) (1µg/ml) peptide for 5h in the presence of Brefeldin A (5µg/ml) for the last 4.5h. Cells were stained at the surface before fixation and permeabilization (Intracellular Fixation & Permeabilization Buffer Set, eBioscience kit: Cat. No. 88-8824) followed by intracellular staining in 1x Perm buffer. For the detection of GzmA and GzmB splenocytes were cultured in the absence of peptide but in the presence of 5µg/ml of Brefeldin A for 4.5h, before intracellular staining as described above.

For LAMP-1 degranulation assay splenocytes were cultured with 1 µM of gp33 peptide for 30min at 37°C, before the addition of 5µg/ml of Brefeldin A and 1µg/ml of PE-Cy7-conjugated CD107a mAb (Biolegend), followed by incubation at 37°C for 4.5h. Mobilization of LAMP-1 was determined by the surface expression of CD107a.

For apoptosis assays splenocytes were cultured for 4h at 37°C in the absence of growth factors. The cells were then stained using the Annexin V-APC Apoptosis Detection Kit (eBioscience), according to manufacturer instructions. 7-AAD was added 5 min prior to data acquisition.

For cell cycle analysis, flow sorted d8 *Tcf7*^{GFPhi} and *Tcf7*$^{GFP-}$ cells were fixed and permeabilized using the Foxp3 kit (eBioscience: Cat. No. 00-5523), followed by intranuclear staining with Ki67-FITC (BD Biosciences 556026) in 1x Perm Buffer. DAPI (2µg/mL) was added for the last 10min of intranuclear staining.

Analysis of the phosphorylation of STAT proteins (pSTAT) was done in flow sorted Wt or Ko d8 *Tcf7*^GFPhi and *Tcf7*^GFP- cells that were stimulated with cytokines at the indicated concentrations for 30min at 37°C. After incubation cells were fixed with a 90% methanol solution at Room Temperature (RT) for 5 min, followed by wash/permeabilization with PBS Tween 0.1% for 20min at RT. Lastly, cells were resuspended with PBS containing the corresponding pSTAT Ab, at the concentration recommended by the manufacturer, and incubated for 45min at RT. Cells were subsequently washed and analyzed directly.

Labelling of cells with Carboxyfluorescein succinimidyl ester (CFSE) or CTV (Thermofisher) was preformed according to manufacturer instructions. Briefly, cells were incubated in warm PBS containing 2 μM of the indicated proliferation dye for 8 min at 37ºC and washed 3x in complete RPMI medium before being used.

Cell surface stained cells were analyzed directly. Flow cytometry measurements of cells were performed on an LSR-II or Fortessa flow cytometer (BD). Data were analyzed using FlowJo (TreeStar).

For cell sorting of P14 cells, splenocytes were enriched for CD8$^+$ T cells using the mouse CD8$^+$ T cell enrichment kit (StemCell Technologies) and stained for CD45.1 (A20) or CD45.2 (clone 104). *Tcf7*^GFPhi and *Tcf7*^GFP- CD45.1$^-$ CD45.2$^+$ cells were flow sorted on a FACSAria (BD) flow cytometer. The purity of sorted cells was greater than 99%, based on post-sort analysis.

Antibody List

Specificity / Fluorochrome	Source	Clone / Identifier
Anti-Mouse CD4 – AF700	eBioscience	Clone GK1.5 RRID:AB_493999
Anti-Mouse CD8α – PerCP-Cy5.5, PE Cy7, APC-eF780 or BV 650	eBioscience / BioLegend	Clone 53.6.7 RRID:AB_1107004 RRID:AB_469583 RRID:AB_1272185 RRID:AB_2563056
Anti-Mouse CD8β – APC	eBioscience	Clone H35-17.2 RRID:AB_657760
Anti-Mouse CD11a (LFA1) - AF647	In house	Clone FD44.8
Anti-Mouse CD19 – AF700	eBioscience	Clone eBio1D3 RRID:AB_837083
Anti-Mouse CD16/32	In house	Clone: 24G2
Anti-Mouse CD25 - APC	Thermo Fisher Scientific	Clone PC61.5 RRID:AB_469366
Anti-Mouse CD44 – APC eF780 or Pacific Blue	eBioscience / In house	Clone IM7 RRID:AB_1272244
Anti-Mouse CD45.1 – BV 785, Pacific Blue or AF647	BioLegend / In house	Clone A20 RRID:AB_2563379

Anti-Mouse CD45.2 – PerCP Cy5.5 or BV 650	eBioscience / BioLegend	Clone 104.2 RRID:AB_953590 RRID:AB_2563065
Anti-Mouse CD49a - APC	BioLegend	Clone HMalpha1 RRID:AB_2562253
Anti-Mouse CD62L – PE, PerCP-Cy5.5, BV 711 or AF647	eBioscience / BioLegend / In house	Clone Mel14 RRID:AB_465722 RRID:AB_996667 RRID:AB_2564215
Anti-Mouse CD69 - PE-Cy7	BD Biosciences	Clone: H1.2F3 RRID:AB_394508
Anti-Mouse CD103 - eFluor450 or PE	Thermo Fisher Scientific	Clone 2E7 RRID:AB_2574032 RRID:AB_465799
Anti-Mouse CD107a (LAMP-1) – PE Cy7	Biolegend	Clone 1D4B; RRID:AB_2562146
Anti-Mouse CD122 - eF450	eBioscience	Clone TM-b1; RRID:AB_2016697
Anti-Mouse CD127 – APC or PE	eBioscience / In house	Clone A7R34 RRID:AB_469435 RRID:AB_465845
Anti-Mouse Cxcr3 - PE	BioLegend	Clone 173 RRID:AB_1027656
Anti-Mouse Cx3cr1 – BV711	BioLegend	Clone SA011F11 RRID:AB_2565939
Anti-Mouse/rat Granzyme A - PE	Santa Cruz Biotechnology	Clone 3G8.5 RRID:AB_2114414
Anti-Mouse/human Granzyme B – AF647	BioLegend	Clone GB11 RRID:AB_2294995
Anti-Mouse IFN-γ - PE or PercPCy5.5	eBioscience	Clone XMG1.2 RRID:AB_466193 RRID:AB_1107020
Anti-Mouse IL-2 – APC	eBioscience	Clone JES6-5H4 RRID:AB_2535421
Anti-Mouse Ki67 – FITC	BD Biosciences	RRID:AB_396302
Anti-Mouse KLRG1 – PE Cy7 or BV 421	eBiosciences / BioLegend	Clone 2F1 RRID:AB_1518768 RRID:AB_10918627
Anti-Mouse/human pStat3 (Tyr705) - PE	BD Biosciences	Clone: 4/P-STAT3 RRID:AB_399860
Anti-Mouse/human pStat4 (Tyr693) - PE	Thermo Fisher Scientific	Clone 4LURPIE RRID:AB_2572688
Anti-Mouse/human pStat5 (pY694) - AF647	BD Biosciences	RRID:AB_399882
Anti-Mouse Sca-1 - PE Cy7 or AF700	eBiosciences / BioLegend	Clone D7 RRID:AB_469669 RRID:AB_2565959
Anti-Mouse TNFα – PE Cy7 or Pacific Blue	eBioscience / BioLegend	Clone MP6-XT22 RRID:AB_11042471 RRID:AB_893639
Anti-Mouse/human TCF1 Rabbit mAb antibody	Cell Signaling Technology	Clone C63D9 RRID:AB_2199302
F(ab')2-Donkey anti-Rabbit IgG (H+L) - PE	eBioscience	RRID:AB_1210761

Goat Anti-Rabbit IgG (H+L) - AF647	Molecular Probes (Invitrogen)	RRID:AB_141663
H-2D^b / gp33-41 – APC (Tetramer)	TC Metrix	N/A
H-2D^b / np396 – APC (Tetramer)	TC Metrix	N/A
H-2K^b / Ova257-264 (SIINFEKL) – APC (Tetramer)	TC Metrix	N/A

Immunofluorescence labeling and microscopy

For immunohistochemistry analysis, the spleens from d8 or d30 infected mice were fixed in 1% PFA in PBS overnight, infiltrated with 30% sucrose the next day (overnight) and then embedded and frozen in OCT compound. Cryostat sections were collected on Superfrost Plus slides (Fisher Scientific), air dried and preincubated with blocking solution containing BSA, normal mouse serum and normal donkey serum (Sigma). Then they were labeled during 1 hour using the following primary reagents: Rat anti-mCD4 (H129), Mouse anti-CD45.2 biotin (AL-1) (both produced in house) and rabbit anti-GFP (Thermofisher). After washing with PBS, the following secondary reagents were applied for 1 hour: Donkey anti-rat IgG Cy3 (Jackson Immunoresearch), streptavidin-APC (Biolegend) and donkey anti-rabbit IgG Alexa488 (Thermofisher). Finally, DAPI (Sigma) was used to stain the nuclei followed by mounting in DABCO (homemade). Images were acquired with a Zeiss AxioImager Z1 microscope and a AxioCam MRC5 camera.

Image analysis and cellular identification

Image quantification was performed using VIS Image Analysis software (Visiopharm, version 2019.02). Splenic tissue was detected applying a 21 pixel mean DAPI$^+$ filter, followed by smoothening the edges and filling holes of the mask using the software's functions "close" and "fill holes", respectively. Next, the mask was converted to a region of interest (ROI), annotated in gray. Within the detected total spleen ROI a similar approach was used to detect regions positive for CD4 expression, in order to identify the T cell zone (TZ), annotated in red. As the architecture of the TZ was altered in d8 spleens, this ROI was subsequently manually adjusted based on a relatively higher mean DAPI$^+$ signal, reflective of an increased nuclear density compared to the red pulp (RP). The ROI for B cell zones (BZ) was manually drawn based on the absence of CD4 signal and relatively higher DAPI$^+$ signal density, ROI annotated in blue. ROI were manually adjusted to exclude areas with high background signal due to artifacts in any of the channels (regions annotated in white).

Nuclear identification was based on the watershed signal of the DAPI$^+$ staining. The nuclear label was expanded with 5 pixels to allow detection of both nuclear and cytoplasmic fluorescent signal. Nuclear labels exceeding the manually set threshold for CD45.2 expression, were converted to CD45.2$^+$ labeled cells. Similarly, CD45.2$^+$ labeled cells

surpassing the threshold for *Tcf7* expression were labeled as *Tcf7*[GFP+] cells. Threshold settings were identical between different samples. Finally, a counting frame was applied to ensure accurate counts for all CD45.2[-], CD45.2[+] and Tcf7[GFP+] cells within the three ROI (total spleen, TZ and BZ). The obtained counts were then used to determine the frequency of single CD45.2^{+} cells (*Tcf7*[GFP-] P14 cells) or of double positive CD45.2[+] *Tcf7*[GFP+] (*Tcf7*[GFP+] P14 cells) in each zone. The frequency of cells in the RP was obtained by subtracting TZ and BZ counts from the cell counts in the total spleen ROI.

RT-qPCR analysis

For the detection of miR449a, T_N, d8 *Tcf7*[GFPhi] or d8 *Tcf7*[GFP-] CD8^{+} T cells were flow sorted and lysed with QIAzol lysis reagent (Qiagen). Total RNA (including small RNAs) was purified using the miRNeasy Mini Kit (Qiagen), as recommended by the manufacturer. Expression of miR449a was analyzed using TaqMan™ MicroRNA Assays mmu-miR-449a-5p (ThermoFisher Scientific, Cat# 4427975 (001030)) and normalized to mouse U6 snRNA (ThermoFisher Scientific, Cat# 4427975 (001973)). Quantification was done as described in TaqMan® Small RNA Assays protocol, using TaqMan® MicroRNA Reverse Transcription Kit and TaqMan® Fast Universal PCR Master Mix (2X), on a 7500 Fast Real-Time PCR System (ThermoFisher Scientific). For *Cdc20b* and *Gpx8*, cDNA was synthesized using the SuperScript III First-Strand Synthesis System (ThermoFisher Scientific). Real-time quantitative PCR was performed using KAPA SYBR FAST qPCR Kit Master Mix (Kapabiosystems) on a LightCycler 480 Instrument (Roche), using primers shown in the Oligonucleotides List. Gene expression was quantified relative to mouse HPRT2.

For the validation of adult stem cell genes knockdown, *in vitro* LV-transduced P14 cells were flow sorted based on mCherry expression at 48h post-transduction. mCherry^{+} cells were lysed using Trizol LS (Life Technologies) and total cellular RNA was extracted using the Direct-zol™ RNA MiniPrep kit (Zymo Research). cDNA synthesis and real-time quantitative PCR were performed as described above (SYBR qPCR kit), using primers shown in the Oligonucleotides List. Gene expression was quantified relative to mouse *β2m*.

Oligonucleotides List

Gene name	Primer sequence
mCdc20b Fw	GAAGGAAAATCTTGCCACCA
mCdc20b Re	CATCTTCCCATCGATTTGCT
mGpx8 Fw	CCTTTCGCTGCCTACCCATTA
mGpx8 Re	GAGTAGAAGCTGTTGGTTCTCG
mHPRT2 Fw	GTTGGATACAGGCCAGACTTTGTTG
mHPRT2 Re	GATTCAACTTGCGCTCATCTTAGGC

mTcf7 Fw	TGCTGAGTGCACACTCAAGG
mTcf7 Re	TGCGGGCCAGTTCATAGTA
mArmcx2 Fw	CTGCACCCAGTCCTAAGGTTC
mArmcx2 Re	TAGCCTCAGTTTTAGCCCCAT
mElovl6 Fw	GAAAAGCAGTTCAACGAGAACG
mElovl6 Re	AGATGCCGACCACCAAAGATA
mPlxdc2 Fw	GCCGCAGCAGGAGTTATGTTA
mPlxdc2 Re	TTCATTCCAAGGAAAAGCGTTTG
mSmad1 Fw	GCTTCGTGAAGGGTTGGGG
mSmad1 Re	CGGATGAAATAGGATTGTGGGG
mKlf4 Fw	GTGCCCCGACTAACCGTTG
mKlf4 Re	GTCGTTGAACTCCTCGGTCT
mKit Fw	GCCACGTCTCAGCCATCTG
mKit Re	GTCGCCAGCTTCAACTATTAACT
mβ2m Fw	AGACTGATACATACGCCTGCAG
mβ2m Re	GCAGGTTCAAATGAATCTTCAG

RNAseq analysis

Flow sorted $Tcf7^{GFPhi}$ CD62L$^+$ CD8$^+$ T cells from naive P14 $Tcf7^{-/-}$ (Ko) or WT $Tcf7^{GFP}$ reporter mice (CD45.2) were used to obtain cellular RNA or were adoptively transferred into B6 hosts (CD45.1/.2) that were infected with LCMV Arm. Eight or 30 days later, splenic $Tcf7^{GFPhi}$ and $Tcf7^{GFP-}$ P14 cells were flow sorted. Sorted cells were lysed and stored in Trizol before extraction of total cellular RNA using the Direct-zol™ RNA MiniPrep kit (Zymo Research).

Library preparation, sequencing and data processing were performed using the methods described [189]. In brief, double stranded cDNA for RNA-seq library preparation was generated using SMART-Seq v4 Ultra Low Input RNA reagents (# 634888, Clontech) according to the protocol provided with the reagents beginning with 5 ng of total RNA and using 9 cycles of PCR. 150 pg of the resulting cDNA were used for library preparation with the Illumina Nextera XT DNA Library reagents (# 15032354, Illumina) using the single cell RNA-seq library preparation protocol developed for the Fluidigm C1 (Fluidigm). Cluster generation was performed with the libraries using the Illumina TruSeq SR Cluster Kit v4 reagents and sequenced on the Illumina HiSeq 2500 using TruSeq SBS Kit v4 reagents. Sequencing data were processed using the Illumina Pipeline Software version 1.82.

Purity-filtered reads were adapters and quality trimmed with Cutadapt (v. 1.3) [201] and filtered for low complexity with seq crumbs (v. 0.1.8). Reads were aligned against *Mus musculus* (version GRCm38) genome using STAR (v. 2.4.2a) [202]. The number of read counts per gene locus was summarized with htseq-count (v. 0.6.1) [203] using *M. musculus* (Ensembl v. GRCm38.82) gene annotation. Quality of the RNA-seq data alignment was assessed using RSeQC (v. 2.3.7) [204].

Differential gene expression analysis was performed using R (version 3.1.2). Genes with low counts were filtered out according to the rule of 1 count per million (cpm) in at least 1 sample, and only protein-coding genes were retained, resulting in 12138 genes analyzed. Library sizes were scaled using TMM normalization (EdgeR, v 3.8.5) [205] and transformed to $\log_2$ cpm. PCA analysis was performed on scaled $\log_2$ normalized cpm of all retained genes. Differential expression was computed using the limma package for R (version 3.22.4 [206]) by fitting data into a linear model correcting for batch effect. Moderated t-test was used for each cell population pairwise comparison and the adjusted p-values were computed by the Benjamini-Hochberg (BH) method controlling for false discovery rate (FDR) independently. Genes were considered as significantly differentially expressed between any two populations of CD8+ T cells at a threshold of absolute $\log_2$ fold change (FC) >1 and FDR<0.05.

The following external gene sets were used for gene set enrichment analysis (GSEA):

1) Genes up-regulated in central memory versus effector memory CD8+ T cells derived from the spleen of LCMV immune mice (T_{CM} *vs* T_{EM}) (GSE70813) [207]. RNAseq data were retrieved form Gene Expression Omnibus (GEO) database (GSM1819914, GSM1819923, GSM1819915, GSM1819924) and raw counts were filtered and genes with at least 1 (cpm) in at least 1 sample were retained (n=12566 genes). Counts were TMM-normalized and converted to $\log_2$ cpm using the edgeR package (version 3.24.3) [205] and the voom function implemented in the limma package (version 3.38.3) [206]. Genes differentially expressed between T_{CM} and T_{EM} CD8+ T cells were determined by fitting a linear model to the normalized gene expression data followed by empirical Bayes moderation using the functions lmFit and eBayes implemented in the limma package. P-values were adjusted using the Benjamini-Hochberg procedure [208]. In total, n=1896 genes were significantly upregulated in T_{CM} compared to T_{EM}. Because genes in Mackay et al (2016) were labeled with Entrez gene IDs, we retrieved available corresponding Ensembl IDs using the biomaRt package (v. 2.38.0) [209], resulting in n=1737 genes used for GSEA.

2) Stem cell-like memory signature [82],

3) Genes up-regulated in hematopoietic stem cells (M8215) [210],

4) Genes up-regulated in adult stem cells (M1999) [211].

5) Genes up-regulated in mature hematopoietic cells (M11205) [210].

For the last three gene sets, we retrieved gene symbols from the Molecular Signatures Database (http://software.broadinstitute.org/gsea/msigdb) [212] and converted human gene symbols to mouse Ensembl IDs and mouse gene symbols using the biomaRt package.

Gene set enrichment analysis was conducted similarly to the method described in [212], for each cell population comparison separately. All protein-coding genes detected by RNA sequencing (12138 genes) were sorted after differential gene expression analysis according to their moderated t-statistic estimate. Upregulated genes and downregulated genes were tested for enrichment separately. An enrichment score (ES) was calculated for each cell subset comparison by increasing or decreasing a running-sum statistic according to the magnitude of the t-statistic of each gene (using $p=1$, see Equation 1 in [212]. The normalized ES (NES) and associated p-value were obtained by randomizing the genes included in the gene set 10^5 times. The NES was calculated by dividing the ES by the mean of the randomized ES values, and the nominal p-value was equal to the proportion of randomized ES values that had a higher (for positive ES) or lower (for negative ES) value than the ES initially calculated. Each p-value was then adjusted for the total number of individual ES calculated across the five gene sets and all cell population comparisons by using the Benjamini-Hochberg procedure [208].

We also performed a GSEA of genes differentially expressed between Wt d8 *Tcf7*^{GFPhi} compared to Ko d8 *Tcf7*^{GFPhi} cells against the hallmark gene set list [213]. The method was the same as the one described above, except that the genes in each gene set were randomized 1000 times.

ATACseq analysis

ATACseq was performed as described [214]. Briefly, 5×10^4 flow sorted CD8$^+$ T cells were washed with cold 1x PBS and resuspended in 50µL of ice-cold lysis buffer (10mM Tris-Cl (pH 7.4), 10mM NaCl, 3mM MgCl$_2$ and 0.1% (v/v) of NP-40). Cells were centrifuged immediately and the resulting pellet (nuclei) was resuspended in 50µL of transposase reaction mix (25 µL 2xTD buffer (Illumina), 2.5 µL Tn5 transposase (Illumina) and 22.5 µL of nuclease-free water), followed by incubation at 37°C for 30min (while gently shacking). Tagmented DNA was cleaned using Qiagen MinElute PCR Purification kit as described in the kit's protocol. Library preparation was performed using Illumina's Unique Dual (UD) Indexes (R#20027213) and NEBNext High-Fidelity 2X PCR Master Mix (M0541), using the following program: 5 min 72°C, 30 sec 98°C ; 10 cycles: 10 sec 98°C, 30 sec 63°C, 1 min 72°C : Hold: 4°C ∞.

The libraries were then cleaned using Agencourt AMPure XP magnetic beads (A63880, Beckman). To remove both excess adapter primers and big DNA fragments we performed double-sided magnetic bead purification. Finally, libraries were quantified using Fragment Analyzer and sequenced on an Illumina HiSeq 4000, with paired end 150 nucleotides at the Lausanne Genomic Technologies Facility.

The bcbio-nextgen pipeline (v. 19.03, https://github.com/bcbio/bcbio-nextgen) was used for

initial computations of the analysis. Each sample was sequenced on 3 independent sequencing lanes, therefore the sequencing reads of each individual lane and sample were first processed separately. Reads were filtered for quality and aligned to the *Mus musculus* reference genome (mm10) using BWA (version 0.7.17-r1188) (Li H. (2013) Aligning sequence reads, clone sequences and assembly contigs with BWA-MEM. arXiv:1303.3997v2 [q-bio.GN]). The three alignment files of each sample were manipulated and merged using samtools (version 1.9) [215]. Peak calling was performed globally for each cell population using Macs2 (version 2.1.1) [216] with the --broad argument.

Tests of differential accessibility of chromatin among cell populations were performed in R (version 3.5.3) using package DiffBind (version 2.10.0). Chromatin regions were considered as significantly differentially accessible between any two cell populations at a threshold of FDR<0.05.

Principal component analysis was performed using reads per kilobase per million mapped reads (RPKM) of all accessible regions called by Macs2 (n=112069). Subsequently, accessible chromatin regions were annotated to genes using the R package CHIPpeakAnno (version 3.16.1) and its precompiled Ensembl mouse TSS annotation (TSS.mouse.GRCm38), retaining only regions laying within ±5kb of a gene subsequent analyses. Heatmaps of read coverage per region were generated using the computeMatrix function of the Galaxy instance of deeptools3 [217]. Regions smaller than 4kb were extended 2kb up- or downstream of the peak center. Read coverage per chromatin region was averaged over the 3 biological replicates of each cell population, and heatmaps were drawn using the ComplexHeatmap package (version 1.20.0) [218].

Figures of coverage tracks were exported from bigwig read alignment files using the Integrative Genomics Viewer [219]. The same y-axis scale was set across all samples.

Data analyses

The fold expansion of T cells was determined relative to an estimated 10% "take" of the transferred cells [15].

All bar and line graphs depict means ±SD. Statistical analyses were performed using Prism 7.0 or 8.0 (Graphpad Software). Non-paired *t* test (two-tailed, 95% confidence level) was used for the comparison of 2 data sets. ANOVA was used for >2 comparison groups. *p*-values (*p*)<0.05 were considered significant (*: $p<0.05$; **: $p<0.01$; ***: $p<0.001$; ****: $p <0.0001$); $p>0.05$ was considered non-significant (ns).

List of Chemicals, Peptides, Recombinant Proteins and Commercial Assays

Reagent or Resource	Source	Identifier
2xTD buffer	Illumina	Cat# 15027866
7-AAD (Viability dye)	Biolegend	Cat# 420404
Ammonium-Chloride-Potassium (ACK) buffer	In house	N/A
AMPure XP magnetic beads	Beckman Coulter	Cat# A63880
Annexin V - APC Apoptosis Detection Kit	eBioscience	RRID:AB_2575165
Brefeldin A	Biolegend	Cat# 420601
CellTrace™ CFSE Cell Proliferation Kit	Invitrogen	Cat# C34554
CellTrace™ Violet Cell Proliferation Kit	Invitrogen	Cat# C34557
DAPI	Life Technlogies	Cat# D1306
Diphtheria Toxin (DT)	Sigma-Aldrich	Cat# D0564
Direct–zol RNA Mini Prep	Zymo Research	Cat# R2050
Dithiothreitol (DTT)	Applichem	Cat# A3668
Dynabeads Mouse T-Activator CD3/CD28	ThermoFisher Scientific	Cat# 11452D
FoxP3/Transcription factor staining buffer set	eBiosciences	Cat# 00-5523
Illumina Nextera XT DNA Library reagents	Illumina	Cat# 15032354
Illumina's Unique Dual (UD) Indexes	Illumina	Cat# 20027213
Intracellular Fix & Perm Buffer set	eBiosciences	Cat# 88-8824
KAPA SYBR FAST qPCR Kit Master Mix	Kapabiosystems	Cat# KR0389
Lipofectamine™ 2000 Transfection Reagent	ThermoFisher Scientific	Cat# 11668019
MACS CD8+ positive selection	Miltenyi Biotec	Cat# 130-116-478
MinElute PCR Purification kit	Qiagen	Cat# 28004
miRNeasy Mini Kit	Qiagen	Cat# 217004
Montanide	SEPPIC, Paris, France	
Mouse CD8+ T cell enrichment kit	StemCell Technologies	Cat# 19853
NEBNext High-Fidelity 2X PCR Master Mix	New England Biolabs	Cat# M0541
NP-40	Caymanchem	Cat# 600009
Pam3CSK4	InvivoGen	Cat# 112208-00-1
Peptide: KL-SLP (KKKKKLEQLEAAYSIINFEKL)	GenScript, NJ	N/A

Peptide: LCMV glycoprotein amino acids 33-41 (gp33) (KAVYNFATM)	TC Metrix	N/A
Peptide: LCMV np396 (FQPQNGQFI)	TC Metrix	N/A
Peptide: Ovalbumin amino acids 257-264 (OVA) (SIINFEKL)	P. Romero, UNIL	N/A
Percoll	GE Heathcare	Cat# 17-0891-01
Polybrene	Sigma-Aldrich	Cat# TR-1003-G
Recombinant human IL-2	Glaxo IMB, Genève, Switzerland	gift from N. Rufer
Recombinant murine IL-12	Peprotech	Cat# 210-12-10ug
Recombinant murine IL-21	Peprotech	Cat# 210-21-2ug
SMART-Seq v4 Ultra Low Input RNA reagents	Clontech	Cat# 634888
SuperScript III First-Strand Synthesis System	ThermoFisher Scientific	Cat# 18080051
TaqMan™ Fast Universal PCR Master Mix (2X), no AmpErase™ UNG	ThermoFisher Scientific	Cat# 4352042
TaqMan™ MicroRNA Reverse Transcription Kit	ThermoFisher Scientific	Cat# 4366596
TDE1, Tagment DNA Enzyme	Illumina	Cat# 15027865
Trizol	Life Technlogies	Cat# 15596026
Tumor Dissociation Kit	Miltenyi Biotec	Cat# 130-096-730
TurboFect Transfection Reagent	Thermo Scientific	Cat# R0531
Zombie Aqua Fixable Viability kit	Biolegend	Cat# 423101

Results

Tcf1 (*Tcf7*) expression during CD8⁺ T cell responses to acute LCMV infection

To follow Tcf1 expression in antigen-specific CD8⁺ T cells during the course of an acute immune response we infected mice with LCMV strains WE or Armstrong (Arm) (as indicated). In addition, we took advantage of P14 transgenic mice, whose CD8⁺ T cells express a TCR specific for the LCMV epitope gp33-41, presented by MHC class I (H-2D^b restricted). Typically, 10^4 naive P14 CD8⁺ T cells (CD45.2⁺) were adoptively transferred (i.v.) into naive C57BL/6J recipient mice (CD45.1⁺ CD45.2⁺) (day -1). The next day mice were infected with LCMV WE or Arm, which cause acute resolved infection in wild type mice. P14 cells were then tracked based on their expression of the congenic marker CD45.2 and absence of CD45.1.

As previously mentioned, Tcf1 is highly expressed in naive cells and in most memory CD8⁺ T cells [126, 127, 128, 176, 177, 178]. However, this TF is downregulated in most CD8⁺ T cells during effector differentiation. So, we sought to pinpoint exactly when the downregulation of Tcf1 first occurred upon acute infection. To do so, we followed the intranuclear expression of Tcf1 in P14 cells from day 2 to day 50 post-LCMV infection (**Fig. 15A**).

We observed high Tcf1 expression in naive and memory cells (**Fig. 15B, C**), corroborating previously published results [126, 127, 128, 176, 177, 178]. While the P14 cells detected at day 2 post-infection (p.i.) still homogeneously expressed Tcf1, downregulation first became evident on day 3 p.i. (**Fig. 15D**). At this stage, Tcf1 protein expression was downregulated in a subset of cells that had divided three times or more, based on the CFSE dilution. We found no evidence for asymmetric Tcf1 partitioning in the first three cell divisions, in agreement with Lin and colleagues [180]. Cells that retained high expression of Tcf1 initially underwent fewer cell divisions, while Tcf1⁻ cells displayed a "fast cycling" phenotype (**Fig. 15E**). Notwithstanding, at day 4 all P14 cells had divided and the frequency of Tcf1⁺ cells was reduced to ~20% (**Fig. 15D**). A similar percentage of Tcf1⁺ cells was observed at the peak of the CD8⁺ T cell response (d8 p.i.) (**Fig. 15B, C**), following which the frequency of these cells started to increase.

We also followed Tcf1-expressing cells using a *Tcf7*^{GFP} reporter mouse strain (described in [189]). These mice were generated using a bacterial artificial chromosome (BAC) containing the entire *Tcf7* locus, which was modified by the insertion of the EGFP coding sequence into *Tcf7* exon 1 exploiting the endogenous translation start codon (**Fig. 15F**). The coding sequence for mCherry was additionally inserted into a translation start codon present in exon 3, to follow the expression of a short Tcf1 isoform (p33), which could act in a dominant-negative fashion. Finally, to follow the expression of *Tcf7* in antigen-specific CD8⁺ T cells we crossed the *Tcf7*^{GFP} reporter mice with P14 transgenic mice.
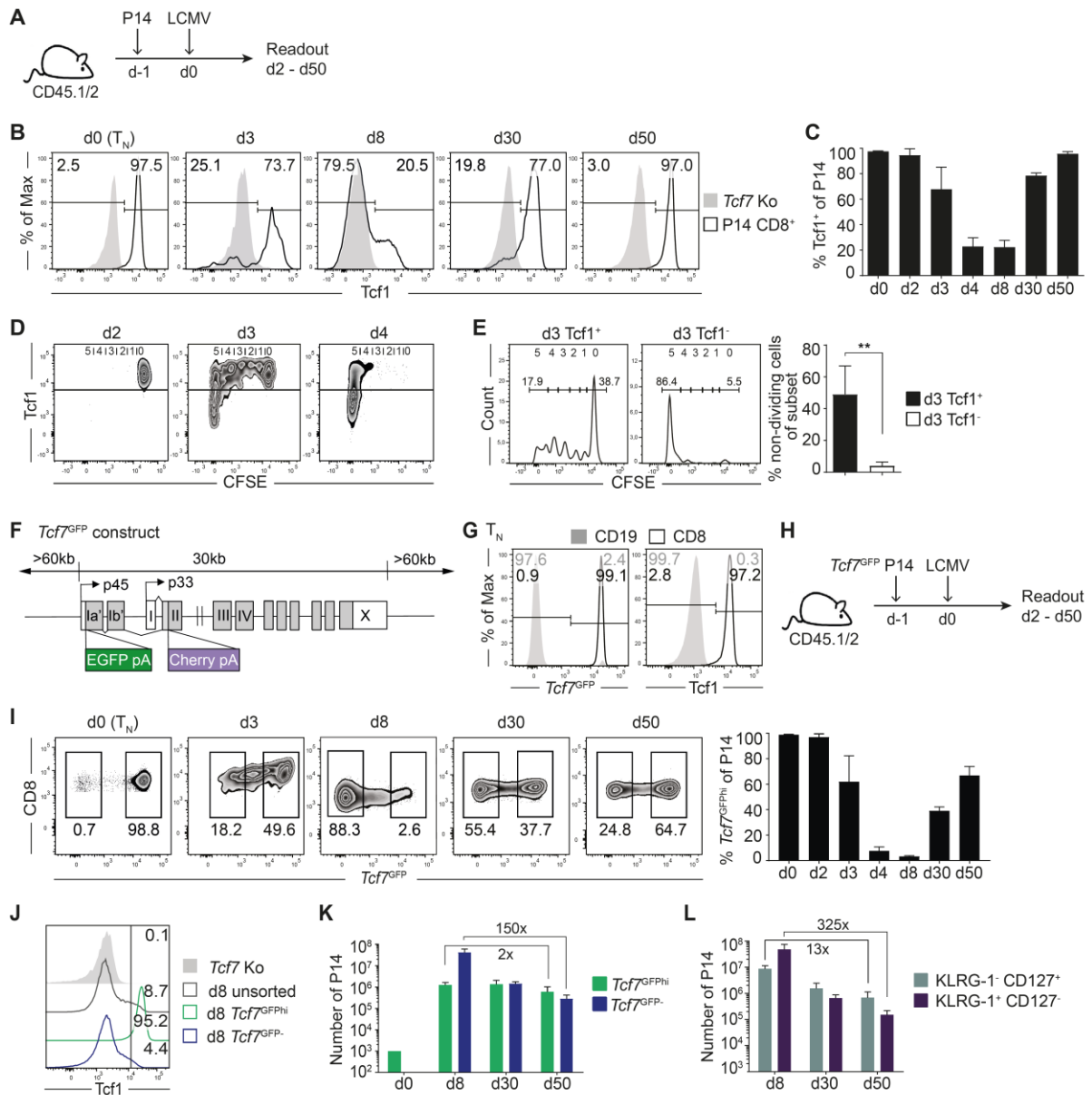
FIGURE 15: Expression pattern of Tcf1 and *Tcf7*^{GFP} in antigen-specific CD8⁺ T cells during the primary immune response to acute LCMV infection.

(**A-E**) B6 (CD45.1/2) mice were adoptively transferred with P14 cells (CD45.2) and infected with LCMV WE on the next day, as schematically shown in (**A**). (**B, C**) Splenic P14 cells were analyzed for the expression of intranuclear Tcf1 at the indicated time point post infection (p.i.), where the percentage of positive cells is depicted in the bar graph (**C**). (**D, E**) P14 cells were labelled with the proliferation dye Carboxyfluorescein succinimidyl ester (CFSE) prior to transfer and infection, and (**D**) analysed at the indicated time point p.i. for the expression of Tcf1 versus CFSE in the spleen; (**E**) the proliferation potential (based on CFSE dilution) of splenic Tcf1⁺ and Tcf1⁻ P14 cells was analyzed at day 3 p.i. (d3). (**F**) *Tcf7*^{GFP} construct: a bacterial artificial chromosome (BAC) containing the murine *Tcf7* locus was modified by inserting EGFP into the first translation codon of the Tcf1 open reading frame. In addition, mCherry, was inserted into a downstream translation codon to follow the expression of the p33 short Tcf1 isoform. The modified BAC was used to generate transgenic mice on a B6 background. (**G**) *Tcf7*^{GFP} (left) and Tcf1 protein expression (right) by splenic CD8⁺ T cells from naive *Tcf7*^{GFP} P14 reporter mice (open) as compared to CD19⁺ B cells (gray fill). (**H-L**) B6 (CD45.1/2) mice were adoptively transferred with *Tcf7*^{GFP} P14 cells (CD45.2) and infected with LCMV WE, as demonstrated in (**H**). (**I**) Splenic P14 cells were analyzed for the expression of *Tcf7*^{GFP} at the indicated time point p.i.. (**J**) Histograms show total P14 cells (grey open) or *Tcf7*^{GFPhi} (green) and *Tcf7*^{GFP-} P14 cells (blue) flow sorted at day 8 (d8) p.i. and analyzed for the expression Tcf1 protein as compared to *Tcf7*^{-/-} (Ko) P14 cells (grey fill). (**K, L**) The bar graphs depict (**K**) the abundance of *Tcf7*^{GFPhi} (green) and *Tcf7*^{GFP-} P14 cells (blue) and (**L**) the abundance of P14 cells with a KLRG-1⁻ CD127⁺ memory precursor (MP) (grey) or a

KLRG-1$^+$ CD127$^-$ terminal effector (TE) (dark purple) phenotype at the indicated time points p.i.. Numbers refer to the fold difference in the abundance of cells at d8 versus d50. In (**B-E, I**) the input number of P14 cells was 2x10^6 cells for the early time points (day 2-4) and 10^4 cells for the remaining time points.
The data shown are pooled from 2 independent experiments with n=5-6 mice per group in (**B, C**) or are representative of 2 independent experiments with n=3-5 mice per group (**D, E, I, K, L**). Mean ±SD are shown. Statistics are based on Non-paired two-tailed Student's test (**E**) with **: $p<0.01$.

While CD19$^+$ B cells lacked both *Tcf7*^{GFP} and Tcf1 protein expression, all naive *Tcf7*^{GFP} P14 CD8$^+$ T cells expressed high levels of *Tcf7*^{GFP}, which corresponded to the Tcf1 protein expression, as demonstrated by intranuclear Tcf1 staining in **Fig. 15G** and in agreement with Utzschneider and colleagues [189].

To confirm and extend the results shown in **Fig. 15B-C**, we studied *Tcf7*^{GFP} expression during CD8$^+$ T cell differentiation in response to acute infections. For this purpose, Wt recipient mice were transplanted with naive *Tcf7*^{GFP} P14 CD8$^+$ T cells one day before infection with LCMV (**Fig. 15H**, as in **15A**). *Tcf7*^{GFP} expression first started to decrease in a subset of P14 cells at day 3 p.i. and reached maximal downregulation at the peak of the acute response (d8) (**Fig. 15I**), similar to the data obtained with Tcf1 protein expression. Nonetheless, a fraction (~2-4%) of cells retained high *Tcf7*^{GFP} expression at d8 p.i.. This fraction then gradually increased following viral clearance and a progressively larger fraction of memory cells expressed high levels of *Tcf7*^{GFP}.

The ability of the *Tcf7*^{GFP} reporter to identify Tcf1 protein expressing cells was validated using flow sorting followed by intranuclear Tcf1 staining. *Tcf7*^{GFPhi} cells sorted at d8 p.i. uniformly exhibited high levels of Tcf1 protein expression, while *Tcf7*$^{GFP-}$ cells were mainly Tcf1 negative, with some cells (~5%) expressed intermediate levels of Tcf1 (**Fig. 15J**). Thus, *Tcf7*^{GFP} faithfully identified Tcf1^{hi} expressing CD8$^+$ T cells.

Even though the frequency of *Tcf7*^{GFPhi} cells at d8 was very low, the number of these cells increased at least 100-fold between d0 and d8 p.i.. The abundance of *Tcf7*^{GFPhi} cells then remained remarkably stable from d8 to d50 (with a minimal 2-fold contraction), while *Tcf7*$^{GFP-}$ cells underwent robust contraction (~150-fold contraction) (**Fig. 15K**). In comparison, the abundance of P14 cells with a memory precursor phenotype (MP, KLRG-1^{lo}CD127^{hi}) decreased more than 10-fold between d8 to d50 (**Fig. 15L**). Therefore, *Tcf7*^{GFPhi} cells present during the effector response seemed to form memory more quantitatively, compared to classically defined MP cells. Additionally, *Tcf7*^{GFPhi} cells seemed to persist better than *Tcf7*$^{GFP-}$ cells.

Tcf7^{GFPhi} memory CD8⁺ T cells have central memory function

We first characterized the phenotype of *Tcf7*^{GFPhi} or *Tcf7*^{GFP-} P14 cells during the early memory phase (d30). Memory *Tcf7*^{GFPhi} cells exhibited higher expression of CD127 and CD62L, and enhanced IL-2 production compared to *Tcf7*^{GFP-} memory cells, which in turn showed increased KLRG-1 expression (**Fig. 16A, B**). Thus, while the latter population displayed a predominant T_{EM} phenotype, the *Tcf7*^{GFPhi} population was enriched for cells with a T_{CM} phenotype.
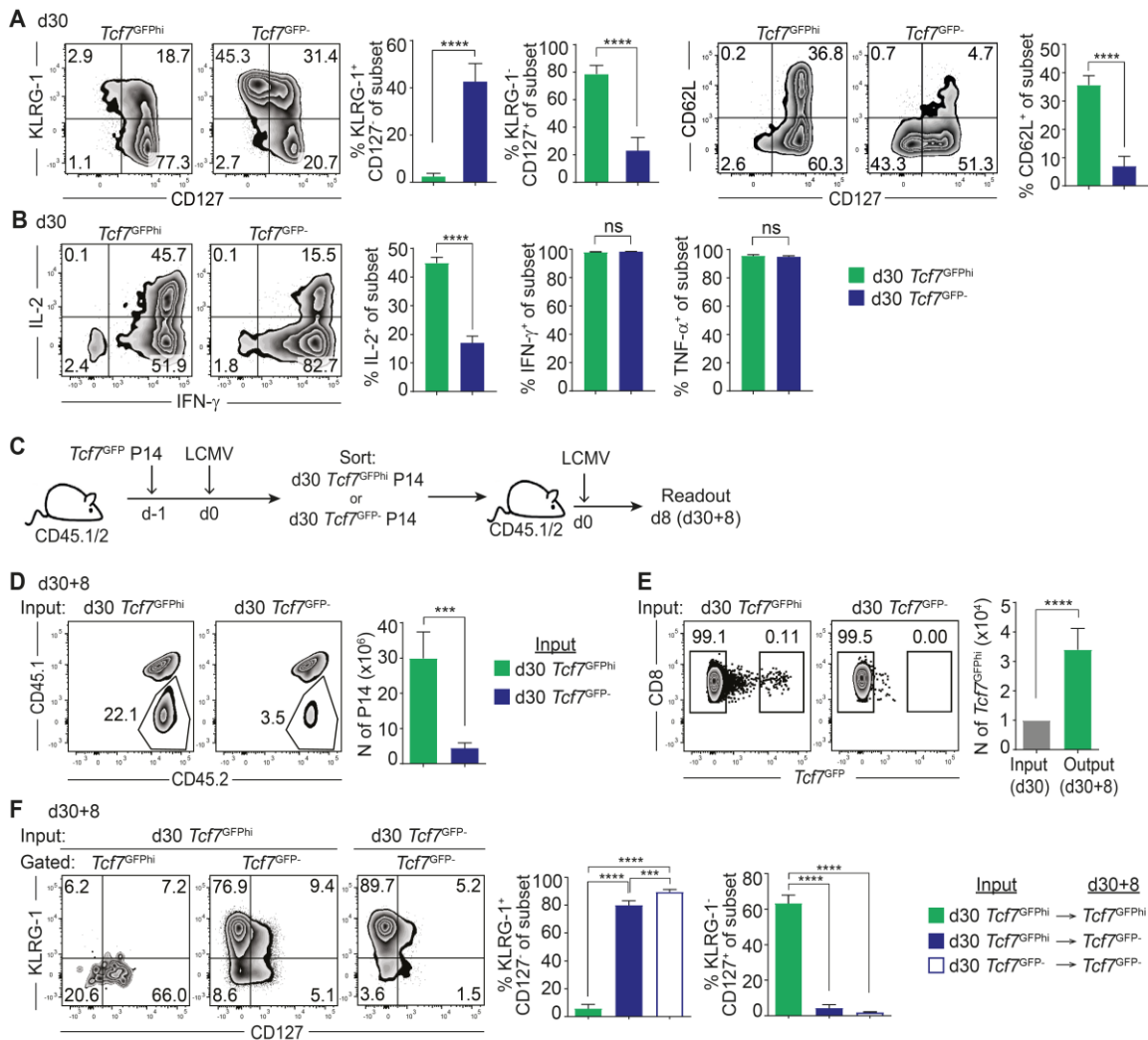
FIGURE 16: High expression of *Tcf7*^{GFP} identifies memory cells with T_{CM} phenotype and function.
(A, B) B6 (CD45.1/2) mice were adoptively transferred with *Tcf7*^{GFP} P14 cells (CD45.2) and infected with LCMV WE. (**A**) Gated *Tcf7*^{GFPhi} and *Tcf7*^{GFP-} P14 memory cells *(*d30) in the spleen were analyzed for the expression of KLRG-1, CD127 and CD62L. (**B**) Splenocytes were re-stimulated for 5 h *in vitro* with gp33 peptide and *Tcf7*^{GFPhi} and *Tcf7*^{GFP-} P14 cells were analyzed for the production of IFN-γ, IL-2 and TNF-α. **(C-F)** Recall expansion and reproduction capacity of d30 *Tcf7*^{GFPhi} (T_{CM}) and d30 *Tcf7*^{GFP-} (T_{EM}) memory cells. (**C**) Equal numbers of d30 *Tcf7*^{GFPhi} and *Tcf7*^{GFP-} P14 cells were transferred into naive B6 (CD45.1/2) mice that were infected with LCMV WE and analyzed 8 days later. P14 cells (d30+8) were analyzed (**D**) for their abundance in the spleen and (**E**) for *Tcf7*^{GFP} expression. (**F**) *Tcf7*^{GFPhi} and *Tcf7*^{GFP-} P14 cells (d30+8) were analyzed for KLRG-1 versus CD127 expression.
Data are representative of at least 2 independent experiments each with n=4 mice per group (**A, B**) or 2 independent experiments with n=4-6 mice per group in (**D-F**). Mean ±SD are shown, and statistics are based

on Non-paired two-tailed Student's test (**A-E**) or on One-Way ANOVA with Tukey's test (**F**) with ***: $p<0.001$; ****: $p<0.0001$ and (ns) $p>0.05$.

A hallmark quality of T_{CM} cells is the capacity to maintain a high proliferation potential upon re-infection [27, 220, 221]. To test this, we sorted $Tcf7^{GFPhi}$ and $Tcf7^{GFP-}$ P14 cells at day 30 p.i. and transferred equal numbers into secondary naive recipients, followed by challenge with high dose of LCMV WE (**Fig. 16C**). At d8 post re-challenge (d30+8), $Tcf7^{GFPhi}$ cells had expanded significantly more than $Tcf7^{GFP-}$ P14 cells (**Fig. 16D**), showing that $Tcf7^{GFPhi}$ memory cells had enhanced re-expansion capacity compared to $Tcf7^{GFP-}$ memory cells. P14 cells derived from $Tcf7^{GFP-}$ cells remained $Tcf7^{GFP-}$ (**Fig. 16E**) and displayed a terminally differentiated phenotype (TE, KLRG-1^{hi}CD127^{lo}) (**Fig. 16F**). On the other hand, d30 $Tcf7^{GFPhi}$ cells mainly gave rise to secondary $Tcf7^{GFP-}$ TE cells, but also yielded a small population of secondary $Tcf7^{GFPhi}$ cells (**Fig. 16E, F**). $Tcf7^{GFPhi}$ cells had significantly expanded compared to input and remained largely undifferentiated (KLRG-1^{low}CD127^{hi}) (**Fig. 16E, F**). Overall, $Tcf7$ expression identified a subpopulation of memory cells with T_{CM} phenotype and function, in part independent of CD62L.

High *Tcf7* expression identifies rare effector-phase cells that resemble T$_{CM}$ cells and lack cytotoxic function

Given that a discrete population of antigen-specific cells expressed high levels of *Tcf7* during the effector phase of the immune response (**Fig. 15E**), we next determined their phenotype. At the peak of the immune response (d8), cells that retained *Tcf7* expression showed a predominant, but not exclusive, KLRG-1^{lo}CD127^{hi} MP phenotype (**Fig. 17A**). In contrast, d8 $Tcf7^{GFP-}$ cells were mostly terminally differentiated (KLRG-1^{hi}CD127^{lo}), consistent with the strong contraction observed in **Fig. 15K**. Consistent with this observation, we noted an increased propensity of d8 $Tcf7^{GFP-}$ cells to undergo apoptosis (high expression of Annexin V following 4h *in vitro* culture) compared to $Tcf7^{GFPhi}$ cells (**Fig. 17B**). Additionally, most $Tcf7^{GFPhi}$ cells were quiescent, i.e. in the G_0 phase of the cell cycle, while $Tcf7^{GFP-}$ cells were in the G_1 phase or cycling (S and G_2/M phase) (**Fig. 17C**). Thus, the maintenance of the d8 $Tcf7^{GFPhi}$ population seemed to correlate with more efficient cell survival and limited cycling.

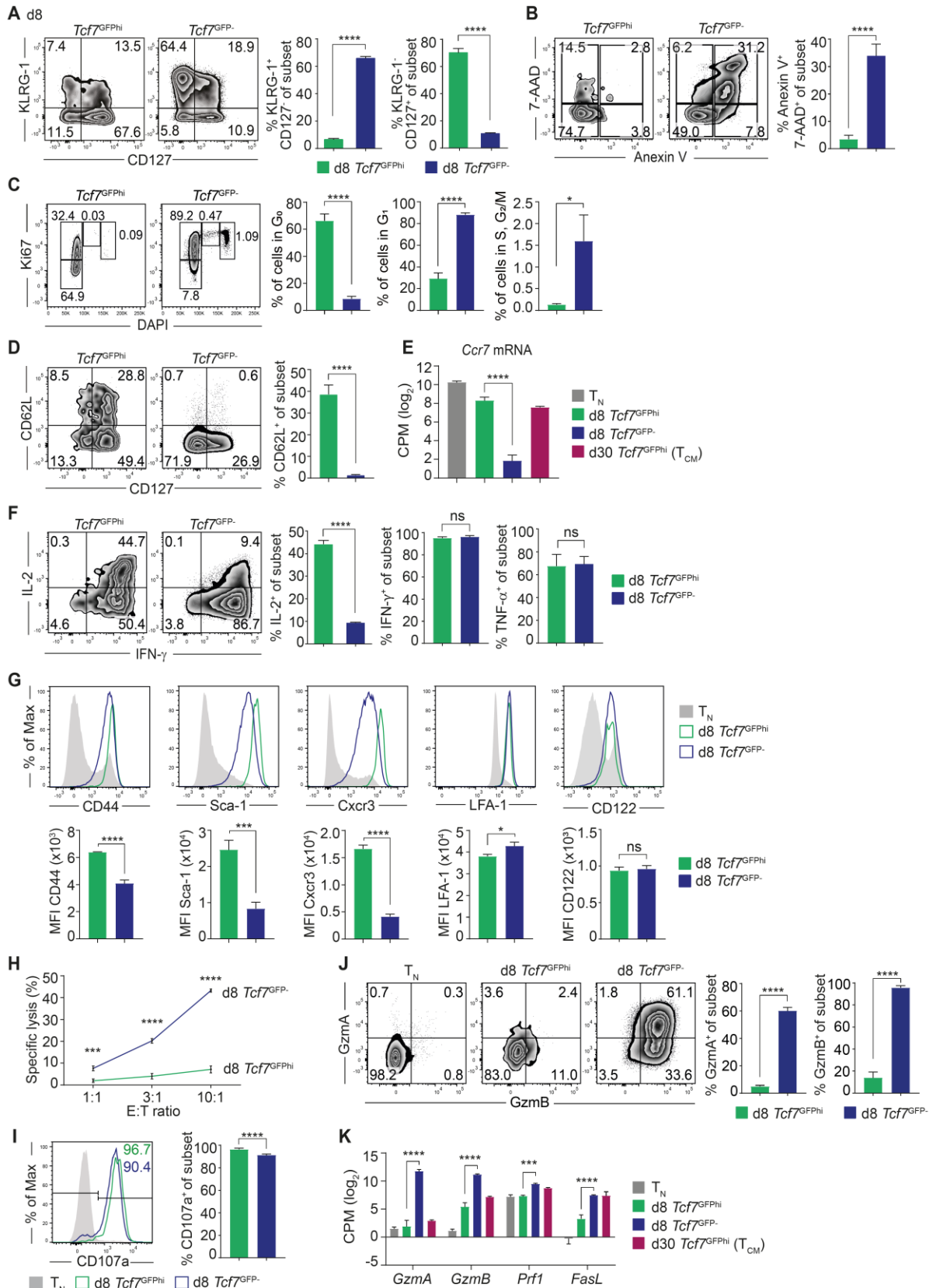**FIGURE 17:** Effector-phase *Tcf7*GFPhi CD8+ T cells resemble central memory cells.
B6 (CD45.1/2) mice were adoptively transferred with *Tcf7*GFP P14 cells (CD45.2) and infected with LCMV WE. At d8 p.i. splenic *Tcf7*GFPhi and *Tcf7*GFP- P14 cells were analyzed (**A**) for the expression of CD127 versus KLRG1; (**B**) for cell survival based on Annexin V versus 7-AAD staining (following 4 h culture in the absence

46

of growth factors); (**C**) for cell cycling based on the staining of flow sorted and permeabilized cells with mKi67 versus the DNA dye DAPI; (**D**) for the expression of CD127 versus CD62L; (**E**) for the expression of *Ccr7* mRNA (based on RNAseq data) relative to that of T_N and d30 *Tcf7*GFPhi (T_{CM}) cells, CPM: Counts per million; (**F**) for the production of IFN-γ, IL-2 and TNF-α following *in vitro* re-stimulation with gp33 peptide; (**G**) for the expression of the indicated markers associated with T_{SCM} cells; (**H**) for lytic activity against gp33-peptide pulsed tumor cells; (**I**) for the release of LAMP1 (CD107a) in response to gp33 peptide re-stimulation; or (**J**) for the expression of GzmA and GzmB protein. (**K**) Expression of the indicated cytotoxic/effector genes (based on RNAseq) by the indicated populations of P14 cells.

The data are representative of at least 2 independent experiments with n=3-5 mice per group in (**A, B, C, D, F, G, H, J**) or from one experiment with n=5 mice in (**I**). RNAseq data are derived from n=3 biological replicates per population (**E, K**). Mean ±SD are shown. Statistics are based on Non-paired two-tailed Student's test (**A, B, C, D, F, G, I, J**); one-Way ANOVA with Tukey's test (**E**); two-way ANOVA with Sidak's test (**H**) or Tukey's test (**K**) with *: $p<0.05$; ***: $p<0.001$; ****: $p <0.0001$ and (ns) $p>0.05$.

Moreover, d8 *Tcf7*GFPhi cells expressed higher levels of the LN homing receptors CD62L (surface expression, **Fig. 17D**) and CCR7 (mRNA expression, **Fig. 17E**), compared to *Tcf7*GFP- cells. The expression levels of these central memory markers in d8 *Tcf7*GFPhi cells were remarkably similar to those observed in d30 *Tcf7*GFPhi T_{CM} cells (**Fig. 16A, Fig. 17E**). Functionally, the production of the effector cytokines IFN-γ and TNF-α was equal among *Tcf7*GFPhi and *Tcf7*GFP- d8 P14 cells (**Fig. 17F**). However, d8 *Tcf7*GFPhi cells produced more IL-2 (**Fig. 17F**), which was similarly seen in d30 *Tcf7*GFPhi T_{CM} cells (**Fig. 16B**). In addition, d8 *Tcf7*GFPhi cells expressed increased levels of certain (Sca-1, Cxcr3), but not all, markers associated with T_{SCM} cells (**Fig. 17G**) [43, 44, 45].

Since T_{CM} do not have lytic activity, we addressed whether effector-stage *Tcf7*GFPhi displayed cytotoxic activity using a flow cytometry-based killing assay (FloKA) [222]. To this end, gp33 peptide-pulsed RMA cells were labelled with Cell Trace Violet (CTV) and co-cultured with flow sorted d8 *Tcf7*GFPhi or *Tcf7*GFP- P14 cells at different Effector to Target (E:T) ratios. 7-AAD uptake by CTV-labelled target cells was used to determine the % of specific lysis. While d8 *Tcf7*GFP- cells proficiently killed their cognate-antigen target cells, the d8 *Tcf7*GFPhi exhibited poor cell-mediated cytotoxicity (**Fig. 17H**). Deficient killing by d8 *Tcf7*GFPhi cells was not due to reduced TCR signalling or impaired exocytosis of granules since they efficiently produced cytokines (**Fig. 17F**) and mobilized LAMP-1 (CD107a) to the cell surface upon re-stimulation with antigen (**Fig. 17I**). Rather, we observed that *Tcf7*GFPhi cells present at the effector phase did not produce cytolytic effector molecules (**Fig. 17J, K**). While d8 *Tcf7*GFP- cells expressed large amounts of both Granzyme (Gzm) A and GzmB, the d8 *Tcf7*GFPhi cells essentially failed to produce these proteins (**Fig. 17J**). Additionally, they also expressed lower mRNA levels of both Perforin (*Prf1*) and Fas ligand (*FasL*), compared to *Tcf7*GFP- cells (**Fig. 17K**). Finally, the levels of these cytolytic proteins were comparable to T_N and often below that of d30 *Tcf7*GFPhi (T_{CM}) cells (**Fig. 17K**). Thus, *Tcf7* expression demarcated rare effector-stage CD8+ T cells that lacked cytotoxic activity and that were remarkably similar to T_{CM} cells.

Polyclonal effector-phase CD8^{+} T cells harbour rare *Tcf7*[GFPhi] cells

We further addressed whether d8 *Tcf7*[GFPhi] cells were also detected during polyclonal CD8^{+} T cell responses to LCMV. To this end, *Tcf7*[GFP] reporter mice were infected with LCMV and CD8^{+} T cells responses to the viral gp33 and np396 epitopes were assessed using MHC-I tetramers 8 days post infection (**Fig. 18A**). Among both tetramer[+] populations we detected a small fraction of cells that retained *Tcf7* expression (~2-3%) (**Fig. 184B**), similar to the above described P14 cells.
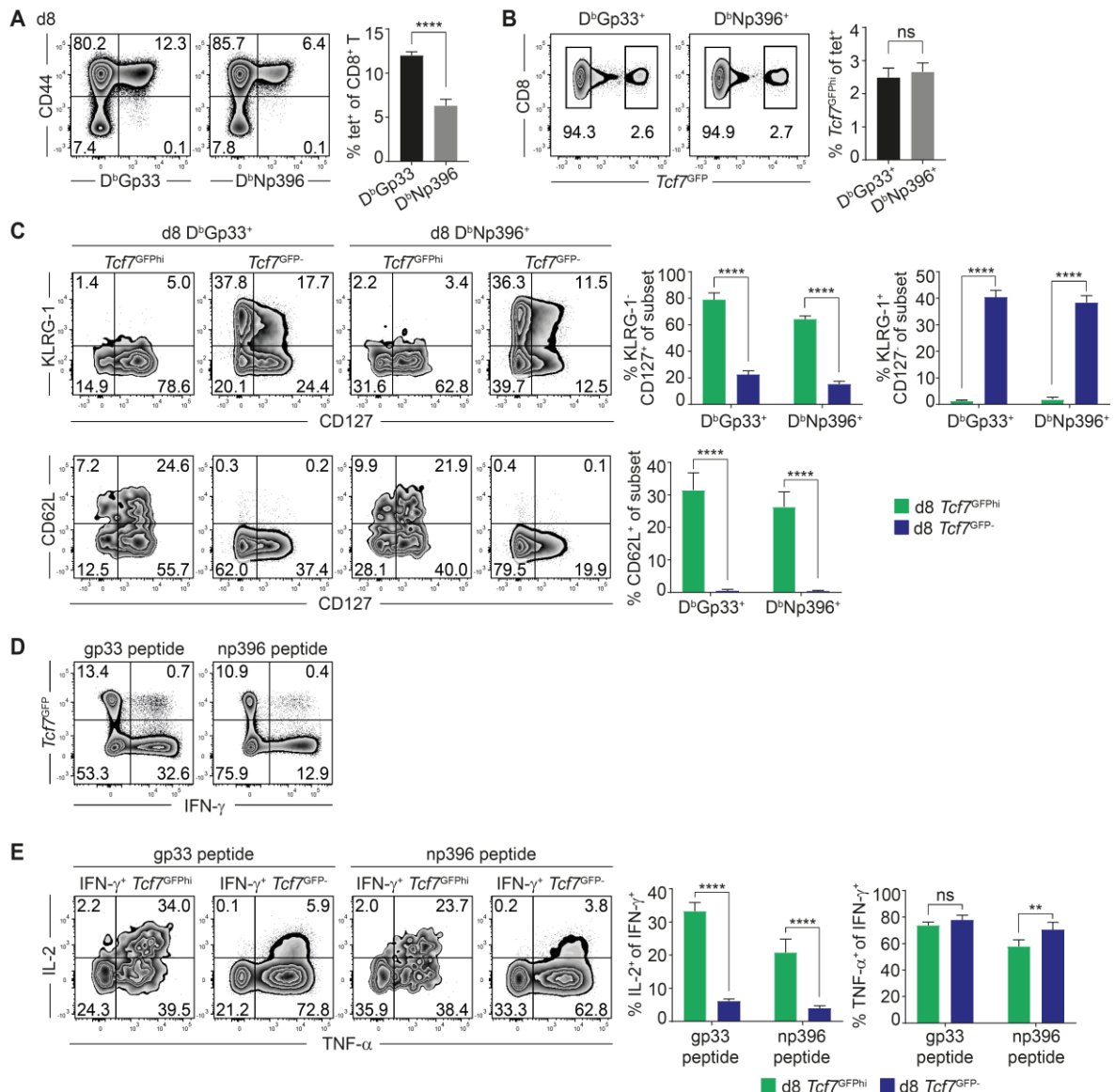
FIGURE 18: Polyclonal *Tcf7*[GFPhi] effector-stage CD8^{+} T cells resemble central memory cells. (**A-E**) *Tcf7*[GFP] mice were infected with LCMV WE and analyzed 8 days later. (**A**) CD8^{+} T cells were stained for CD44 and D[b]Gp33 or D[b]Np396 tetramers. (**B**) Gated D[b]Gp33^{+} or D[b]Np396^{+} CD44^{+} CD8^{+} T cells were analyzed for the expression of *Tcf7*[GFP]. (**C**) *Tcf7*[GFPhi] and *Tcf7*[GFP-] D[b]Gp33^{+} or D[b]Np396^{+} cells were analyzed for the expression of KLRG-1, CD127 and CD62L. (**D, E**) Splenocytes were re-stimulated for 5 h *in vitro* with gp33 or np396 peptide and *Tcf7*[GFPhi] and *Tcf7*[GFP-] IFN-γ^{+} CD8^{+} T cells were analyzed for the production of IL-2 or TNF-α.

Polyclonal *Tcf7*GFPhi effector-stage cells also had a prominent MP phenotype and displayed augmented expression of CD62L, compared to the *Tcf7*GFP- cells (**Fig. 18C**). Finally, polyclonal *Tcf7*GFPhi cells responding to either gp33 or np396 peptide stimulation (IFN-γ^+) showed enhanced IL-2 production (**Fig. 18D, E**). Overall, polyclonal populations of CD8$^+$ T cells with high *Tcf7* expression also exhibited hallmark features of T$_{CM}$ cells.

Effector-phase *Tcf7*GFPhi cells can be detected in multiple tissues

Since T$_{CM}$ reside in secondary lymphoid organs and have the capacity to recirculate [39], we determined the presence of *Tcf7*GFPhi cells in various hematopoietic and non-hematopoietic tissues. *Tcf7*GFPhi effector-phase cells were present in hematopoietic tissues, such as the spleen, lymph nodes (LN) and Bone Marrow (BM), as well as in the circulation (peripheral blood) (**Fig. 19A**). Interestingly, cells with high expression of *Tcf7* could also be detected in the parenchyma of non-hematopoietic tissues, including in the liver, lung, and among Intraepithelial lymphocytes (IEL) of the small intestine (**Fig. 19A**). CD8α^+ cells present in the circulation of the respective organs were excluded from the analysis by injecting anti-CD8α mAb prior to sacrifice.

Given that d8 *Tcf7*GFPhi cells were most abundant in the spleen we next determined their location in this tissue using multicolor immunofluorescence staining combined with digital image analysis. The spleen is organized in 2 major zones, the red pulp (RP) and the white pulp. The latter is further compartmentalized between T (TZ) and B cell zone (BZ) [223]. DAPI and CD4 staining of spleen cross sections allowed us to discriminate between RP, TZ and BZ (**Fig. 19B**). We then looked at the distribution of P14 cells (CD45.2$^+$, blue), some of which expressed *Tcf7*GFP (blue plus green), within each zone (**Fig. 19C**). *Tcf7*GFP+ P14 cells could be detected in both the RP and TZ, but not in the BZ (**Fig. 19D**). The Visiopharm software then allowed us to quantify *Tcf7*GFP+ and *Tcf7*GFP- P14 cells in each zone as seen based on a mask created by the digital analysis (**Fig. 19E**). *Tcf7*GFP+ cells are highlighted by arrows. The abundance of P14 and of *Tcf7*GFP+ P14 cells detected in this way corresponded well to that obtained after tissue homogenization and flow cytometry (**Fig. 19F**). While the vast majority of d8 *Tcf7*GFP- cells were located in the RP (~90%), d8 *Tcf7*GFP+ cells followed a different distribution pattern (**Fig. 19G**). Only 57% of *Tcf7*GFP+ cells were located in the RP and 40% were located in the TZ (**Fig. 19G**). Similar distributions were observed for d30 *Tcf7*GFP+ (T$_{CM}$) as well as naive *Tcf7*GFP+ (T$_N$) cells (**Fig. 19H**). Therefore, *Tcf7*GFP+ cells present both at d8 or d30 p.i. followed a similar distribution pattern in the spleen.

FIGURE 19: Tissue distribution of d8 and d30 $Tcf7^{GFPhi}$ CD8$^+$ T cells.
(**A**) Flow cytometry analysis for the presence of $Tcf7^{GFPhi}$ P14 cells in the indicated tissues at d8 p.i. For liver, lung and Intraepithelial lymphocytes (IELs) of the small intestine, circulating cells were excluded from the analysis based on positive signal for the i.v. injected anti-CD8α mAb. (**B-H**) Naive B6 mice (CD45.1) were transferred with $Tcf7^{GFP}$ P14 cells (CD45.2) and analyzed one day later (d0). Alternatively mice were infected

with LCMV WE and analyzed on d8 or d30 p.i.. (**B-E**) Representative multicolor immunofluorescence (IF) staining of the spleen at d8 post infection. (**B, C**) Spleen cross sections were stained for CD45.2 (P14 cells) (blue), GFP (*Tcf7*GFP) (green), CD4 (red) and DAPI (grey) and used to discriminate the T cell zone, the B cell zone and the red pulp. (**D**) Higher magnification of a representative region stained for CD45.2 (P14 cells) (blue) and GFP (*Tcf7*GFP) (green), (**E**) with further magnification showing the original IF staining (top) and the digital image (bottom) used to identify *Tcf7*GFP+ or *Tcf7*GFP- P14 cells among nucleated cells (DAPI+). (**F**) Spleens were analyzed either by immunofluorescence (IF) staining (Visiopharm; left panels) or by flow cytometry (FACS; right panels) for the frequency of P14 cells among nucleated cells (DAPI+) or among gated live cells, respectively. The frequency of *Tcf7*GFP+ cells amongst P14 cells was determined by IF staining and by FACS in the spleen at d0, d8 or d30 p.i. (**G**) Relative distribution of d8 *Tcf7*GFP+ or *Tcf7*GFP- P14 cells in the B cell zone (blue), the T cell zone (red) and the red pulp (grey) as quantified using the Visiopharm image analysis software or (**H**) relative distribution of d0, d8 *Tcf7*GFP+ or d30 *Tcf7*GFP+ (T$_{CM}$) P14 cells to each zone. (**I-L**) B6 (CD45.1/2) mice were adoptively transferred with *Tcf7*GFP P14 cells (CD45.2) and infected with LCMV WE. At d30 p.i. mice were injected i.v. with an anti-CD8α mAb and sacrificed 5 min later. (**I**) P14 cells were analyzed for their abundance within IELs of the small intestine and for *Tcf7*GFP expression. (**J**) *Tcf7*GFPhi and *Tcf7*GFP- P14 cells among IELs were analyzed for CD69 versus CD103 expression. (**K**) P14 cells were analyzed for their abundance in the lung where CD8α- cells were considered resident and in which the expression of *Tcf7*GFP was evaluated. (**L**) Lung resident *Tcf7*GFPhi and *Tcf7*GFP- P14 cells were analyzed for the expression of CD69 versus CD49a.

IF staining and image acquisition was performed by Dr. Leonardo Scarpellino, Prof. Sanjiv Luther's Lab, UNIL; Roeltje Maas, Prof. Johanna Joyce's Lab, UNIL, helped with Visiopharm analysis. Data described in (**A**) are from 1 experiment with n=3 mice/group. Data in (**B-H**) are representative of 3-4 mice per group with one cross-section/mouse. The data shown in (**I, J**) are pooled from 2 independent experiments with n=5 mice in or are representative of 2 independent experiments with n=3 mice (**K, L**). Mean ±SD are shown. Statistics are based on Two-Way ANOVA with Tukey's test (**G, H**) with *: $p < 0.05$; ***: $p < 0.001$ and (ns) $p > 0.05$.

The fact that *Tcf7*GFPhi cells were present among non-hematopoietic tissues at d8 prompted us to investigate the expression of *Tcf7* among CD8+ tissue resident memory cells (T$_{RM}$) at d30 post-LCMV infection (**Fig. 19I-L**). CD8α- P14 cells resident in either the small intestine's IEL (**Fig. 19I**) or the lung (**Fig. 19K**) contained a substantial population of cells expressing high levels of *Tcf7*GFP. The expression of T$_{RM}$ markers CD69, CD103 and CD49a, was greatly reduced among the *Tcf7*GFPhi population compared to *Tcf7*GFP- (**Fig. 19J, L**). The data thus suggested that the T$_{RM}$ compartment contained relatively undifferentiated *Tcf7*GFPhi cells.

The transcriptome of effector-phase *Tcf7*GFPhi cells resemble that of T$_{CM}$ cells

To globally compare *Tcf7*GFPhi effector-phase cells to other CD8+ T cell types, we performed RNA sequencing. The analysis included naive (T$_N$), d30 *Tcf7*GFPhi (T$_{CM}$) and d30 *Tcf7*GFP- (T$_{EM}$) cells in addition to d8 *Tcf7*GFPhi and d8 *Tcf7*GFP- cells.

Principal component analysis (PCA) of normalized sequencing reads identified d8 *Tcf7*GFPhi cells as a unique class of CD8+ T cells, which were transcriptionally different from their *Tcf7*GFP- counterparts (**Fig. 20A**). In fact, while they were both distinct from T$_N$ cells, d8 *Tcf7*GFPhi cells seemed to cluster substantially closer to d30 *Tcf7*GFPhi as compared to *Tcf7*GFP- cells (**Fig. 20A**). We found 1'204 differently expressed genes (DEGs) between d8 *Tcf7*GFPhi and d8 *Tcf7*GFP- cells (FC>2, FDR<0.05) (**Fig. 20B**). Half of these genes (n=602) were upregulated by

d8 *Tcf7*[GFP-] cells and these were enriched in effector associated genes including cytotoxic effector molecules, as previously described, but also TE markers (*Klrg1* and *Cx3cr1*) and TFs (*Prdm1* and *Zeb2*) (**Fig. 20B, C**). The gene expression program of these cells thus corresponded to the phenotypic analysis (**Fig. 17**) and established the d8 *Tcf7*[GFP-] cells as the *bona fide* effector/cytotoxic population. On the other hand, the d8 *Tcf7*[GFPhi] cells overexpressed multiple T$_{CM}$ associated genes, many of which are also shared with naive cells, such as *Ccr7*, *Sell*, *Il7ra*, *Id3* and *Bcl2* (**Fig. 20B, C**). Interestingly, several of these genes were expressed at an equivalent level in T$_N$ or d30 *Tcf7*[GFPhi] T$_{CM}$ cells. Thus, effector-phase cells that retain high *Tcf7* expression seemed to represent a population with a central memory gene signature.

We then compared the transcriptomes of T$_N$, d8 *Tcf7*[GFPhi] and d30 *Tcf7*[GFPhi] (T$_{CM}$) populations relative to that of d8 *Tcf7*[GFP-] effector cells (FDR<0.05). T$_N$ (n=6'336) and d30 *Tcf7*[GFPhi] (n=4'533) cells had more DEGs compared to d8 *Tcf7*[GFPhi] cells (n=2'998), suggesting that the first populations were more distinct from the effector *Tcf7*[GFP-] cells. Nonetheless, d8 *Tcf7*[GFPhi] cells shared 71% of their DEGs (2'130 out of 2'998) with d30 *Tcf7*[GFPhi] (T$_{CM}$) cells (**Fig. 20D**). 519 additional d8 *Tcf7*[GFPhi] DEGs were also shared with T$_N$ cells, thus only 12% (349 out of 2'998) of genes were uniquely expressed by the effector-stage *Tcf7*[GFPhi] cells (**Fig. 20D**). Next, we performed gene set enrichment analysis (GSEA) of d8 *Tcf7*[GFPhi] versus d8 *Tcf7*[GFP-] cells against our own d30 *Tcf7*[GFPhi] (T$_{CM}$) versus d30 *Tcf7*[GFP-] (T$_{EM}$) gene set or against an independent T$_{CM}$ signature (CD62L$^+$ T$_{CM}$ vs CD62L$^-$ T$_{EM}$ samples) [207]. In all comparisons we observed a significant enrichment for a T$_{CM}$ signature among effector-stage *Tcf7*[GFPhi] cells (**Fig. 20E**). GSEA of d30 *Tcf7*[GFPhi] versus d30 *Tcf7*[GFP-] cells also significantly overlapped with the independent T$_{CM}$ gene signature (**Fig. 20F**). Thus, *Tcf7*^{hi} and *Tcf7*^{-} memory populations corresponded to T$_{CM}$ and T$_{EM}$, respectively. In addition, genes overexpressed by d8 *Tcf7*[GFPhi] cells, compared to *Tcf7*[GFP-] counterparts, were also enriched in a recently proposed stem cell-like memory signature [82] (**Fig. 20H**), an hematopoietic stem cell [210] (**Fig. 20G, H**) and an adult stem cell signature [211] (**Fig. 20H**), but not with a mature hematopoietic cell signature [210] (**Fig. 20G, H**). Finally, many of the stem cell signatures were also observed in d30 *Tcf7*[GFPhi] (T$_{CM}$) and T$_N$ cells (**Fig. 20H**). Thus, effector-phase *Tcf7*[GFPhi] cells were transcriptionally similar to T$_{CM}$ and T$_N$ cells and displayed stem cell-related genes.

Gzma, *Gpx8* and *Cdc20b* were the 3 most highly up-regulated genes in d8 *Tcf7*[GFP-], as compared to d8 *Tcf7*[GFPhi] cells (log$_2$FC: -9.8, -8.3 and -7.5, respectively). Interestingly, these 3 genes are closely linked on mouse Chromosome 13 and this locus further includes the microRNA cluster 449 (miR449), which is located in intron 2 of the *Cdc20b* gene (**Fig. 20I**). miR449, which includes miR449 a, b and c, belongs to the miR34 family of miRNAs that is known to induce cell death and differentiation [224]. qPCR analysis of T$_N$, d8 *Tcf7*[GFPhi] and d8

Tcf7^{GFP-} cells confirmed increased expression of both *Gpx8* and *Cdc20b* in *Tcf7*^{GFP-} cells, and also demonstrated that d8 *Tcf7*^{GFP-} cells overexpressed miR449a (**Fig. 20J**). Thus, *Tcf7* may negatively regulate the expression of the *Cdc20b*/miR449 locus in CD8$^+$ T cells and overexpression of miR449a by d8 *Tcf7*^{GFP-} cells may contribute to the increased terminal differentiation and apoptosis of these cells (**Fig. 17A, B**).
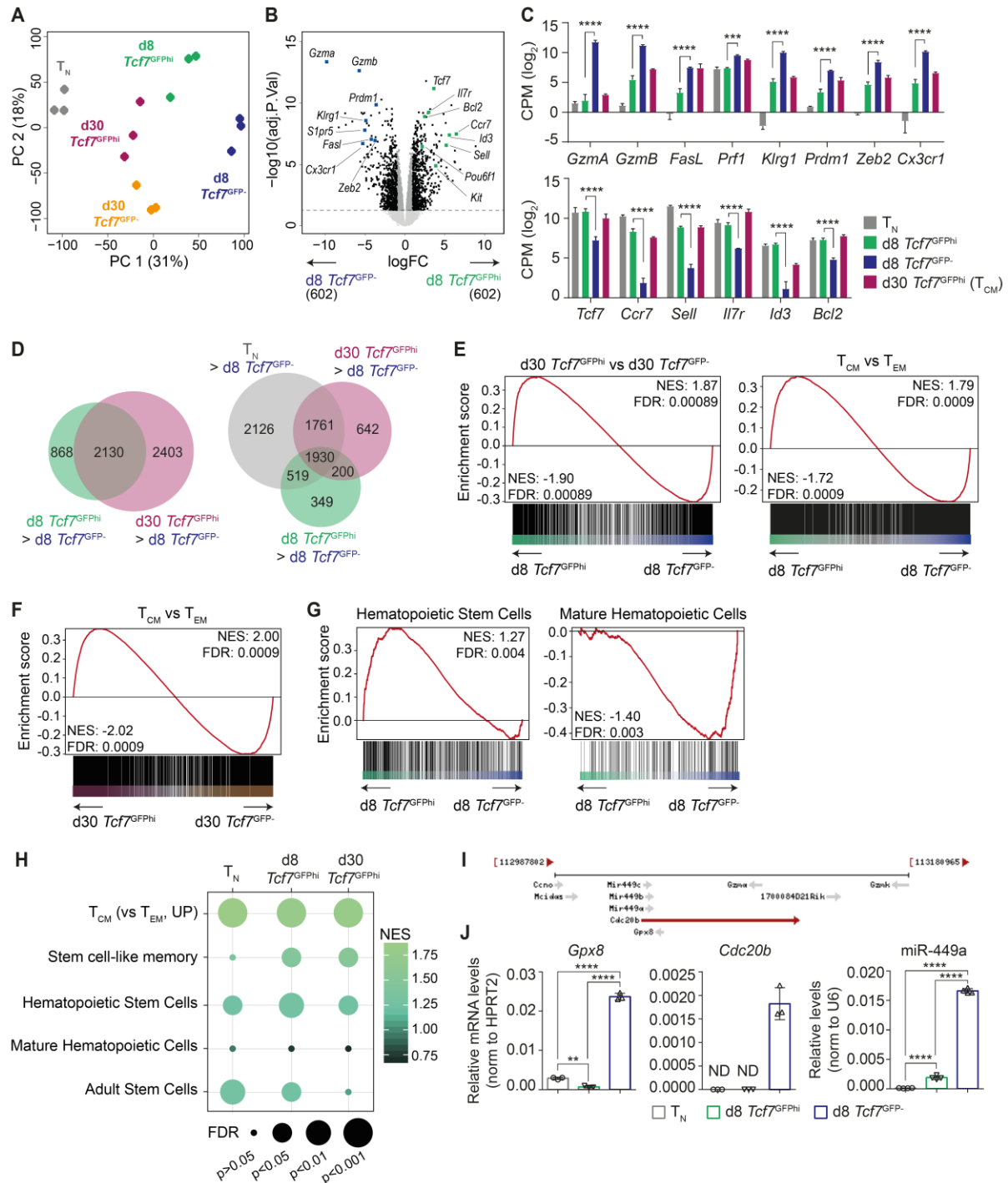
FIGURE 20: *Tcf7*^{GFPhi} effector-phase CD8$^+$ T cells exhibit a T$_{CM}$ gene expression signature. B6 (CD45.1/2) mice were adoptively transferred with *Tcf7*^{GFP} P14 cells (CD45.2) and infected with LCMV Arm. Splenic *Tcf7*^{GFPhi} and *Tcf7*^{GFP-} P14 cells were flow sorted on d8 or d30 p.i. and subjected to RNAseq analysis. **(A)** Principal component analysis (PCA) of normalized and scaled gene expression counts

(n=12138) of naive (T$_N$) (grey), d8 *Tcf7*[GFPhi] (green), d8 *Tcf7*[GFP-] (blue), d30 *Tcf7*[GFPhi] (purple) and d30 *Tcf7*[GFP-] (orange) P14 cells. Each dot represents a biological replicate. (**B**) Volcano plot showing genes differentially expressed between d8 *Tcf7*[GFPhi] and *Tcf7*[GFP-] cells (log$_2$ FC (fold change) >1 and adj. p<0.05). (**C**) Expression of selected effector/cytotoxic (up) and memory genes (down) in the indicated CD8$^+$ T cell populations based on RNAseq analysis. CPM: counts per million. (**D**) Venn diagrams showing genes differentially expressed between d8 *Tcf7*[GFPhi] and d30 *Tcf7*[GFPhi] cells (left) or T$_N$, d8 *Tcf7*[GFPhi] and d30 *Tcf7*[GFPhi] cells (right), each relative to d8 *Tcf7*[GFP-] cells. (**E-H**) Gene set enrichment analysis (GSEA) of (**E**) d8 *Tcf7*[GFPhi] vs d8 *Tcf7*[GFP-] cells testing for enrichment of genes differentially expressed in d30 *Tcf7*[GFPhi] vs d30 *Tcf7*[GFP-] cells (left) or in the T$_{CM}$ vs T$_{EM}$ cell signatures [207] (right); (**F**) d30 *Tcf7*[GFPhi] vs d30 *Tcf7*[GFP-] cells testing for enrichment of genes differentially expressed in T$_{CM}$ vs T$_{EM}$ cells [207] and (**G**) d8 *Tcf7*[GFPhi] vs d8 *Tcf7*[GFP-] cells testing for enrichment of a hematopoietic stem cell signature (left) or mature hematopoietic cell signature (right) [210]. (**H**) GSEA results of T$_N$, d8 *Tcf7*[GFPhi] and d30 *Tcf7*[GFPhi] cells (each versus d8 *Tcf7*[GFP-] cells) testing enrichment in genes upregulated in T$_{CM}$ vs T$_{EM}$ samples [207], in a stem cell-like memory signature [82], in hematopoietic stem cells and in mature hematopoietic cells [210] or in adult stem cells [211]. The dot size and color scale are proportional to the false discovery rate (FDR) and the normalized enrichment score (NES), respectively. (**I**) Schematic representation of the *Cdc20b* locus on mouse chromosome 13 which hosts the miR449 cluster. (**J**) Isolated T$_N$, d8 *Tcf7*[GFPhi] and d8 *Tcf7*[GFP-] cells were analysed for the expression of *Gpx8*, *Cdc20b* or miR449a using RT-qPCR. Expression levels were normalized to HPRT2 or to U6, as indicated. ND = Non detected.
Bioinformatic analyses were performed by Dr. Tania Wyss, UNIL. Data are derived from n=3 biological replicates per population (**A-H**) or representative of 2 experiments with n=3-4 replicates per group (**J**). Mean ±SD are shown. Statistics are based on two-way ANOVA with Tukey's test (**C**) or One-Way ANOVA with Tukey's test (**J**) with **: $p<0.01$; ***: $p<0.001$; ****: $p <0.0001$.

Epigenetic landscape of *Tcf7*[GFPhi] effector-phase cells

Next, we assessed the epigenetic landscape of effector-phase *Tcf7*[GFPhi] cells in comparison to T$_{CM}$ and T$_N$ cells. To address this, we performed ATACseq (Assay for Transposase Accessible Chromatin with high-throughput sequencing) to map accessible DNA regions. PCA of differentially accessible regions (DARs) revealed that d8 *Tcf7*[GFPhi] cells clustered separately from their *Tcf7*[GFP-] counterparts (**Fig. 21A**), demonstrating that the two acute phase populations were epigenetically distinct. Moreover, d8 *Tcf7*[GFPhi] and d30 *Tcf7*[GFPhi] (T$_{CM}$) cells clustered closer to T$_N$ than d8 *Tcf7*[GFP-] or d30 *Tcf7*[GFP-] (T$_{EM}$) cells (**Fig. 21A**).

The analyses identified 17'676 DARs (FDR<0.05) between the d8 *Tcf7*[GFPhi] and d8 *Tcf7*[GFP-] cells, of which 7'194 were more accessible in effector-phase *Tcf7*[GFPhi] cells (**Fig. 21B**). To compare accessible regions across all populations, we generated peak-centered heatmaps of ATACseq read coverage based on regions more accessible in d8 *Tcf7*[GFPhi] compared to *Tcf7*[GFP-] cells. These regions were also more accessible in d30 *Tcf7*[GFPhi] (T$_{CM}$) and T$_N$ cells, but less accessible in d30 *Tcf7*[GFP-] (T$_{EM}$) cells (**Fig. 21B**). Conversely, regions more accessible in *Tcf7*[GFP-] effector cells (n=10'482) were also more accessible in d30 *Tcf7*[GFP-] (T$_{EM}$) cells but less accessible in d30 *Tcf7*[GFPhi] (T$_{CM}$) and T$_N$ cells (**Fig. 21C**). Thus, the chromatin accessibility of d8 *Tcf7*[GFPhi] cells was globally similar to that of T$_{CM}$ and T$_N$ cells, but different from T$_{EM}$ and *Tcf7*[GFP-] effector cells.
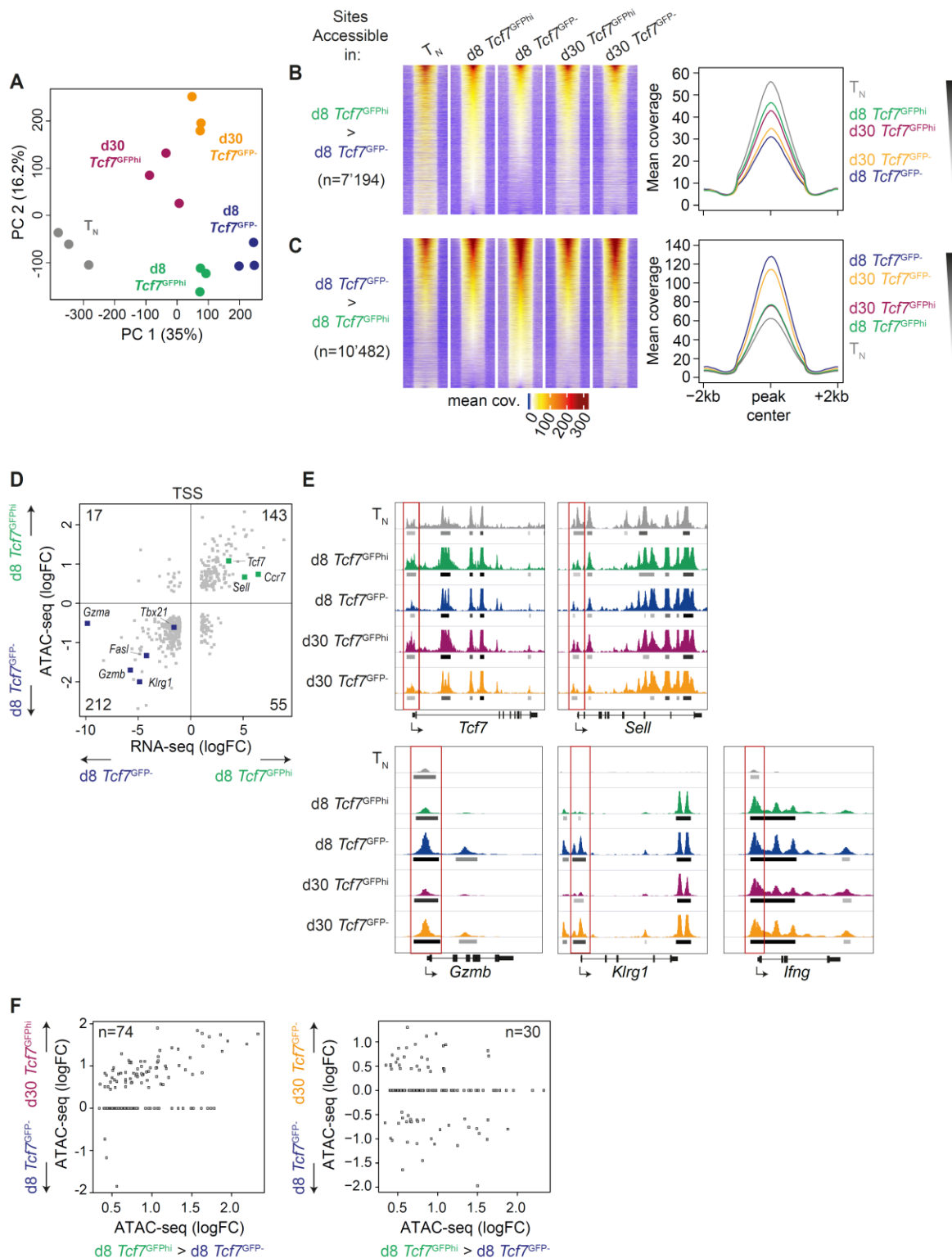
FIGURE 21: Chromatin accessibility of effector-stage *Tcf7*^GFPhi CD8⁺ T cells.
B6 (CD45.1/2) mice were adoptively transferred with *Tcf7*^GFP P14 cells (CD45.2) and infected with LCMV Arm. Splenic *Tcf7*^GFPhi and *Tcf7*^GFP- P14 cells were flow sorted on d8 or d30 p.i. and subjected to ATACseq analysis. (**A**) PCA of accessible regions (n=112069) in T_N (grey), d8 *Tcf7*^GFPhi (green), d8 *Tcf7*^GFP- (blue), d30 *Tcf7*^GFPhi (purple) and d30 *Tcf7*^GFP- (orange) P14 cells. Each dot represents an individual sample. (**B, C**) Peak centered heat maps (± 2kb flanking region in 25bp-long windows) of ATACseq read coverage. The coverage of regions more accessible in (**B**) d8 *Tcf7*^GFPhi cells or (**C**) in d8 *Tcf7*^GFP- cells are shown for T_N, d30 *Tcf7*^GFPhi (T_CM) and d30 *Tcf7*^GFP- (T_EM) cells, averaged over the 3 biological replicates and sorted according to their

coverage level in d8 *Tcf7*^{GFPhi} cells (**B**) or d8 *Tcf7*^{GFP-} cells (**C**). Corresponding line graphs show the mean intensity of the read coverage. (**D**) Transcription start sites (TSS) differentially accessible in d8 *Tcf7*^{GFPhi} versus d8 *Tcf7*^{GFP-} cells (FDR p<0.05) were correlated with genes differentially expressed in d8 *Tcf7*^{GFPhi} versus d8 *Tcf7*^{GFP-} cells (absolute log$_2$FC>1 and adj. p<0.05). Selected genes are indicated by a colored dot. (**E**) Read coverage track for selected memory (*Tcf7, Sell* (CD62L)) (top) and cytotoxic/effector genes (*Gzmb, Klrg1, Ifng*) (bottom) in the indicated populations of cells. The region surrounding the TSS is highlighted using a red outline. The horizontal lines depict accessible regions based on peak calling, where color intensity correlates with p-value. (**F**) Regions more accessible in d8 *Tcf7*^{GFPhi} cells were correlated with differentially accessible regions in d30 *Tcf7*^{GFPhi} versus d8 *Tcf7*^{GFP-} cells (left) or d30 *Tcf7*^{GFP-} versus d8 *Tcf7*^{GFP-} cells (right) (FDR p<0.05). Number inside plots indicates the number of genes more accessible in both d8 *Tcf7*^{GFPhi} and d30 *Tcf7*^{GFPhi} cells (left) or in d8 *Tcf7*^{GFPhi} and d30 *Tcf7*^{GFP-} cells (right).
Bioinformatic analyses were performed by Dr. Tania Wyss, UNIL. Data are derived from n=3 biological replicates per population.

We then focused our analysis on accessibility changes at the transcriptional start site (TSS), which are known to be functionally relevant. This identified 4'049 genes associated with a differentially accessible TSS in d8 *Tcf7*^{GFPhi} compared to d8 *Tcf7*^{GFP-} cells (783 more accessible and 3'266 less accessible TSS) (FDR p<0.05). To correlate accessibility changes with gene expression, we combined these differently accessible TSS regions with the 1'204 differently expressed genes identified in the d8 *Tcf7*^{GFPhi} vs d8 *Tcf7*^{GFP-} cells based on RNAseq analysis (**Fig. 20B**). Of the 602 genes overexpressed in d8 *Tcf7*^{GFPhi} cells, 143 (23.8%) had increased TSS accessibility (**Fig. 21D**). This class of *Tcf7*^{GFPhi} genes included central memory genes such as *Tcf7, Sell or Ccr7* (**Fig. 21D, E**). In addition, more than half of these genes were also more accessible in T$_{CM}$ (74 of 143), but fewer were more accessible in T$_{EM}$ (30 of 143) (**Fig. 21F**). Conversely, the TSS was more open in 212 of the 602 (35.2%) genes specifically expressed in d8 *Tcf7*^{GFP-} cells (**Fig. 21D**), including effector genes such as *Gzma, Gzmb, Klrg1, FasL* and *Tbx21* (T-bet) (**Fig. 21D, E**). Strikingly, while the TSS of *Gzmb* was open in d8 *Tcf7*^{GFP-} or T$_{EM}$ cells, it was essentially inaccessible in d8 *Tcf7*^{GFPhi} and T$_{CM}$ cells, as well as in T$_N$ cells (**Fig. 21E**). In comparison, the *Ifng* locus was equally open in antigen-experienced populations but closed in T$_N$ cells (**Fig. 21E**). Thus, even though *Ifng* is used as a marker for effector differentiation, it rather identifies antigen-experienced cells.

The epigenetic data suggested that sustained expression of T$_{CM}$-associated genes among d8 *Tcf7*^{GFPhi} cells might be the result of increased accessibility, in particular of their TSS. Conversely, downregulation of these genes in *Tcf7*^{GFP-} effector cells was likely regulated in part by reduced TSS accessibility. On the other hand, reduced accessibility of effector-loci likely contributed to the low expression of this class of genes in *Tcf7*^{GFPhi} cells. Epigenetically, *Tcf7*^{GFPhi} cells resembled T$_{CM}$ and T$_N$ in particular with regard to key lineage determining factors.

Effector-phase *Tcf7*GFPhi cells show efficient recall expansion, differentiation and self-renewal capacity

Because d8 *Tcf7*GFPhi cells were phenotypically, transcriptionally and epigenetically similar to T_{CM} cells, we asked if they performed central memory functions. Such functions, which include recall expansion, differentiation and self-renewal capacity, are currently believed to be acquired late during the contraction phase of an acute immune response (~d22 p.i.) [68]. However, since *Tcf7*GFPhi cells are rare among effector cells, we hypothesized that recall expansion may not be evident when testing the bulk effector population. We thus sorted *Tcf7*GFPhi or *Tcf7*GFP- P14 d8 cells and transferred equal numbers into secondary naive recipients, which were challenge with LCMV (as schematically shown in **Fig. 22A**). Eight days later (d8+8), the d8 *Tcf7*GFPhi cells yielded considerably more progeny than *Tcf7*GFP- P14 cells (**Fig. 22B**). Interestingly, the recall expansion capacity of d8 *Tcf7*GFPhi cells was identical to that of d30 *Tcf7*GFPhi cells (**Fig. 22C**). Additionally, we tested whether increased expansion correlated with higher protection. To do so, we engrafted Vβ5 transgenic hosts with either d8 *Tcf7*GFP-, d8 *Tcf7*GFPhi or d30 *Tcf7*GFPhi cells and measured splenic LCMV Plaque Forming Units (PFU) eight days post LCMV challenge. Vβ5 transgenic hosts cannot control virus infection. Preliminary analyses showed that the adoptive transfer of d8 *Tcf7*GFP- cells lead to a minimal reduction in splenic virus titers, as compared to mice that received no cell transfer (**Fig. 22C**). In contrast, transfer of either d8 or d30 *Tcf7*GFPhi cells strongly and comparably reduced the splenic virus titers (**Fig. 22C**). Therefore, effector-stage *Tcf7*GFPhi cells protected from systemic infection as effectively as T_{CM}.

We also followed the fate of transferred d8 cells upon re-challenge. The progeny of d8 *Tcf7*GFP- cells were homogeneously *Tcf7*GFP- (**Fig. 22E**) with a TE phenotype (**Fig. 22F**). This data further supported that downregulation of *Tcf7* favors terminal differentiation and that *Tcf7*GFP- cells cannot re-express *Tcf7*. On the other hand, d8 *Tcf7*GFPhi cells generated secondary *Tcf7*GFP- as well as rare *Tcf7*GFPhi progeny (**Fig. 22E**). The number of *Tcf7*GFPhi cells robustly increased during re-challenge, indicating that these cells can reproduce themselves (**Fig. 22E**). In agreement with this conclusion, secondary d8 *Tcf7*GFPhi cells remained chiefly undifferentiated (KLRG-1lo CD127hi) (**Fig. 22F**).
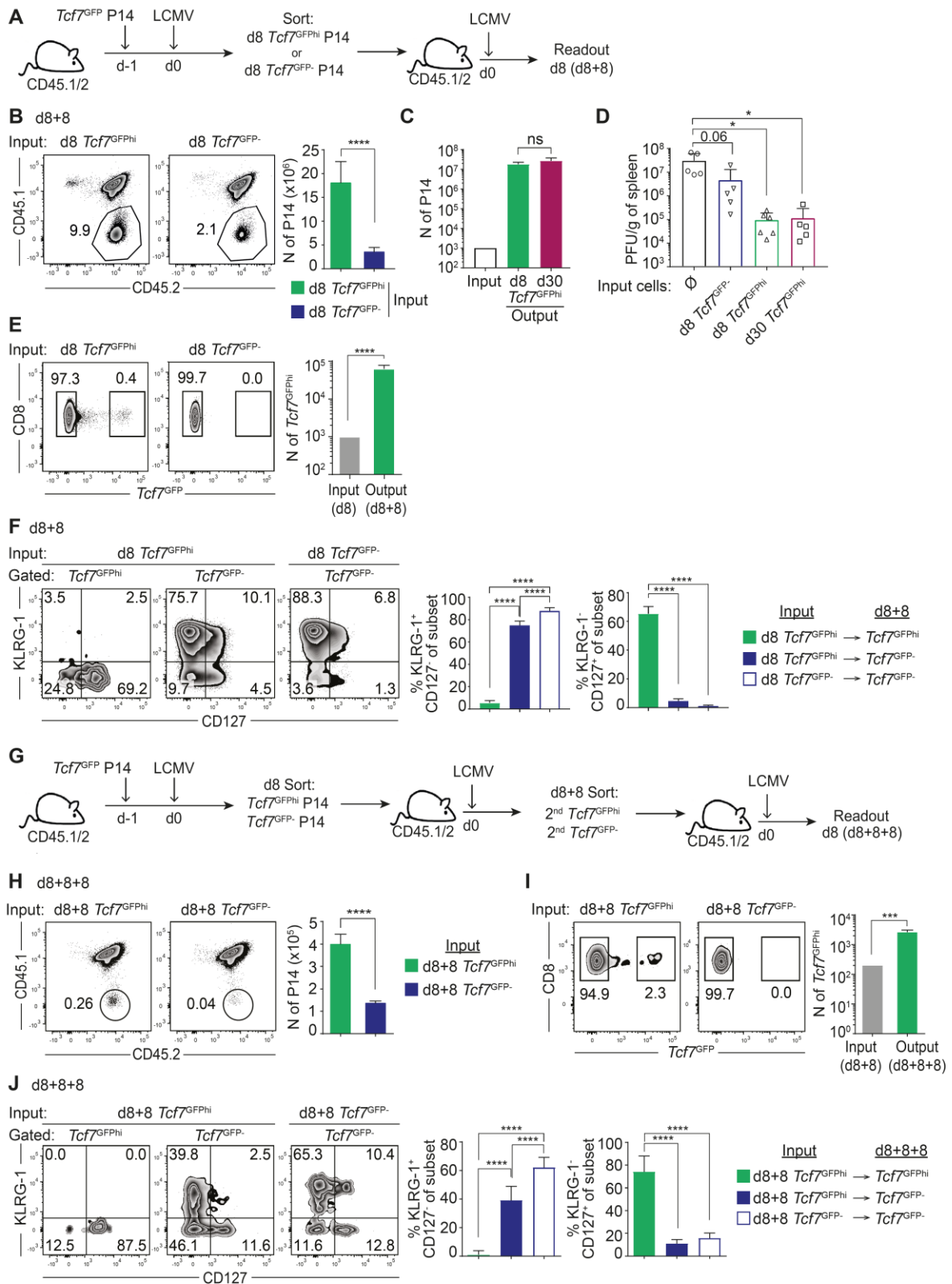
FIGURE 22: Effector-phase *Tcf7*[GFPhi] cells have central memory function.
(**A-F**) B6 (CD45.1/2) mice were transplanted with *Tcf7*[GFP] P14 cells (CD45.2) and infected with LCMV WE. Eight days later, *Tcf7*[GFPhi] or *Tcf7*[GFP-] P14 cells were flow sorted and equal numbers were transferred to naïve secondary B6 (CD45.1/2) recipients. These were infected with LCMV WE and analyzed on d8 (d8+8), as depicted in (**A**). (**B**) Recall expansion capacity of d8 *Tcf7*[GFPhi] or *Tcf7*[GFP-] P14 cells was analyzed at d8 (d8+8) and (**C**) was compared to that of d30 *Tcf7*[GFPhi] (T$_{CM}$) cells. (**D**) Vβ5 TCR transgenic mice were transplanted

with equal numbers of d8 *Tcf7*^{GFPhi}, d8 *Tcf7*^{GFP-} or d30 *Tcf7*^{GFPhi} (T_{CM}) cells (or no cells Ø) and infected with LCMV Arm. Splenic LCMV titers (PFU = Plaque forming units) were determined 8 days later. (**E**) Splenic d8+8 P14 cells were analyzed for the expression of *Tcf7*^{GFP} and (**F**) gated *Tcf7*^{GFPhi} and *Tcf7*^{GFP-} cells were analyzed for the expression of KLRG-1 versus CD127. The bar graph in (**E**) depicts the abundance of secondary *Tcf7*^{GFPhi} cells compared to input (assuming 10% take). (**G-J**) Recall expansion and self-renewal capacity of d8 *Tcf7*^{GFPhi} cells. Secondary *Tcf7*^{GFPhi} and *Tcf7*^{GFP-} P14 cells (d8+8) were flow sorted and equal numbers were transferred into naive B6 (CD45.1/2) mice that were infected with LCMV WE, as schematically demonstrated in (**G**). Tertiary P14 cells (d8+8+8) were analyzed (**H**) for their abundance in the spleen and (**I**) for *Tcf7*^{GFP} expression. The bar graph depicts the abundance of tertiary *Tcf7*^{GFPhi} *P14 cells* compared to input (assuming 10% take). (**J**) Tertiary *Tcf7*^{GFPhi} *and Tcf7*^{GFP-} P14 cells were analyzed for KLRG-1 versus CD127 expression.

The data are representative of 2 independent experiments with n=6 mice per group in (**B, C, E, F, H, I**) or from one experiment with n=5-6 mice in (**D**) or pooled from 2 independent experiments with n=11 mice per group (**J**). Mean ±SD are shown. Statistics are based on Non-paired two-tailed Student's test (**B, E, H, I**) or on One-Way ANOVA with Tukey's test (**C, D, F, J**) with *: $p<0.05$; ***: $p<0.001$; ****: $p <0.0001$ and (ns) $p>0.05$.

To formally test if d8 *Tcf7*^{GFPhi} cells can self-renew we performed tertiary transfers as shown in **Fig. 22G**. At d8 following the third LCMV challenge (d8+8+8) the secondary *Tcf7*^{GFPhi} P14 cells had undergone robust re-expansion (**Fig. 22H**), showing that they maintained their expansion potential. Furthermore, the resulting progeny again included both terminally differentiated *Tcf7*^{GFP-} effector cells as well as tertiary undifferentiated *Tcf7*^{GFPhi} cells (**Fig. 22I, J**). Finally, the abundance of tertiary *Tcf7*^{GFPhi} cells had increased during re-stimulation. Thus, serial transfers demonstrated that effector-phase *Tcf7*^{GFPhi} cells can self-renew in response to antigen re-challenge.

We further tested the recall expansion, differentiation and self-renewal capacity of polyclonal effector-stage *Tcf7*^{GFPhi} CD8⁺ T cells (**Fig. 23**). Total *Tcf7*^{GFPhi} and *Tcf7*^{GFP-} CD8⁺ T cells were sorted from the spleen of *Tcf7*^{GFP} reporter mice 8 days post-LCMV infection (**Fig. 23A**). At this stage, the *Tcf7*^{GFPhi} population contained a substantially lower frequency of either D^bGp33⁺ or D^bGp396⁺ cells compared to the *Tcf7*^{GFP-} population (**Fig. 23B**). Thus, in order to re-challenge comparable numbers of tetramer⁺ cells, we adoptively transferred 150'000 *Tcf7*^{GFPhi} cells or 40'000 *Tcf7*^{GFP-} cells into secondary recipient mice (CD45.1/.2), followed by LCMV infection. In this way, the *Tcf7*^{GFPhi} and *Tcf7*^{GFP-} input cells contained 3'960 D^bGp33⁺ *Tcf7*^{GFPhi} and 5'360 D^bGp33⁺ *Tcf7*^{GFP-} cells, respectively. Eight days later (d8+8) we observed that *Tcf7*^{GFPhi} cells specific for either the gp33 or the gp396 LCMV epitope expanded significantly more than the *Tcf7*^{GFP-} cells (**Fig. 23C**). In addition, the d8 polyclonal *Tcf7*^{GFPhi} cells had mostly differentiated into *Tcf7*^{GFP-} TE cells, but also regenerated *Tcf7*^{GFPhi} cells (**Fig. 23D, E**). Thus, *Tcf7*^{GFP} expression marked CD8⁺ T cells with T_{CM} hallmark aptitudes (robust recall expansion, differentiation and self-renewal capacity), which were already evident at the effector phase of the primary immune response.
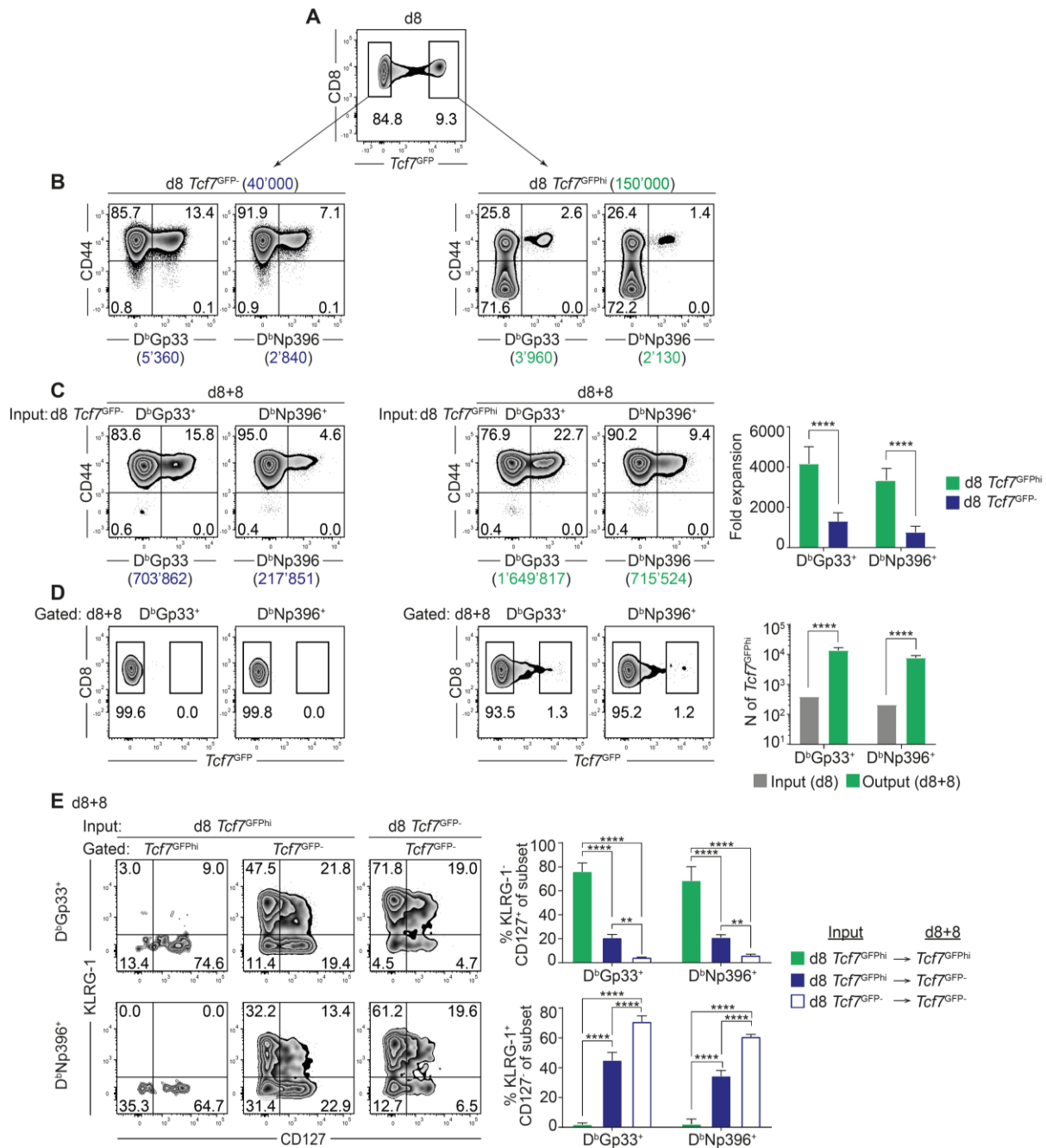
FIGURE 23: Recall expansion and re-production of polyclonal d8 *Tcf7*GFPhi CD8+ T cells.
(**A-E**) *Tcf7*GFP mice (CD45.2) were infected with LCMV WE. (**A**) Eight days later *Tcf7*GFPhi and *Tcf7*GFP- CD8+ T cells were flow sorted. (**B**) Tetramer staining showed that the 150'000 sorted *Tcf7*GFPhi cells contained 3'960 DbGp33+ and 2'130 DbNp396+ CD8+ T cells and that the 40'000 sorted *Tcf7*GFP- cells contained 5'360 DbGp33+ and 2'840 DbNp396+ CD8+ T cells. The sorted cells were transferred into naive secondary recipients (CD45.1) that were infected with LCMV WE. (**C**) Eight days later (d8+8) donor-derived CD8+ T cells were stained using tetramer. The 3'960 *Tcf7*GFPhi DbGp33+ input cells had yielded 1'649'817 DbGp33+ cells. The corresponding bar graph depicts the expansion of the different populations compared to input (assuming a 10% take of the latter)[15]. (**D**) Secondary DbGp33+ and DbNp396+ cells (d8+8) were analyzed for the expression of *Tcf7*GFP. The corresponding bar graph depicts the number of secondary tetramer+ *Tcf7*GFPhi cells compared to input (assuming a 10% take). (**E**) Gated d8+8 *Tcf7*GFPhi or *Tcf7*GFP- tetramer+ cells were analyzed for the expression of KLRG-1 versus CD127.
Data are representative of 2 independent experiments with n=4-5 mice per group. Mean ±SD are shown. Statistics are based on Two-Way ANOVA with Tukey's test with **: $p<0.01$; and ****: $p<0.0001$.

Effector-phase *Tcf7*^{GFPhi} cells can generate the entire array of memory subtypes

The above data suggested that d8 *Tcf7*^{GFPhi} cells have stem-like properties. However, stemness includes not only the capacity to expand, differentiate and self-renew but also the capacity to generate the entire range of effector and memory cell subsets, i.e. multipotency [225]. As described above, upon antigen re-stimulation d8 *Tcf7*^{GFPhi} cells reproduced and generated secondary effector cells (**Fig. 22E, F**). Next, we extended this analysis by determining the ability of d8 *Tcf7*^{GFPhi} cells to generate distinct memory subtypes. For this purpose, d8 *Tcf7*^{GFPhi} cells were transferred into naive Wt recipients, that were infected with LCMV and analyzed 30 days later (d8+30) (**Fig. 24A**).

Compared to mice that received d8 *Tcf7*^{GFPhi} cells, the splenic memory compartment was markedly reduced (~5 fold) in mice engrafted with d8 *Tcf7*^{GFP-} cells (**Fig. 24B**). Memory cells derived from the *Tcf7*^{GFPhi} effector-phase cells included a large population of *Tcf7*^{GFPhi} cells (**Fig. 24C**), many of which expressed CD62L and produced IL-2 (**Fig. 24D**) and thus corresponded to T_{CM}. *Tcf7*^{GFPhi} effector-phase cells also yielded CD62L$^-$ T_{EM} (**Fig. 24D**). In contrast, the memory cells derived from the d8 *Tcf7*^{GFP-} cells were essentially *Tcf7*^{GFP-} (**Fig. 24C**) and few were producing IL-2 (**Fig. 24D**). Thus, only the *Tcf7*^{GFPhi} cells had the capacity to give rise to both T_{CM} and T_{EM} memory subsets. Comparable results were also seen in the LN memory compartment (**Fig. 24E-G**).

Moreover, d8 *Tcf7*^{GFPhi} cells yielded significantly larger memory compartments in non-hematopoietic tissues compared to d8 *Tcf7*^{GFP-} cells. This was evident among IELs present in the small intestine (**Fig. 24H**) and among lung resident CD8$^+$ T cells, from which re-circulating CD8α^+ cells had been excluded (**Fig. 24I**). Therefore, besides failing to generate T_{CM} cells, d8 *Tcf7*^{GFP-} cells also yielded considerable fewer T_{EM} and T_{RM} cells. In contrast, effector-phase *Tcf7*^{GFPhi} cells displayed multi-lineage differentiation potential as they generated all memory populations in addition to effector cells.
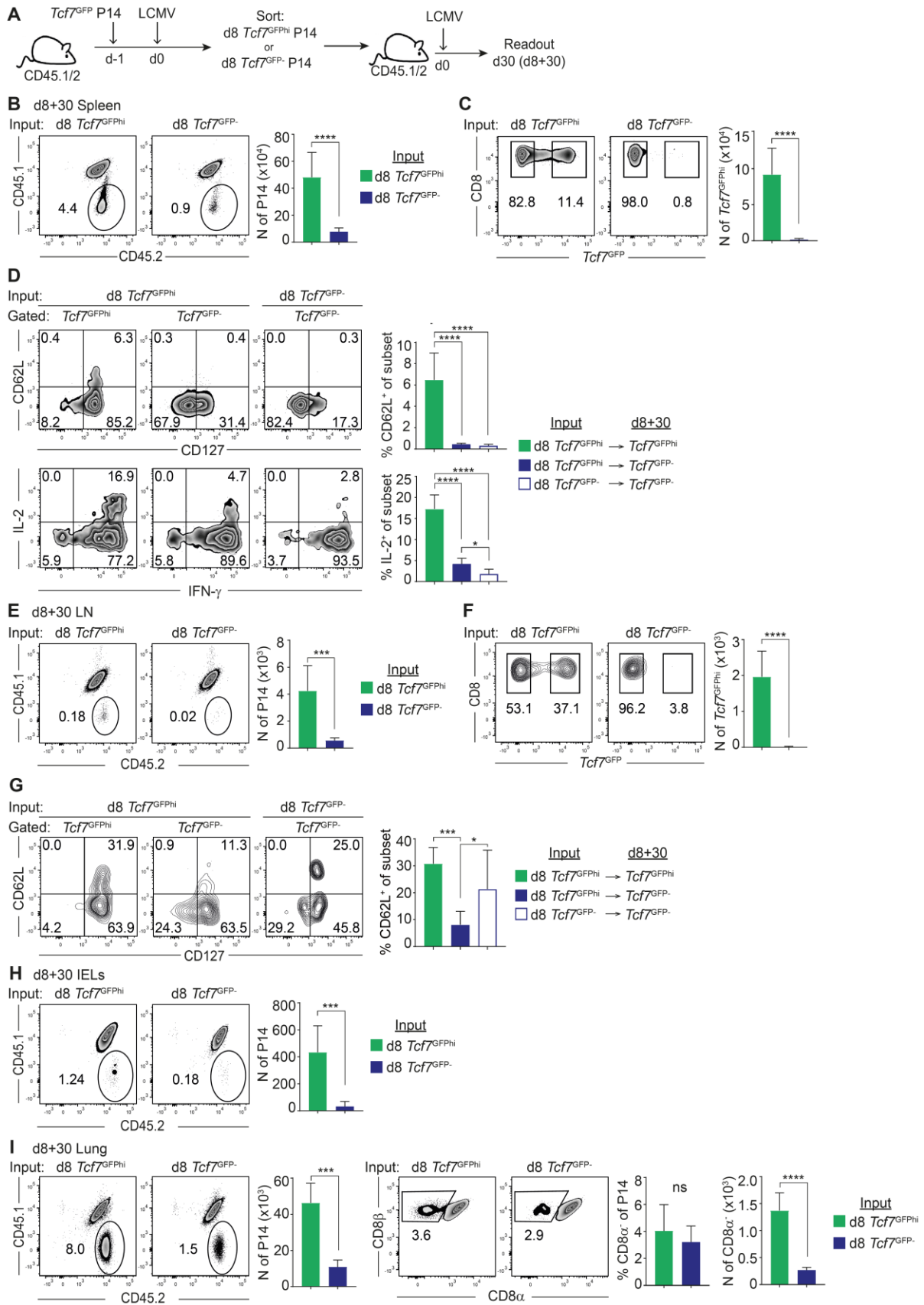
FIGURE 24: Effector-phase *Tcf7*^{GFPhi} CD8⁺ T cells have multipotency.

B6 (CD45.1/2) mice were transplanted with *Tcf7*^{GFP} P14 cells (CD45.2) and infected with LCMV WE. Eight days later, *Tcf7*^{GFPhi} or *Tcf7*^{GFP-} P14 cells were flow sorted and equal numbers were transferred to naïve

secondary B6 (CD45.1/2) recipients. These were infected with LCMV WE and analyzed on d30 p.i. (d8+30), as seen in (**A**). Before analysis mice were injected i.v. with an anti-CD8α mAb and sacrificed 5 min later. (**B-D**) Splenic P14 cells (d8+30) were analyzed for (**B**) their abundance, for (**C**) the expression of *Tcf7*GFP and (**D**) gated *Tcf7*GFPhi and *Tcf7*GFP- cells were analyzed for the expression of CD62L versus CD127 (top) and the production of IFN-γ and IL-2 (bottom). (**E-G**) P14 memory cells (d8+30) present in the LN were analyzed (**E**) for their abundance, (**F**) the expression of *Tcf7*GFP and (**G**) *Tcf7*GFPhi and *Tcf7*GFP- P14 memory cells (d8+30) were analyzed for the expression CD62L and CD127. (**H**) Abundance of P14 cells (d8+30) among Intraepithelial lymphocytes (IELs) of the small intestine, or (**I**) resident in the lung, i.e. CD8+ T cells not stained with the i.v. injected anti-CD8α mAb.

Data are compiled from of 3 independent experiments with n=11-12 mice per group (**B, C, D**), pooled from 2 experiments with n=6-7 mice per group (**E, F, G, H**) or representative of 2 experiments with n=5 mice per group (**I**). Mean ±SD are shown. Statistics are based on Non-paired two-tailed Student's test (**B, C, E, F, H, I**) or on One-Way ANOVA with Tukey's test (**D, G**) with *: $p<0.05$; ***: $p<0.001$; ****: $p <0.0001$ and (ns) $p>0.05$.

Ablation of effector-phase *Tcf7*GFPhi CD8+ T cells impairs TCM formation

To determine the relationship between *Tcf7*GFPhi effector-stage cells and central memory cells in intact mice we used mice expressing a *Tcf7*DTR-GFP construct (**Fig. 25A**) [192]. Similar to the *Tcf7*GFP reporter mice, *Tcf7*DTR-GFP mice were generated by the insertion of a diphtheria toxin receptor (DTR) - T2A - GFP fusion gene into the *Tcf7* locus present on a Bacterial Artificial Chromosome (BAC). *Tcf7*DTR-GFP mice were then crossed with P14 transgenic mice, in order to deplete LCMV-specific *Tcf7*+ CD8+ T cells *in vivo* using diphtheria toxin (DT). Naive P14 cells from *Tcf7*DTR-GFP mice homogenously expressed GFP, which corresponded to the expression of Tcf1 protein (**Fig. 25B**). The intensity of GFP expression was, however, lower compared to cells expressing the *Tcf7*GFP construct. *Tcf7*DTR-GFP or control *Tcf7*GFP P14 cells from naive mice were then adoptively transferred into Wt recipients (termed chimeric mice hereafter) that were then infected with LCMV. As expected, only a minority of P14 cells (2.2%) expressed high levels of *Tcf7*DTR-GFP at d8 p.i. (**Fig. 25C, left**). These cells were flow sorted to perform intranuclear Tcf1 staining. d8 *Tcf7*DTR-GFP+ cells expressed uniformly high levels of endogenous Tcf1 protein (**Fig. 25C, right**), demonstrating that the *Tcf7*DTR-GFP construct was properly regulated.

To investigate the developmental potential of effector-phase *Tcf7*GFP+ cells, as well as to assess the contribution of *Tcf7*GFP- cells to the central memory compartment, mice were treated with DT (or PBS - Ø) starting at day 10 p.i. (**Fig. 25D**). The treatment started when approximately 6% of the P14 cells expressed *Tcf7*DTR-GFP and consisted of 4 DT injections. One day after the last injection (d16), mice were analyzed to verify the efficacy of the DT mediated deletion (**Fig. 25E**). While both the PBS (Ø) treated *Tcf7*DTR-GFP and the DT treated *Tcf7*GFP chimeras harbored considerable populations of GFP+ P14 cells (~30%), such cells were largely absent in DT treated *Tcf7*DTR-GFP chimeras (0.21%) (~100 cells/spleen) (**Fig. 25E**). Thus, DT treatment efficiently depleted *Tcf7*DTR-GFP+ P14 cells.
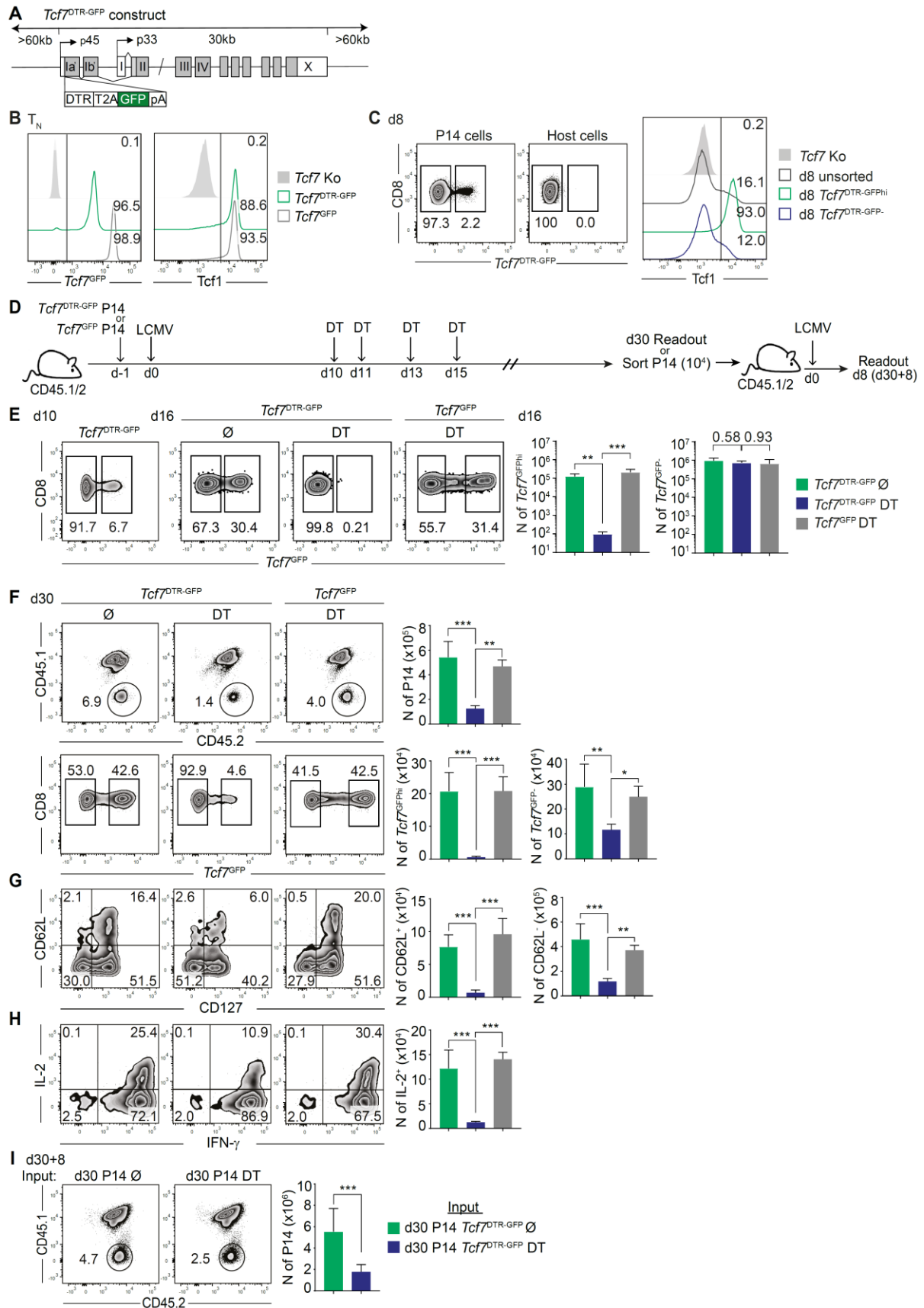
FIGURE 25: Central memory development is compromised upon lineage ablation of effector-phase *Tcf7*[GFPhi] CD8+ T cells.

(**A**) Schematic representation of the *Tcf7*[DTR-GFP] construct. A diphtheria toxin receptor (DTR) T2A green fluorescent protein (GFP) fusion gene was inserted into the first exon of the *Tcf7* locus (present on a > 150kb

BAC) and was used to generate $Tcf7^{DTR-GFP}$ transgenic mice. (**B**) Histogram plots show CD8$^+$ T P14 cells from naïve $Tcf7$ Ko mice (grey fill), $Tcf7^{DTR-GFP}$ mice (green open) or $Tcf7^{GFP}$ mice (grey open), analysed for the expression of GFP (left) or intranuclear Tcf1 (right). (**C**) $Tcf7^{DTR-GFP}$ P14 cells (CD45.2) were transferred into WT (CD45.1/2) recipients that were then infected with LCMV Arm. Splenic P14 $Tcf7^{DTR-GFP}$ cells were analyzed for GFP expression at d8 p.i. (left). GFP^{hi} (green) and GFP$^-$ P14 cells (blue) were flow sorted and analyzed for Tcf1 expression compared to total unsorted P14 cells (grey) or $Tcf7$ Ko cells (grey fill). (**D**) $Tcf7^{DTR-GFP}$ or control $Tcf7^{GFP}$ P14 cells (CD45.2) were transferred into WT (CD45.1/2) recipients that were infected with LCMV Arm. Mice were left untreated (Ø) or were injected with Diphtheria Toxin (DT) starting on d10 p.i., with a total of 4 injections (i.p.). Spleen cells were analyzed (**E**) one day after the last DT injection (i.e. d16 p.i.) or (**F-H**) on d30 p.i.. (**E**) $Tcf7^{GFP}$ expression prior to (d10) and upon DT treatment (d16) in P14 cells. The bar graph depicts the abundance of $Tcf7^{GFPhi}$ (left) and $Tcf7^{GFP-}$ (right) P14 cells in DT treated and untreated mice at d16. Splenic P14 memory cells (d30) were analyzed for (**F**) their abundance (top) and expression of $Tcf7^{DTR-GFP}$ (or control $Tcf7^{GFP}$) (bottom), for (**G**) their expression of CD62L versus CD127 or for (**H**) their production of IFN-γ and IL-2 after 5h of *in vitro* gp33 peptide re-stimulation. (**I**) Recall expansion capacity. The abundance of secondary splenic P14 cells (d30+8) was analyzed 8 days after equal numbers of flow sorted total d30 P14 cells from DT treated or untreated mice (Ø) were transferred to naive secondary mice, challenged with LCMV WE.

Data shown are representative of 2 independent experiments with n=4-5 mice per group. Mean ±SD are shown. Statistics are based on Non-paired two-tailed Student's test (**I**) or on One-Way ANOVA with Tukey's test (**E-H**) with *: $p<0.05$; **: $p<0.01$; ***: $p<0.001$; and (ns) $p>0.05$.

DT treated $Tcf7^{DTR-GFP}$ chimeras were then analyzed on d30 post-infection. The overall splenic memory compartment was significantly reduced (~4 fold) following DT treatment, as judged by the number of P14 cells (**Fig. 25F**). Thus, depletion of rare $Tcf7$ expressing effector-stage cells (6%) had a considerable effect on the total memory compartment. More remarkably, based on the abundance of P14 cells expressing $Tcf7^{DTR-GFP}$, CD62L or IL-2, T$_{CM}$ cells were reduced 10-20 fold in these mice (**Fig. 25F-H**). This reduction was not due to DT toxicity since the memory compartment of DT treated mice harboring $Tcf7^{GFP}$ P14 control cells was of normal size and phenotype (**Fig. 25F-H**). The number of $Tcf7^{DTR-GFP-}$ and CD62L$^-$ memory cells was also diminished in DT treated mice (**Fig. 25F, G**). Finally, the recall expansion capacity of P14 memory cells was significantly impaired when mice had been treated with DT (**Fig. 25I**), suggesting an overall dysfunctional central memory compartment when effector-stage $Tcf7^{GFP+}$ cells were depleted.

$Tcf7^{DTR-GFP+}$ cells were stably and almost quantitatively depleted by DT treatment (**Fig. 25F**). Despite the substantial reduction of $Tcf7^{DTR-GFP+}$ cells in DT treated mice, some central memory phenotype P14 cells were detected at d30 p.i. (~5000 $Tcf7^{DTR-GFP+}$ P14 /spleen) and these were more abundant than on d16 p.i. (~100 $Tcf7^{DTR-GFP+}$ P14 /spleen). An occasional conversion of $Tcf7^-$ cells into central memory phenotype cells could thus not be excluded. However, their contribution to the central memory pool (10^5 cells) was minor (5%), demonstrating that central memory chiefly derived from $Tcf7^+$ effector-stage cells.

Tcf1 ensures the recall expansion and self-renewal capacities of *Tcf7*^{GFPhi} effector-phase cells

Given that *Tcf7* expression defined a population of effector-stage cells with T_{CM} function, we next explored the importance of Tcf1 for the development and function of these cells. To address this, we generated *Tcf7*^{-/-} (Ko) *Tcf7*^{GFP} P14 mice, that lacked the endogenous Tcf1 protein expression (**Fig. 26A**). P14 cells isolated from naive Ko reporter mice retained high levels of *Tcf7*^{GFP} expression (**Fig. 26A**), showing that *Tcf7* expression is not dependent on Tcf1 protein and that these mice could be used to track *Tcf7*^{GFPhi} cells lacking Tcf1 protein.
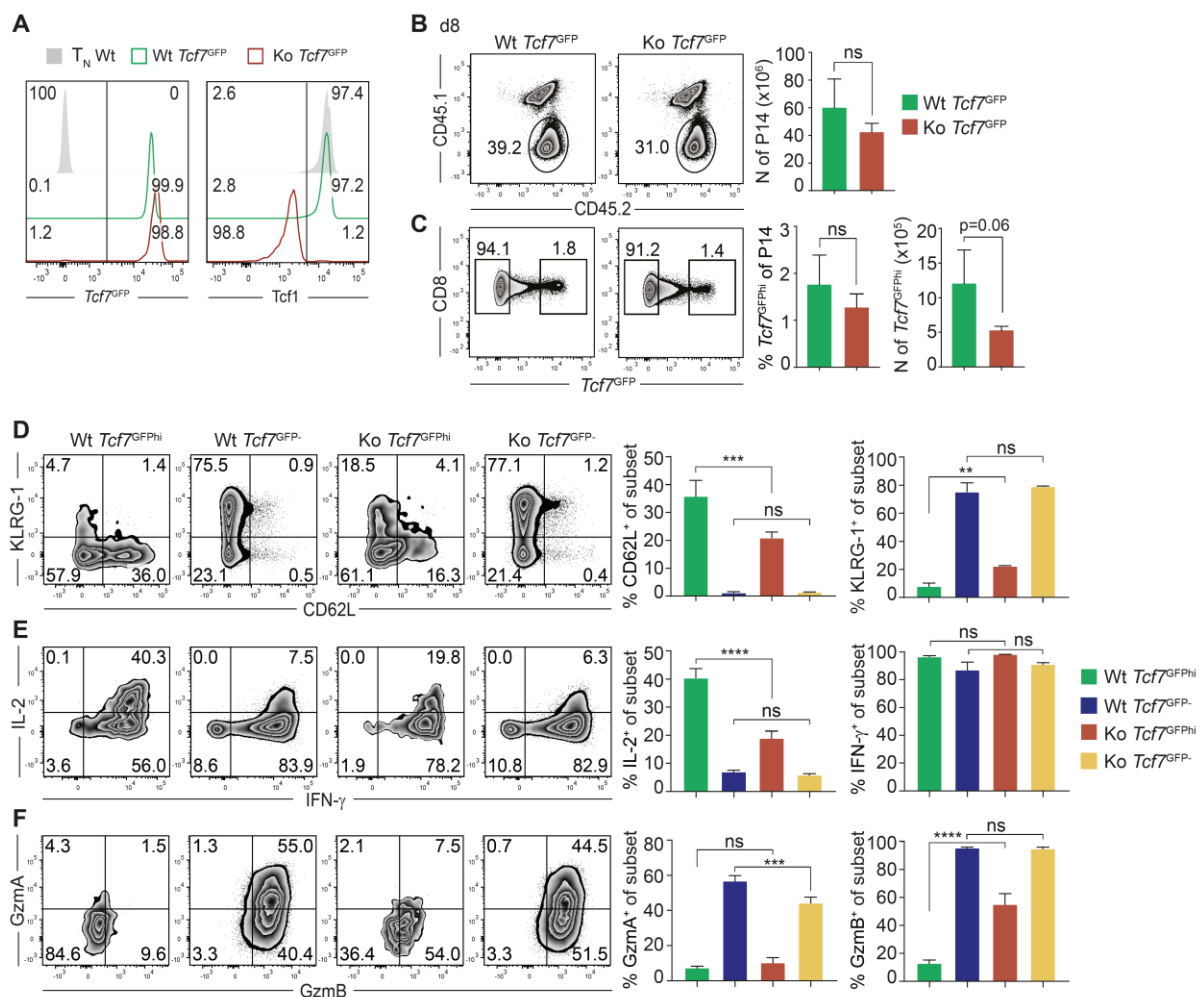
FIGURE 26: Primary expansion and phenotype of *Tcf7*^{-/-} (Ko) *Tcf7*^{GFPhi} effector-phase cells. (**A**) CD8⁺ T cells from naive Wt *Tcf7*^{GFP} P14 (green), *Tcf7*^{-/-} (Ko) *Tcf7*^{GFP} P14 (red) or Wt P14 mice (grey) were analyzed for the expression of GFP (*Tcf7*^{GFP}) (left) and Tcf1 protein (right). (**B-F**) B6 (CD45.1/2) mice were transplanted with Wt or Ko *Tcf7*^{GFP} P14 cells (CD45.2), infected with LCMV WE and analyzed 8 days later. Primary Wt or Ko P14 cells (d8) were analyzed for (**B**) their abundance in the spleen, (**C**) the expression of *Tcf7*^{GFP} and gated *Tcf7*^{GFPhi} and *Tcf7*^{GFP-} P14 cells were analyzed for (**D**) the expression of KLRG-1 and CD62L, for (**E**) the ability to produce IL-2 and IFN-γ or for (**F**) the expression of GzmA and GzmB.
Data are representative of at least 3 experiments with n=4 mice per group (**B, C, D**), representative of 2 experiments with n=5-6 mice per group (**E**) or from one experiment with n=5 mice in (**F**). Mean ±SD are shown. Statistics are based on Non-paired two-tailed Student's test (**B, C**) or on One-Way ANOVA with Tukey's test (**D, E, F**) with **: $p<0.01$; ***: $p<0.001$; ****: $p<0.0001$ and (ns) $p>0.05$.

Following adoptive transfer and acute LCMV stimulation, the d8 Wt and Ko $Tcf7^{GFP}$ P14 compartments were of similar size (~35% of CD8$^+$ T cells) (**Fig. 26B**), suggesting that Ko cells mount a normal primary immune response to LCMV infection. Additionally, both P14 populations contained a comparable fraction of $Tcf7^{GFPhi}$ cells (~1.5%) (**Fig. 26C**). Nonetheless, the number of d8 $Tcf7^{GFPhi}$ cells was modestly reduced among Ko P14 cells and their phenotype was different from that of the corresponding Wt cells (**Fig. 26D-F**). Ko $Tcf7^{GFPhi}$ effector-stage cells exhibited increased KLRG-1 expression, but decreased CD62L expression, when compared to Wt $Tcf7^{GFPhi}$ cells (**Fig. 26D**). In addition, upon peptide re-stimulation, production of IL-2 was reduced, while IFN-γ production was equivalent among Wt and Ko $Tcf7^{GFPhi}$ effector-phase cells (**Fig. 26E**). Finally, the latter cells produced significantly more GzmB, but not GzmA, compared to Wt $Tcf7^{GFPhi}$ cells (**Fig. 26F**). Notably, the phenotype of Wt and Ko $Tcf7^{GFP-}$ cells was not different (**Fig. 26D-F**). Overall, effector-phase $Tcf7^{GFPhi}$ cells could be generated in the absence of Tcf1, however they displayed a more differentiated phenotype.

Since Ko $Tcf7^{GFPhi}$ effector-phase cells displayed a diminished T$_{CM}$ phenotype we next addressed their stemness (as schematically shown in **Fig. 27A**). Upon re-challenge (d8+8) we found that Wt P14 $Tcf7^{GFPhi}$ cells had expanded significantly more than the Ko $Tcf7^{GFPhi}$ cells (**Fig. 27B**), indicating that recall expansion capacity of $Tcf7^{GFPhi}$ cells was compromised in the absence of Tcf1. Consistent with the results described above, re-stimulation of Wt d8 $Tcf7^{GFPhi}$ cells yielded a sizable population of secondary $Tcf7^{GFPhi}$ cells that had expanded compared to input (**Fig. 27C, D**). In sharp contrast, Ko d8 $Tcf7^{GFPhi}$ cells essentially failed to generate secondary $Tcf7^{GFPhi}$ cells. Therefore, effector-phase $Tcf7^{GFPhi}$ cells lacking Tcf1 failed to self-renew in response to antigen re-challenge.

In addition, we determined if Tcf1 expression was necessary for the homeostatic expansion / maintenance of $Tcf7^{GFPhi}$ cells. For this purpose, we adoptively transferred either Wt or Ko $Tcf7^{GFPhi}$ cells into Rag2$^{-/-}$ γc$^{-/-}$ recipient mice, which lack mature T, B and NK cells (**Fig. 27E**). T cells transferred into such hosts undergo homeostatic proliferation [226]. In order to avoid LCMV carry over, P14 cells were sorted and transferred at day 15 p.i.. Eight days later (d15+8) Wt but not Ko $Tcf7^{GFPhi}$ cells had undergone considerable homeostatic expansion (**Fig. 27F**). Moreover, transferred Ko $Tcf7^{GFPhi}$ cells yielded significantly fewer $Tcf7^{GFPhi}$ progeny during homeostatic conditions (**Fig. 27G**). Lastly, the expression of CD62L was drastically reduced in P14 cells derived from the Ko $Tcf7^{GFPhi}$ cells compared to Wt cells (**Fig. 27H**). Wt and Ko $Tcf7^{GFP-}$ cells had undergone comparable and reduced homeostatic expansion (**Fig. 27F**).

Overall, the data suggested that both the antigen-driven and cytokine-driven (homeostatic) expansion potential of effector-phase $Tcf7^{GFPhi}$ cells relied on Tcf1 protein expression. Tcf1

thus seemed to ensure the stem cell-like properties of $Tcf7^{GFPhi}$ cells by preventing differentiation and maintaining self-renewal capacity.
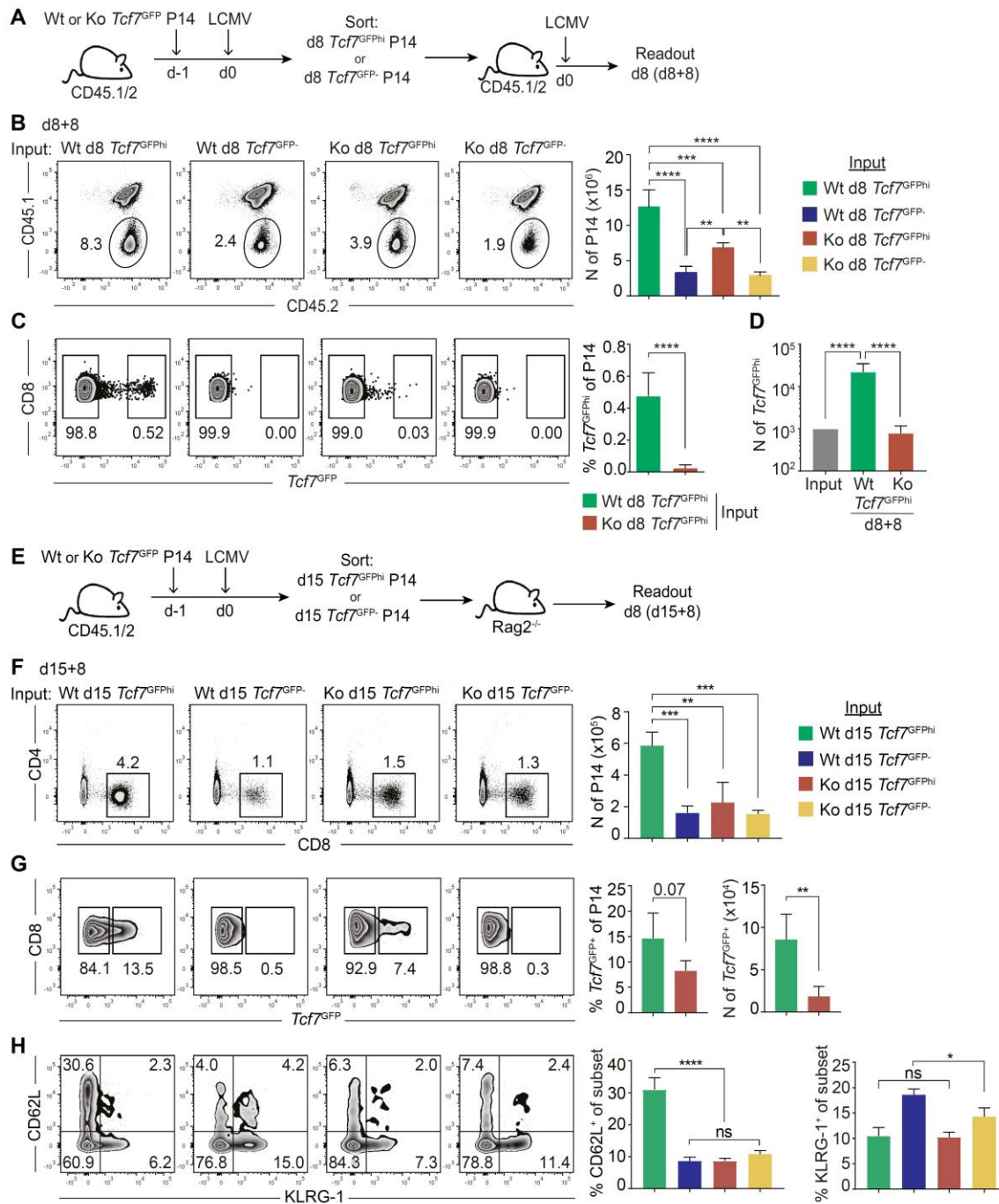
FIGURE 27: Tcf1 is essential for the stemness of $Tcf7^{GFPhi}$ effector-phase CD8^{+} T cells. (**A-D**) Wt and Ko $Tcf7^{GFPhi}$ or $Tcf7^{GFP-}$ P14 cells (CD45.2) were flow sorted at d8 p.i. and equal numbers of cells were transplanted into B6 (CD45.1/2) mice that were infected with LCMV WE, as schematically seen in (**A**). Eight days later (d8+8), P14 cells were analyzed for (**B**) their abundance in the spleen and (**C**) the expression of $Tcf7^{GFP}$. (**D**) The bar graph depicts the abundance of secondary $Tcf7^{GFPhi}$ cells compared to input. (**E-H**) Wt and Ko $Tcf7^{GFPhi}$ or $Tcf7^{GFP-}$ P14 cells (CD45.2) were flow sorted at d15 p.i. and equal numbers of cells were transplanted into Rag2^{-/-} γc^{-/-} recipient mice (**E**). T cell populations were investigated eight days later (d15+8), in which (**F**) donor CD8^{+} T cells (P14) were gated. Gated P14 CD8^{+} T cells were analyzed for (**G**) their expression of $Tcf7^{GFP}$ or (**H**) their expression of CD62L versus KLRG-1.

The data shown are compiled from 2 independent experiments with n=5-7 mice per group in (**B-D**) or are representative of 2 independent experiments with n=4 mice per group (**F-H**). Mean ±SD are shown. Statistics are based on Non-paired two-tailed Student's test (**C, G**) or on One-Way ANOVA with Tukey's test (**B, D, F, H**) with *: p<0.05; **: p<0.01; ***: p<0.001; ****: p <0.0001 and (ns) p>0.05.

Tcf7^{GFPhi} effector-phase cells lacking Tcf1 display an effector gene signature

To begin to address the basis for the impaired stemness of Tcf1 deficient effector-phase cells, we performed RNA sequencing analysis of Wt and Ko d8 *Tcf7*^{GFPhi} cells. The Wt and Ko d8 *Tcf7*^{GFPhi} populations displayed unique transcriptomic states based on Principal Component Analysis (PCA) (**Fig. 28A**), but also based on the number of differentially expressed genes (DEGs) (n=607, 318 up and 289 down, based on FDR <5%, FC>2). On the other hand, the Wt and Ko d8 *Tcf7*^{GFP-} cells co-clustered in the PCA and few genes were differentially expressed (DEG n=72, 35 up, 37 down). The data indicated that absence of Tcf1 expression mostly impacted the *Tcf7*^{GFPhi} population and further supported the lack of phenotypic differences in *Tcf7*^{GFP-} cells observed in **Fig. 26D-F**. We then compared the transcriptome of either d8 *Tcf7*^{GFPhi} population to that of Wt *Tcf7*^{GFP-} effector cells (**Fig. 28B**). Significantly fewer genes were differently regulated between the Ko *Tcf7*^{GFPhi} versus Wt *Tcf7*^{GFP-} cells (n=2'197), compared to Wt *Tcf7*^{GFPhi} versus Wt *Tcf7*^{GFP-} cells (n=2'998). The data thus suggested that Ko *Tcf7*^{GFPhi} cells were less distinct from the *Tcf7*^{GFP-} cells, compared to Wt *Tcf7*^{GFPhi} cells. In agreement with this notion, Ko d8 *Tcf7*^{GFPhi} cells overexpressed multiple effector genes, including cytotoxic effector proteins (*Gzms*, *FasL*), effector cell markers (*Cx3cr1*, *IL2ra*) and transcription factors (*Prdm1*) (**Fig. 28C**). Therefore, Tcf1 expression counteracted the differentiation of effector-phase *Tcf7*^{GFPhi} cells.

Interestingly, GSEA revealed that Ko d8 *Tcf7*^{GFPhi} cells were enriched in an IL-2 STAT5 signaling signature (**Fig. 28D**). We thus assessed the activation of several STAT proteins in Wt and Ko d8 *Tcf7*^{GFPhi} cells in response to cytokines. We saw no difference in the activation i.e. phosphorylation of STAT3 (pSTAT3) among Wt and Ko d8 *Tcf7*^{GFPhi} cells in response to IL-21 stimulation (**Fig. 28E**). However, following stimulation with IL-12, Ko *Tcf7*^{GFPhi} cells expressed slightly more pSTAT4 than Wt (**Fig. 28E**). STAT4 promotes effector differentiation [118, 227] and IL-12 (via STAT4) has been shown to downregulate Tcf1 in activated T cells [182]. Most impressively, IL-2 stimulation of Ko d8 *Tcf7*^{GFPhi} cells induced strong STAT5 activation (~55% pSTAT5⁺), while pSTAT5 in Wt *Tcf7*^{GFPhi} cells was weak (~14%) (**Fig. 28E**). Thus, Ko *Tcf7*^{GFPhi} cells had an increased responsiveness to IL-2 and IL-12, which may account for their increased differentiation.

Increased IL-2 STAT5 signaling induces the expression of the transcription factor Blimp1 (*Prdm1*) [89, 97, 228, 229], which in turn contributes to elevated expression of effector molecules,

such as KLRG-1, perforin and GzmB [88, 89, 230]. Thus, high IL-2 STAT5 signaling seemed to favor the differentiation of Tcf1 deficient effector-phase *Tcf7*^{GFPhi} cells.
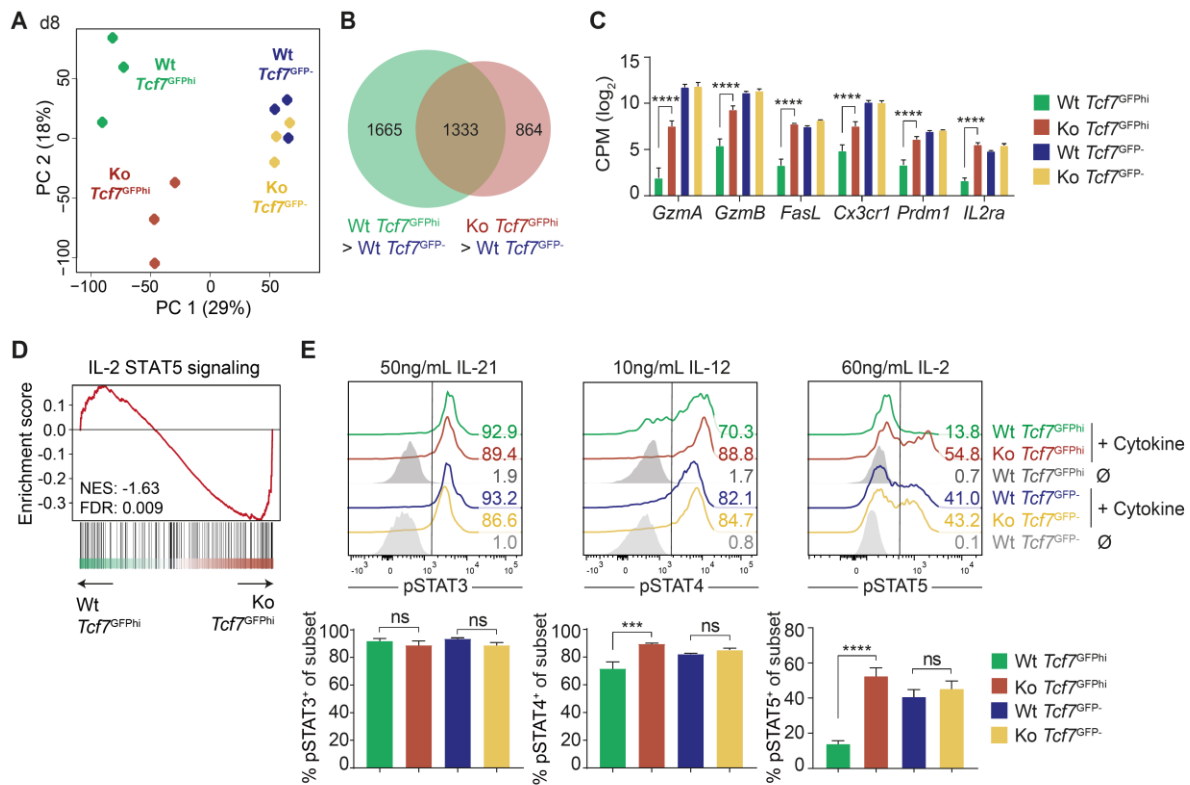
FIGURE 28: Ko *Tcf7*^{GFPhi} effector-phase cells show increased effector differentiation.
(**A-D**) B6 (CD45.1/2) mice were transplanted with Wt or Ko *Tcf7*^{GFP} P14 cells (CD45.2), infected with LCMV Arm and flow sorted P14 subsets were subjected to RNAseq analysis at d8 p.i.. (**A**) PCA of Wt and Ko *Tcf7*^{GFPhi} and *Tcf7*^{GFP-} cells. Each dot represents an individual sample, n=3 samples per condition. (**B**) Venn diagram showing the number of genes differentially expressed between Wt and Ko *Tcf7*^{GFPhi} cells each relative to Wt *Tcf7*^{GFP-} cells. (**C**) Expression of the indicated cytotoxic/effector genes (based on RNAseq) by the indicated populations of d8 Wt or Ko P14 cells. CPM: counts per million. (**D**) Gene set enrichment analysis of Wt d8 *Tcf7*^{GFPhi} vs Ko d8 *Tcf7*^{GFPhi} cells identified a significant enrichment of the IL-2 STAT5 signaling pathway in Ko d8 *Tcf7*^{GFPhi} cells. (**E**) Wt and Ko *Tcf7*^{GFPhi} and *Tcf7*^{GFP-} P14 cells were flow sorted at d8 p.i., stimulated with IL-21, IL-12 or IL-2 and analyzed for phosphorylated STAT3 (pSTAT3), pSTAT4 or pSTAT5, respectively. Some samples were left un-stimulated (Ø) for a negative staining control.
Bioinformatic analyses were performed by Dr. Tania Wyss, UNIL. Data are derived from n=3 biological replicates per population (**A-D**) or representative of 2 independent experiments with n=3 mice per group in (**E**). Mean ±SD are shown. Statistics are based on Two-Way ANOVA with Tukey's test (**C**) or on One-Way ANOVA with Tukey's test (**E**) with ***: $p<0.001$; ****: $p <0.0001$ and (ns) $p>0.05$.

Forced expression of IL2rα is not sufficient to impair the generation and/or function of Wt *Tcf7*^{GFPhi} effector-phase cells

CD8⁺ T cells with increased expression of the high-affinity IL-2 receptor subunit α (IL2rα or CD25) during the early phase of LCMV infection are more likely to terminally differentiate [88, 89]. Since Ko *Tcf7*^{GFPhi} cells displayed increased IL-2 STAT5 signaling and *IL2ra* mRNA (**Fig.**

28C), we addressed whether overexpression of IL2rα favored the differentiation of Wt *Tcf7*^{GFPhi} cells. Naive Wt *Tcf7*^{GFP} P14 CD8$^+$ T cells were activated *in vitro* and transduced with a Retrovirus (RV) construct containing murine IL2rα and RFP. Alternatively, the cells were transduced with a control (Ctrl) RV expressing RFP only. Transduced *Tcf7*^{GFP} P14 cells (CD45.2) were adoptively transferred into Wt recipient mice (CD45.1), which had been infected with LCMV the day before (**Fig. 29A**). Alternatively, the cells were kept *in vitro* to verify the efficiency of the transduction (**Fig. 29B**). After 48 hours of culture we observed that the majority of the transduced cells expressed RFP (**Fig. 29B**).

At day 8 post-infection, Ctrl and IL2rα RV-infected cells harbored a comparable population of RFP$^+$ P14 cells (**Fig. 29C, D**), suggesting that the primary response to acute infection was not impacted by enforced CD25 expression. While the expression of IL2rβ (CD122) was equivalent among RFP$^+$ cells, IL2rα RV-transduced cells (RFP$^+$) indeed overexpressed cell surface CD25 (**Fig. 29E**). The number of d8 *Tcf7*^{GFPhi} cells expressing CD25 was equivalent to the control (**Fig. 29F**), demonstrating that the formation of *Tcf7*^{GFPhi} effector-phase cells was not influenced by increased IL2rα expression.

In addition, the phenotype of transduced Wt d8 *Tcf7*^{GFPhi} cells was also not significantly altered upon overexpression of IL2rα (**Fig. 29G-J**). The expression of T$_{CM}$ / stem cell-like memory markers, such as CD62L (**Fig. 29G**) or Sca-1 (**Fig. 29H**), was equivalent and we found no evidence for increased KLRG-1 or Cx3cr1 expression (**Fig. 29I**). If anything, we saw a decreased expression of these effector markers in IL2rα$^+$ d8 *Tcf7*^{GFPhi} cells. Moreover, upon peptide re-stimulation, IL-2 and IFN-γ production was equivalent (**Fig. 29J**), while IL2rα$^+$ *Tcf7*^{GFPhi} cells produced higher amounts of TNF-α, compared to Ctrl cells (**Fig. 29J**).

Finally, we evaluated the recall expansion capacity of transduced d8 *Tcf7*^{GFPhi} and *Tcf7*^{GFP-} cells (as schematically shown in **Fig. 29A**). Eight days following re-challenge (d8+8) the re-expansion of both *Tcf7*^{GFPhi} populations was similar (**Fig. 29K**). If anything, we detected a trend towards increased expansion of IL2rα$^+$ d8 *Tcf7*^{GFPhi} cells. A similar trend in favor of the IL2rα$^+$ d8 *Tcf7*^{GFPhi} population was noted for the number of secondary *Tcf7*^{GFPhi} cells (**Fig. 29L, M**).

In conclusion, overexpression of IL2rα did not impair the recall expansion or self-renewal of Wt *Tcf7*^{GFPhi} effector-phase cells. Rather, expression of IL2rα might improve stemness. Thus, the high expression of *IL2ra* observed in Ko *Tcf7*^{GFPhi} cells was not sufficient to explain differentiation of *Tcf7*^{GFPhi} cells.
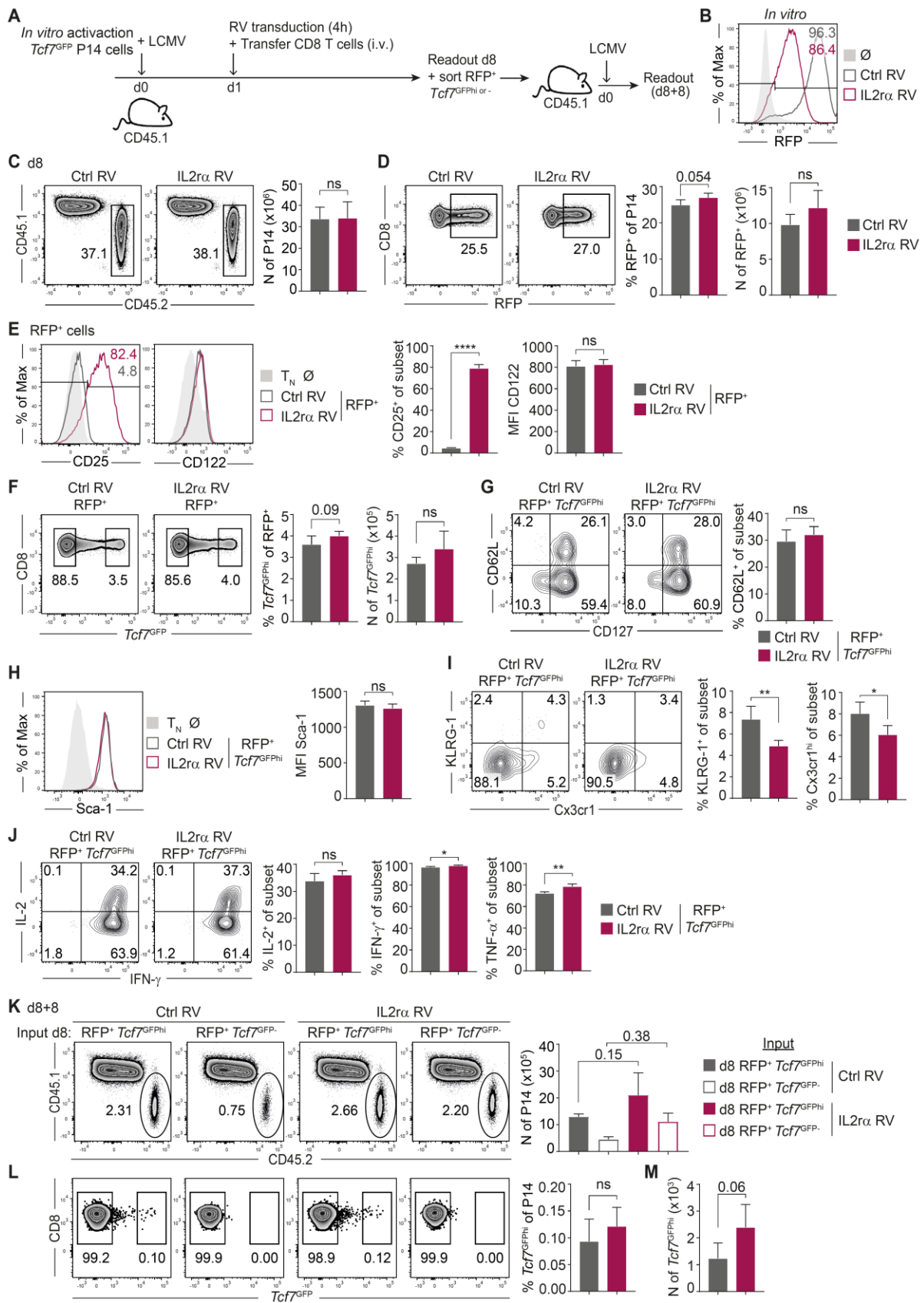
FIGURE 29: Overexpression of IL2rα does not affect the function of Wt d8 *Tcf7*^{GFPhi} cells.
In vitro activated *Tcf7*^{GFP} P14 CD8⁺ T cells (CD45.2) were transduced with Retroviral construct containing IL2rα and RFP (IL2rα RV) or with a control construct (Ctrl RV) and were transferred into B6 CD45.1 mice that had been infected with LCMV WE one day before. Splenic P14 cells were analyzed eight days later, as

schematically represented in (**A**). Alternatively, cells were kept in culture for 48h and (**B**) the transduction efficiency was determined, based on RFP expression (non-transduced – Ø). (**C-J**) On d8 p.i. P14 cells transduced with the indicated RV construct were analyzed for (**C**) their abundance in the spleen and (**D**) the expression of RFP. Transduced P14 cells (RFP⁺) were analyzed for the expression of (**E**) CD25 and CD122 or of (**F**) *Tcf7*^GFP. Gated RFP⁺ *Tcf7*^GFPhi P14 cells transduced with the indicated RV were analyzed for (**G**) the expression of CD62L versus CD127; (**H**) the expression of Sca-1; (**I**) the expression of KLRG-1 versus Cx3cr1 or (**J**) the production of IL-2, IFN-γ and TNF-α. (**K-M**) Transduced (RFP⁺) *Tcf7*^GFPhi and *Tcf7*^GFP- P14 cells (CD45.2) were flow sorted at d8 p.i. and transplanted into secondary B6 (CD45.1) mice that were infected with LCMV WE. Eight days later (d8+8), P14 cells were analyzed for (**K**) their abundance in the spleen and (**L**) for the expression of *Tcf7*^GFP. (**M**) The bar graph depicts the abundance of secondary *Tcf7*^GFPhi cells in each RV-transduced population.

The data are representative of 2 independent experiments with n=4-5 mice per group in (**C-J**) or from one experiment with n=3-4 mice in (**K-M**). Mean ±SD are shown. Statistics are based on Non-paired two-tailed Student's test (**C-J, L, M**) or on One-Way ANOVA with Tukey's test (**K**) with *: $p<0.05$; **: $p<0.01$; ****: $p <0.0001$ and (ns) $p>0.05$.

Tcf1 preserves the expression of a set of adult stem cell-associated genes

Since the phenotypic differences observed between Wt and Tcf1-deficent *Tcf7*^GFPhi effector-stage cells remained unexplained, we continued to explore their molecular differences. GSEA revealed that the transcriptome of Ko d8 *Tcf7*^GFPhi cells still overlapped extensively with a T_CM gene signature [207] and even with a stem cell-like memory signature [82] (**Fig. 30A**). Moreover, the expression of genes known to be important for central memory formation and function, such as *Bcl6*, *Foxo1, Id3, Myb* or *STAT3*, were also not affected (**Fig. 30B**). However, we noted that *Tcf7*^GFPhi effector-phase cells lacking Tcf1 no longer overlapped with the hematopoietic stem cell [210] or the adult stem cell [211] gene signatures (**Fig. 30A**). To identify relevant and conserved targets, we combined the genes upregulated in the hematopoietic stem cell (n=517), the adult stem cell (n=494) and the Wt d8 *Tcf7*^GFPhi (n=602) lists. This approach identified 18 adult stem cell genes that were shared among the 3 gene signatures. Eight of these genes were reduced in Ko d8 *Tcf7*^GFPhi cells (*Armcx2*, *Cpq*, *Cyp4v3*, *Elovl6*, *Kit*, *Klf4*, *Plxdc2* and *Smad1*) (**Fig. 30C**). Thus, the compromised stemness of Ko *Tcf7*^GFPhi effector-stage cells correlated with reduced expression of adult stem cell genes.

To test their importance for CD8⁺ T cell stemness, we generated lentivirus (LV) based short-hairpin (sh) RNA constructs for 6 of the 8 Tcf1-dependent adult stem cell genes, including *Armcx2*, *Elovl6*, *Kit*, *Klf4*, *Plxdc2* and *Smad1*. We also designed sh LV constructs for *Tcf7* as a positive control (because there was a possibility that the results obtained with the Ko *Tcf7*^GFP mice could be secondary to impaired T cell development [231]) and included a scrambled shRNA construct (Ctrl sh) as a negative control. Sh constructs were chosen in order to reproduce the partial reduction of gene expression observed in *Tcf7*^GFP- cells. Each gene of interest was targeted with 2 or 3 independent LV sh constructs that included a mCherry reporter.
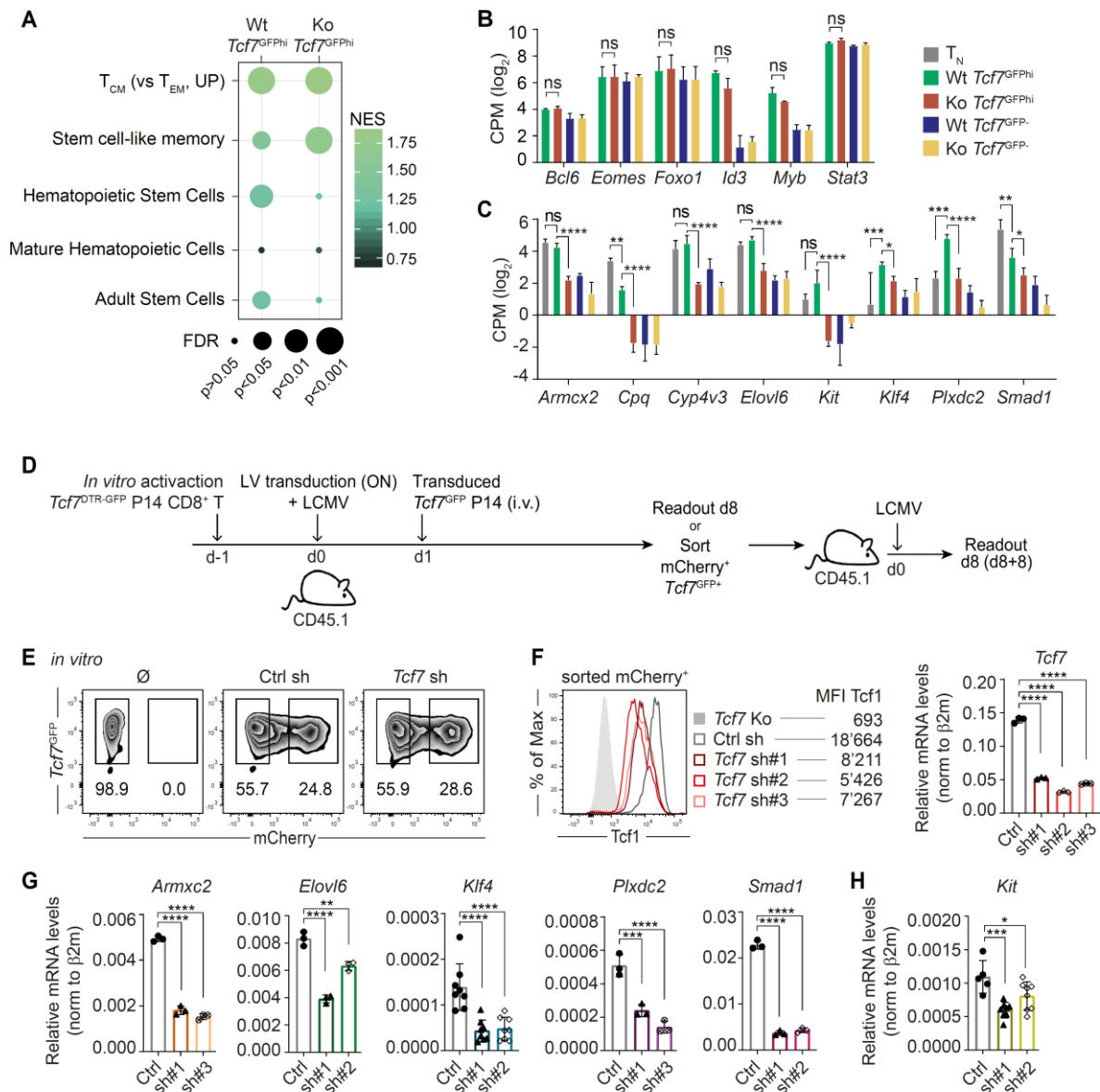
FIGURE 30: Tcf1 maintains an adult stem cell gene expression program in d8 *Tcf7*^{GFPhi} cells. (**A-C**) B6 (CD45.1/2) mice were transplanted with Wt or Ko *Tcf7*^{GFP} P14 cells (CD45.2), infected with LCMV Arm and flow sorted *Tcf7*^{GFPhi} and *Tcf7*^{GFP-} P14 subsets were subjected to RNAseq analysis at d8 p.i.. (**A**) Compiled GESA data of Wt and Ko *Tcf7*^{GFPhi} cells (each versus Wt *Tcf7*^{GFP-}) relative to upregulated genes in T_{CM} (vs T_{EM}) [207], in a stem cell-like memory signature [82], in hematopoietic stem cells and in mature hematopoietic cells [210] and in adult stem cells [211]. The dot size and color indicate the FDR and the normalized enrichment score (NES), respectively. Expression of (**B**) the indicated central memory/stemness genes or of (**C**) 8 out of 18 genes shared between the hematopoietic and the adult stem cell signatures and Wt d8 *Tcf7*^{GFPhi} cells, showing Tcf1-dependence, by the indicated populations of d8 Wt or Ko P14 cells or naïve Wt *Tcf7*^{GFP} P14 cells. CPM: counts per million. (**D**) Schematic representation of the approach used to study the function of Tcf1-conserved genes: *Tcf7*^{DTR-GFP} (abbreviated hereafter to *Tcf7*^{GFP}) P14 (CD45.2) cells activated *in vitro* were transduced with Lenti-based sh RNA constructs or control (Ctrl) Sh construct, containing a scrambled sequence. All sh constructs have a mCherry reporter. Transduced CD8⁺ T cells were transferred into B6 CD45.1 mice that had been infected with LCMV Arm one day before. Alternatively, cells were kept in culture for 48h. (**E**) P14 cells transduced with indicated sh constructs (or non-transduced - Ø) were analyzed for transduction efficiency (mCherry⁺) 48 h post Lentivirus infection. Transduced P14 cells (mCherry⁺) (**F**) expressing *Tcf7* sh constructs were flow sorted and analyzed for Tcf1 protein and mRNA expression or (**G**) expressing the indicated sh constructs were flow sorted and analyzed using RT-qPCR for the gene of interest. (**H**) *Kit* sh transduced P14 cells (mCherry⁺) were flow sorted on d8 p.i. and analyzed using RT-qPCR for *Kit* expression. Expression levels were normalized to β2m.

Briefly, *in vitro* activated $Tcf7^{DTR-GFP}$ (abbreviated hereafter to $Tcf7^{GFP}$) P14 CD8+ T cells (CD45.2) were transduced overnight with LV and transplanted into recipient mice (CD45.1) that had been infected with LCMV one day earlier (**Fig. 30D**). Alternatively, transduced cells were kept in culture and analyzed for the expression of mCherry 48 hours later. Compared to untransduced cells (Ø), we observed a substantial population of transduced mCherry+ cells (~25%) with both the Ctrl sh and the gene targeting sh constructs (**Fig. 30E**). For simplicity FACS plots are only shown for the Ctrl and the *Tcf7* sh constructs. The transduction with all other sh LV constructs yielded comparable results in several experiments. Transduction with *Tcf7* sh reduced *Tcf7* expression among mCherry+ cells, as compared to Ctrl sh transduced cells, both based on FACS or qPCR analysis (**Fig. 30F**). Expression of the respective sh constructs reduced *Armcx2*, *Elovl6*, *Klf4*, *Plxdc2* and *Smad1* expression 48 hours post-transduction (**Fig. 30G**) or *ex vivo* at d8 p.i. (*Kit*) (**Fig. 30H**). Thus, all sh constructs significantly reduced the expression of their target gene.

We then performed individual gene knockdown in Wt $Tcf7^{GFP}$ cells and evaluated their expansion 8 days following primary LCMV infection. Even though the percentage of mCherry+ cells was similar at input, mCherry+ cells were severely reduced following knockdown of *Tcf7* (**Fig. 31A, B**). More impressively, *Tcf7* sh reduced the abundance of $Tcf7^{GFP+}$ mCherry+ cells by 16-fold (**Fig. 31A, B**). Thus, the development of Wt $Tcf7^{GFP+}$ effector-phase cells was considerably impaired when *Tcf7* was knocked down.

Compared to non-transduced cells (mCherry-), the residual d8 $Tcf7^{GFP+}$ mCherry+ *Tcf7* sh cells displayed reduced expression of CD62L and showed evidence of terminal differentiation, as determined by the increased expression of KLRG-1 and Cx3cr1 (**Fig. 31C**). In addition, while there was no difference in the production of IFN-γ, IL-2 production was reduced (**Fig. 31D**). The phenotype of mCherry+ $Tcf7^{GFP+}$ cells transduced with the Ctrl sh was not distinct from the mCherry- $Tcf7^{GFP+}$ cells (**Fig. 31C, D**). Finally, both the recall expansion (**Fig. 31E**) and self-renewal potential (**Fig. 31F**) of d8 $Tcf7^{GFP+}$ mCherry+ cells were also diminished following *Tcf7* knockdown. Overall, transduction of Wt $Tcf7^{GFP}$ P14 cells with *Tcf7* sh reproduced the results obtained with Ko $Tcf7^{GFP}$ cells (**Fig. 26, 27**). These data suggested that results obtained with Ko $Tcf7^{GFP}$ cells were not due to T cell developmental defects and they validated our approach to test the function of the adult stem cell genes.

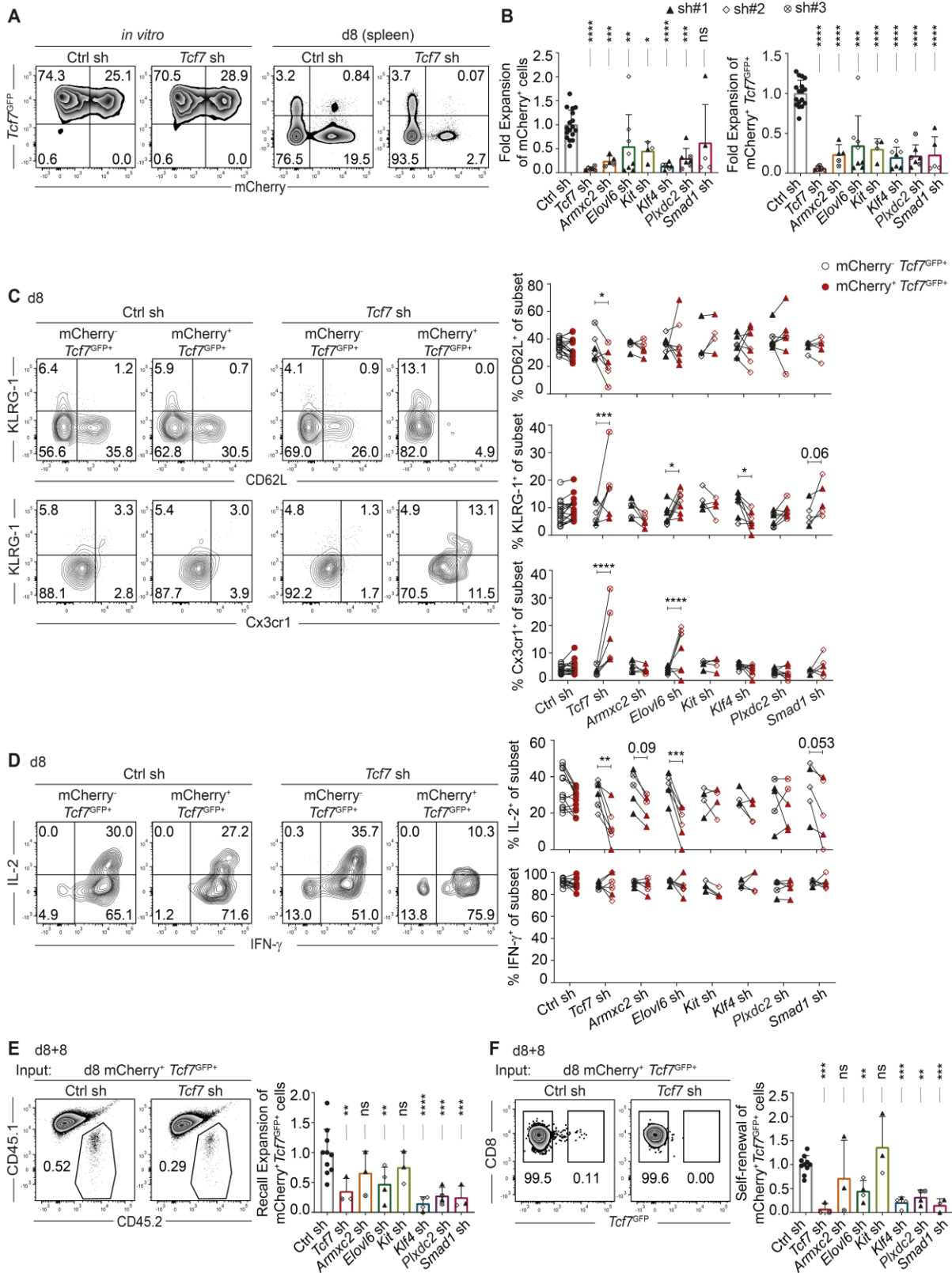**FIGURE 31:** Tcf1-dependent adult stem cell genes are essential for CD8^{+} T cell stemness. Activated P14 *Tcf7*[GFP] cells were transduced with Lentiviral sh RNA constructs to the indicated genes or a scrambled control (Ctrl) construct. (**A**, left) Transduction efficiency was determined *in vitro* based on mCherry expression. P14 cells (containing 20-30% transduced cells) (CD45.2) were transferred into B6 CD45.1 mice

that had been infected with LCMV Arm one day before. On d8 p.i. P14 cells were analyzed for (**A**, right) the presence of mCherry$^+$ and $Tcf7^{GFP+}$ cells, (**B**) the abundance of (left) total mCherry$^+$ cells and (right) of mCherry$^+$ $Tcf7^{GFP+}$ cells both relative to input (taking into account the percentage of mCherry$^+$ cells at input). Data shown in bar graphs are normalized to the Ctrl sh (= 1). Non-transduced (mCherry$^-$) and mCherry$^+$ $Tcf7^{GFP+}$ P14 cells were analyzed on d8 p.i. for (**C**) the expression of CD62L, KLRG-1 and Cx3cr1 or (**D**) the production of IL-2 and IFN-γ. (**C, D**) The line graphs depict the expression of the indicated marker by mCherry$^+$ $Tcf7^{GFP+}$ (red filled) compared mCherry$^-$ $Tcf7^{GFP+}$ (black open) cells in each sample. (**E, F**) mCherry$^+$ $Tcf7^{GFP+}$ P14 cells (CD45.2) were flow sorted at d8 p.i. and transplanted into secondary B6 (CD45.1) mice that were infected with LCMV Arm. Eight days later (d8+8), P14 cells were analyzed for (**E**) their abundance in the spleen and (**F**) for the expression of $Tcf7^{GFP}$. Fold expansion shown in bar graphs (**E, F**) are normalized to input number of cells and to the Ctrl sh (=1.0).

Data shown are based on at least 2 distinct sh constructs per gene (on for the Ctrl sh) tested in at least 2 independent experiments with a total of n=4-15 mice per group (**A-D**) or n=3-10 mice per group (**E, F**). Means ±SD are shown. Statistics are based on One-Way (**B, E, F**) or Two-Way (**C, D**) ANOVA with Fisher's LSD test with *: $p<0.05$; **: $p<0.01$; ***: $p<0.001$; ****: $p<0.0001$ and (ns) $p>0.05$. Absence of statistics in (**C, D**) refers to $p>0.05$.

Similar to *Tcf7* sh, knockdown of all 6 Tcf1-dependent adult stem cell genes reduced the generation of mCherry$^+$ d8 $Tcf7^{GFP+}$ cells, compared to Ctrl sh (**Fig. 31B**). The data suggested that all target genes were individually required for the generation of $Tcf7^{hi}$ effector-phase cells. In addition, *Elovl6* or *Smad1* knockdown altered the phenotype of d8 $Tcf7^{GFP+}$ mCherry$^+$ cells (**Fig. 31C, D**). The expression of KLRG-1 and Cx3cr1 (*Elovl6* sh only) was increased (**Fig. 31C**), while the production of IL-2 was decreased (**Fig. 31D**). Knockdown of the remaining Tcf1-dependent adult stem cell genes did not significantly impact the phenotype of effector-stage $Tcf7^{GFP+}$ cells. However, *Elovl6, Smad1*, *Klf4* and *Plxdc2* sh reduced the re-expansion and self-renewal of d8 $Tcf7^{GFP+}$ mCherry$^+$ cells (**Fig. 31E, F**). Normal expression of *Armxc2* or *Kit* was only required for the initial generation of $Tcf7^{GFP+}$ cells (**Fig. 31F**).

Finally, we used our molecular analyses to gain insights into the regulation of these adult stem cell genes. Based on ATACseq analysis, the TSS of 6 of the 8 genes was more accessible in d8 $Tcf7^{GFPhi}$ cells compared to their $Tcf7^{GFP-}$ counterparts (**Fig. 32A, B**). The remaining genes (*Elovl6, Klf4*) were bound by Tcf1 in naive CD8$^+$ T cells (**Fig. 32C**), based on published ChIPseq data (Xing et al., 2016), indicating Tcf1-dependent transcriptional regulation. Interestingly, both the expression (**Fig. 30C**) and the accessibility of the TSS (**Fig. 32B**) of most adult stem cell genes in d8 $Tcf7^{GFPhi}$ cells was equivalent or lower compared to T$_N$ cells. These data thus suggested that an important part of the CD8$^+$ T cell stemness program is maintained, rather than activated, during a primary immune response and negatively regulated via epigenetic mechanisms during effector differentiation.
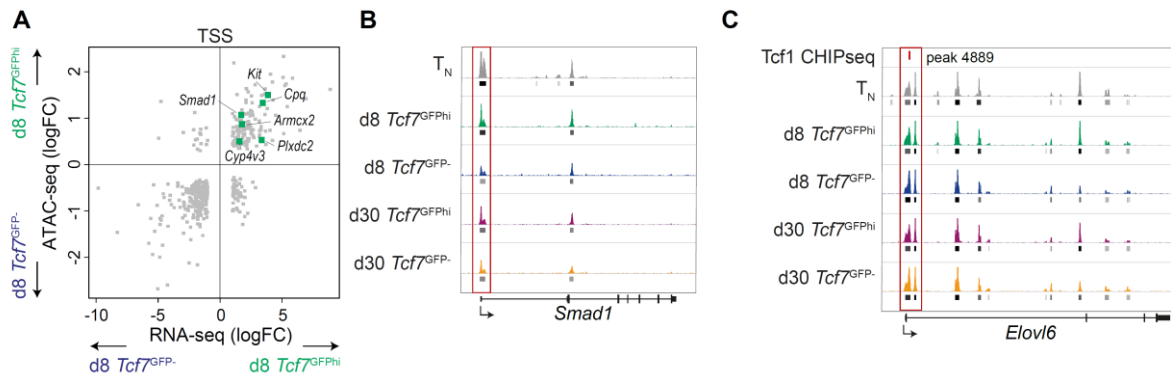
FIGURE 32: Epigenetic regulation of Tcf1-dependent adult stem cell genes.
B6 (CD45.1/2) mice were adoptively transferred with *Tcf7*GFP P14 cells (CD45.2) and infected with LCMV Arm. Splenic *Tcf7*GFPhi and *Tcf7*GFP- P14 cells were flow sorted on d8 or d30 p.i. and subjected to ATACseq analysis. (**A**) Transcription start sites (TSS) differentially accessible in d8 *Tcf7*GFPhi versus d8 *Tcf7*GFP- cells (FDR p<0.05) were correlated with genes differentially expressed in d8 *Tcf7*GFPhi versus d8 Tcf7GFP- cells (absolute log$_2$ FC>1 and adj. p<0.05) and stem cell associated genes more accessible and more expressed in d8 *Tcf7*GFPhi cells are indicated. (**B, C**) Representative read coverage of the stem cell associated gene (**B**) *Smad1* and (**C**) *Elovl6*. The latter track further includes the Tcf1 binding peak (peak 4889) present in naive CD8$^+$ T cells based on published ChIPseq data [232]. The region surrounding the TSS is highlighted using a red outline. The horizontal lines depict accessible regions based on peak calling, where color intensity correlates with p-value.
Bioinformatic analyses were performed by Dr. Tania Wyss, UNIL. Data are derived from n=3 biological replicates per population.

Stem-like *Tcf7*GFPhi CD8$^+$ T cells can also be detected following vaccination

The data thus far identified a minor population of stem-like *Tcf7*GFPhi CD8$^+$ T cells during the acute response to infection. Because the induction of potent T$_{CM}$ responses is a major goal of vaccination regimens, we next assessed whether vaccination generated such stem-like *Tcf7*GFPhi cells. To do so, *Tcf7*GFP transgenic mice were primed (d0) and boosted (d14) using a long synthetic Ovalbumin (Ova) peptide (KL-SLP) and the TLR1/2 agonist Pam3CSK4 emulsified together in Montanide (**Fig. 33A**). Control mice (Ø) received only Pam3CSK4 emulsified in Montanide. The peripheral blood of these mice was then analyzed either one week (d21) or 3 weeks after the boost (d35) for the presence of H-2K^b Ova (SIINFEKL) tetramer (K^{b}Ova)-positive CD8$^+$ T cells.

Compared to control mice, PBMCs of mice vaccinated with Ova contained a population of K^{b}Ova$^+$ CD8$^+$ T cells at the peak of the response (d21) (**Fig. 33B**). Such cells were equally abundant 3 weeks after boost (**Fig. 33C**). At both time points we observed K^{b}Ova$^+$ CD8$^+$ T cells that expressed high levels of *Tcf7*GFP and CD62L (**Fig. 33D**). A similar population of K^{b}Ova$^+$ *Tcf7*GFPhi CD8$^+$ T cells was detected in the spleen of vaccinated mice three weeks after boost (**Fig. 33E, F**). Splenic K^{b}Ova$^+$ *Tcf7*GFPhi cells showed low expression of KLRG-1, but enhanced expression of CD62L and IL-2 (**Fig. 33G, H**), compared to *Tcf7*GFP- cells. Thus, endogenous antigen-specific *Tcf7*$^+$ CD8$^+$ T cells were present at the peak of the vaccination

response and these cells persisted. Therefore, CD8⁺ T cells with stem-like properties can be detected during vaccination, but these cells were rare compared to natural infection.
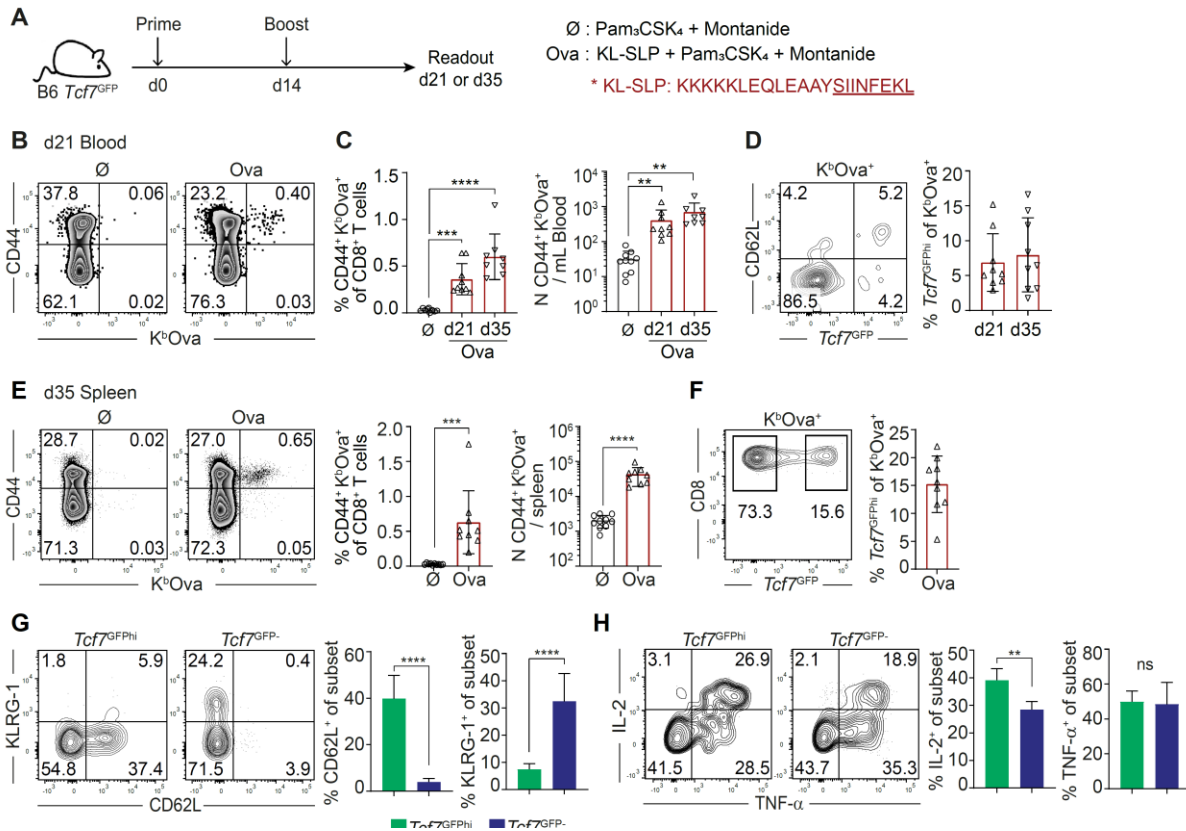
FIGURE 33: *Tcf7*^GFPhi CD8⁺ T cells can be generated by vaccination.
B6 *Tcf7*^GFP mice were primed with a modified synthetic long peptide (KL-SLP) derived from Ovalbumin (Ova) and Pam3CSK4 (TLR1/2 ligand) in Montanide (Ova) or with Pam3CSK4 (TLR1/2 ligand) in Montanide (Ø) at d0 and boosted at d14, as schematically seen in (**A**). Peripheral blood was analyzed for (**B, C**) the presence of K^bOva⁺ CD8⁺ T cells on d21 and d35 and (**D**) K^bOva⁺ CD8⁺ T cells were analyzed for the expression of *Tcf7*^GFP and CD62L. (**E-H**) The spleen was analyzed on d35 post vaccination for (**E**) the presence of K^bOva⁺ CD8⁺ T cells and (**F**) their expression of *Tcf7*^GFP. Gated *Tcf7*^GFPhi and *Tcf7*^GFP- cells were analyzed for (**G**) the expression of KLRG-1 versus CD62L and (**H**) the production of IL-2 and TNF-α.
The data are pooled from 2 independent experiments with n=9-10 mice per group (**B-G**) or are representative of 2 experiments with n=4 mice (**H**). Means ±SD are shown. Statistics are based on Non-paired two-tailed Student's test (**E, G, H**) or on One-Way ANOVA with Tukey's test (**C**) with **: $p<0.01$; ***: $p<0.001$; ****: $p<0.0001$ and (ns) $p>0.05$.

Personal contributions for additional published work by this Lab

Siddiqui, I., K. Schaeuble, V. Chennupati, S. A. Fuertes Marraco, S. Calderon-Copete, **D. Pais Ferreira**, S. J. Carmona, L. Scarpellino, D. Gfeller, S. Pradervand, S. A. Luther, D. E. Speiser & W. Held (2019). Intratumoral Tcf1^{+} PD-1^{+} CD8^{+} T Cells with Stem-like Properties Promote Tumor Control in Response to Vaccination and Checkpoint Blockade Immunotherapy. *Immunity*, 50, 195-211.e10.

- Performed *in vitro* killing assays with isolated Tcf1^{+} PD-1^{+} TILs (not shown).
- Provided critical mouse strain (*Tcf7*^{-/-} (Ko) *Tcf7*[GFP] P14 mice) to address the importance of Tcf1 in the generation / maintenance of Tcf1^{+} PD-1^{+} memory-like TILs.

Utzschneider, D. T., M. Charmoy, V. Chennupati, L. Pousse, **D. Pais Ferreira**, S. Calderon-Copete, M. Danilo, F. Alfei, M. Hofmann, D. Wieland, S. Pradervand, R. Thimme, D. Zehn & W. Held (2016). T Cell Factor 1-Expressing Memory-like CD8^{+} T Cells Sustain the Immune Response to Chronic Viral Infections. *Immunity*, 45, 415-27.

- Contributed for the preparation of samples for RNA sequencing. GEO accession number: GSE83978.
- Performed *in vitro* cell proliferation assays of chronically stimulated Tcf1^{+} memory-like CD8^{+} T cells (not shown).

Discussion

CD8$^+$ T lymphocytes play a key role in the initial clearance of intracellular pathogens and the subsequent protection against re-infection, via the generation of both effector and memory cells, respectively. However, the mechanisms that determine effector versus memory fates, and the stage of the immune response at which this lineage separation happens, have remained long-standing open questions. Resolving these questions has important clinical implications, for instance for improving vaccination regimens that aim at generating long-lived multipotent memory cells. Due to their stem cell-like properties, eliciting central memory (T$_{CM}$) CD8$^+$ T cell responses is a major goal of vaccines and adoptive T cell transfer (ACT) therapy. Thus, understanding the mechanisms that promote the emergence of T$_{CM}$ are essential steps towards the development of more effective T cell therapies.

In the past decade numerous studies have followed the role of the transcription factor Tcf1 in the control of CD8$^+$ T cell differentiation [125, 126, 127, 128, 129]. While a relatively normal primary CD8$^+$ T cell responses occurs in the absence of Tcf1, this TF is selectively required for the generation of the stem cell-like T$_{CM}$ and their function [125, 127]. More recently, Tcf1 was also shown to preserve the stemness of CD8$^+$ T cells that sustain the immune response to chronic infections and tumors [189, 192]. These findings suggest a major role of Tcf1 in the control of stem-like properties of memory CD8$^+$ T cells. This prompted us to follow the expression of Tcf1 by CD8$^+$ T cells during acute viral infection in order to address the genealogy of effector and memory CD8$^+$ T cells.

Using *Tcf7* reporter mice we uncovered a discrete population of *Tcf7*^{hi} effector-phase CD8$^+$ T cells that were epigenetically, transcriptionally, functionally and phenotypically similar to T$_{CM}$ cells. These effector-stage cells retained high *Tcf7* expression, lacked cytotoxic activity and had stem cell properties (i.e. recall expansion, multipotency, differentiation and self-renewal capacity), a function associated with T$_{CM}$. Direct comparison revealed comparable recall expansion and protective capacity of T$_{CM}$ and *Tcf7*^{hi} effector-phase cells. Thus, the data suggested that *Tcf7*^{hi} cells present at the peak of an immune response already possessed T$_{CM}$ hallmark qualities. Since these cells are rare among the effector population, their central memory traits were previously missed when testing the bulk population.

Features of effector-phase *Tcf7*^{hi} CD8$^+$ T cells:

(i) Cytotoxicity / effector functions

Several studies provided evidence that long-lived memory CD8$^+$ T cells derive from cells that passed through a cytotoxic/effector phase [74, 79, 81]. Even MP effector cells, that have increased survival potential, have potent lytic activity and predominantly lack the expression of CD62L

[90]. Unlike MP cells, the *Tcf7*^{hi} cells present at the effector-phase identified herein, frequently expressed CD62L, produced IL-2 and lacked cell-mediated cytotoxicity.

The inefficiency of *Tcf7*^{hi} effector-phase cells to kill target cells resulted from the relative absence of cytolytic proteins, such as GzmB. Tcf1 was shown to directly repress the expression of GzmB in NK cells, by binding to an upstream regulatory element of the *Gzmb* locus [139]. Therefore, it seems likely that Tcf1 directly suppresses *Gzmb* transcription in CD8^{+} T cells.

(ii) Gene expression profile

Compared to *Tcf7*^{-} cells, the transcriptome of *Tcf7*^{hi} effector-phase cells also revealed low expression of many effector-associated genes, including genes coding for effector surface markers (*Klrg1, Cx3cr1*) but also key effector transcription factors (*Tbx21, Prdm1, Zeb2*). These data suggested that *Tcf7*^{hi} cells lacked an effector gene expression profile. Indeed, this was dependent on Tcf1, as several effector-associated genes were induced in effector-phase *Tcf7*^{hi} cells that lacked Tcf1 expression. Therefore, the absence of Tcf1 appeared to facilitate effector differentiation, in agreement with previous studies [176, 182]. Interestingly, this Tcf1 function can be observed across several immune cell types. While in NK cells Tcf1 limits the expression of cytotoxic effector molecules allowing the survival and maturation of these cells [139], in CD4^{+} T cells Tcf1 is known to curb IFN-γ production and thus impair T_H1 differentiation [173]. These observations provide evidence of a general role for Tcf1 in restricting effector fate determination.

The molecular basis for the terminal differentiation of CD8^{+} T cells is however poorly understood. Our RNAseq analysis identified an overexpression of the microRNA 449 (miR449) cluster in d8 *Tcf7*^{-} cells, compared to d8 *Tcf7*^{hi} cells (**Fig. 20**). This family of miRNAs is known to induce cell cycle arrest, cell death and/or differentiation [224], consistent with the observed elevated apoptosis of d8 *Tcf7*^{-} cells. It would thus be interesting to assess exactly when miR449 is upregulated during the primary response and to further explore a potential role of miR449 in the terminal differentiation of CD8^{+} T cells.

(iii) Chromatin accessibility

The lack of an effector gene expression program in *Tcf7*^{hi} effector-phase cells could be explained by epigenetic mechanisms. Indeed, the chromatin accessibility of the TSS of multiple effector-loci was markedly reduced in effector-stage *Tcf7*^{hi} compared to *Tcf7*^{-} cells, likely explaining the reduced expression of such genes. Particularly, the TSS of *Gzmb* was nearly inaccessible in T_N and *Tcf7*^{hi} compared to *Tcf7*^{-} cells. This contrasts with the equivalent

accessibility of *Gzmb* in TE or MP cells [233], supporting the view that the later population includes differentiated effector cells.

At the same time, the TSS of many T_{CM} associated genes (*Ccr7*, *Sell*, etc) was more accessible in *Tcf7*hi effector-phase cells and this correlated with elevated transcription. Conversely, both the accessibility and mRNA expression of this class of genes was severely reduced in *Tcf7*- effector cells. Importantly, the chromatin accessibility of regions relevant for T_{CM} associated genes was similar between T_N, d8 *Tcf7*hi cells and T_{CM}. Thus, our data suggested that a T_{CM} gene expression program was maintained in CD8+ T cells that retain high expression of *Tcf7*. Additionally, this program seemed to be epigenetically repressed upon *Tcf7* silencing and this further coincided with opening of effector-associated loci. Finally, this suggested a role for epigenetic regulation in CD8+ T fate determination. Nevertheless, the mechanisms that allow/drive these epigenetic alterations still need to be identified.

(iv) Location

We observed an increased localization of the *Tcf7*hi cells in the splenic T cell zone (TZ), compared to *Tcf7*- cells, which might also contribute to their disparate fates. Similar to the lymph nodes, the splenic TZ displays a dense network of fibroblast reticular cells (FRCs) [223]. These stromal cells are known to produce the chemokines CCL19 and CCL21, which are ligands for CCR7, and thus direct the trafficking of T_N and T_{CM} cells to this zone [234]. Effector-phase *Tcf7*hi cells had increased *Ccr7* expression, which likely explains the preferential homing of these cells to the TZ. Additionally, FRCs can also produce IL-7 and IL-15 allowing the homeostasis of MP and T_{CM} cells [234]. The particular localization of *Tcf7*hi effector-phase cells in the TZ might therefore protect them against terminal differentiation.

Developmental potential of effector-phase *Tcf7*hi CD8+ T cells:

(i) At steady state (in intact mice)

The frequency of *Tcf7*hi cells gradually increased following pathogen clearance, however their number remained remarkably stable throughout the immune response. Since re-expression of *Tcf7* by *Tcf7*GFP- cells was very rare, as judged by the low abundance of *Tcf7*DTR-GFP+ memory cells in mice depleted of *Tcf7*DTR-GFP+ effector-phase cells, the data indicated that *Tcf7*hi effector-phase cells survived long-term. Indeed, these cells showed enhanced survival upon growth factor withdrawal *in vitro*. Therefore, *Tcf7*hi effector-phase cells seemed to quantitatively form central memory. This conclusion was further supported by lineage tracing experiments performed in this lab (Joana Gomes da Silva, unpublished).

Conversely, the T_{CM} memory compartment and central memory function (i.e. IL-2 production and re-expansion) was severely compromised upon the ablation of $Tcf7^+$ effector-phase cells. Thus, our data strongly suggested that T_{CM} cells quantitatively derived from effector-phase CD8$^+$ T cells that retain high levels of $Tcf7$.

Additionally, when $Tcf7^{hi}$ effector cells were depleted *in vivo* the abundance of CD62L$^-$ T_{EM} cells was also reduced (**Fig. 25**). These results indicated that T_{EM} also derived from the effector-stage $Tcf7^{hi}$ population after pathogen clearance. However, further studies using lineage tracing approaches are required to resolve the developmental relationship between T_{CM} and T_{EM}.

(ii) Upon re-challenge

Adoptive transfer and re-stimulation of effector-stage $Tcf7^{hi}$ cells revealed their multilineage differentiation potential. $Tcf7^{hi}$ cells yielded terminal effector cells, CD62L$^-$ T_{EM} and T_{RM} as well as T_{CM} cells (**Fig. 24**).

Besides multilineage potential, re-stimulation of effector-phase $Tcf7^{hi}$ cells also yielded an expanded population of undifferentiated $Tcf7^{hi}$ cells. Re-transfer and re-stimulation of the latter cells formally showed that $Tcf7^{hi}$ cells could self-renew. The limited proliferation/cell cycling of $Tcf7^{hi}$ cells observed during early activation (d3 p.i.) or at the peak of the response (d8) might reduce the risk for replicative senescence and thus help to maintain the stemness state.

Conversely, the re-stimulation of $Tcf7^-$ cells yielded only KLRG-1^{hi} $Tcf7^-$ effector cells, reduced numbers of T_{EM} or T_{RM} and no evidence of T_{CM}. The latter suggested that there was no evidence of de-differentiation of $Tcf7^-$ cells into $Tcf7^{hi}$ cells. Silencing of $Tcf7$ thus seemed to be stable and heritable.

T_{RM} cells were thought to lack recall expansion capacity [33, 34]. However, a recent study showed that mucosal CD8$^+$ T_{RM} cells are able to divide (although not accumulate in number) *in situ* in response to local antigen re-challenge [235]. This raises the possibility that T_{RM} cells include a population with stem-like properties. Indeed, we detected a substantial population of undifferentiated $Tcf7^{hi}$ cells in the T_{RM} compartment. Given the stemness properties of splenic $Tcf7^{hi}$ cells it is possible that $Tcf7^{hi}$ T_{RM} mediate similar functions within specific tissues. It will also be interesting to investigate whether the tissue resident $Tcf7^{hi}$ cells are responsible to maintain the T_{RM} compartment.

Implications for the models of memory CD8^{+} T cell differentiation

Numerous reports support the idea that memory differentiation takes place following virus clearance [68, 70, 71, 73], in favor of the so-called linear model for memory CD8^{+} T cell differentiation. Further, it has been recently suggested that the formation of functional memory cells results from the de-differentiation of certain effector cells [81]. If so, differentiated effector cells would need to re-acquire stem-like properties upon virus clearance.

A large number of studies have used a small set of cell surface markers to study effector versus memory differentiation. However, the expression of most of these markers is not stable, the ability to distinguish cells with distinct potential is not clear-cut and the functional relevance of these markers is limited. For instance, KLRG-1 typically defines short-lived effector cells [90]. However some KLRG-1^{+} CD8^{+} T cells can be detected 5 months after acute LCMV infection [90]. Thus, not all KLRG-1^{+} cells are short-lived [91]. On the other hand, T_{CM} cells have classically been defined by the expression of CD62L [84]. While occasional CD8^{+} T cells express intermediate levels of CD62L at the peak of the immune response [236], CD62L expression is unstable. During the early phase of the immune response, CD62L can be cleaved off the surface of activated T cells by a disintegrin metalloprotease [237, 238]. Most importantly, the expression of these markers is not required for effector or memory differentiation/function [239, 240, 241]. Indeed, lack of CD62L expression did not impact the generation of CCR7^{+} T_{CM} cells (in the spleen) nor did it alter the protective capacity of memory CD8^{+} T cells [239]. CD127 is downregulated in most CD8^{+} T cells during a primary immune response [69, 242]. These cells are predominantly short-lived, while cells that retain CD127 have a higher propensity to survive [69, 90]. However, enforced expression of CD127 in CD8^{+} T cells does not increase the number or function of memory cells [241]. Thus, expression of CD127 during the acute phase of the immune response is not sufficient to drive CD8^{+} T cell memory formation [240, 241]. In contrast, Tcf1 is stably expressed in a subset of effector-phase cells and there is essentially no evidence that Tcf1 is reacquired by cells that have downregulated it. Finally, Tcf1 is essential for T_{CM} formation and function, i.e. to ensure stemness of CD8^{+} T cells (see below).

The identification of cells with T_{CM} functions (i.e. recall expansion, multipotency and self-renewal capacity) at the peak of the immune response challenges the linear differentiation model. Indeed, effector-stage cells that retained *Tcf7*, which lacked cytotoxic function, were required for T_{CM} formation and function. Therefore, T_{CM} do not arise from cytotoxic effector cells that undergo de-differentiation following the elimination of pathogen. Instead, they derive form a subpopulation of acutely antigen-exposed *Tcf7*^{hi} cells with stem cell properties (**Fig. 34A**). Besides self-renewal, i.e. generating more cells with T_{CM} function, effector-phase *Tcf7*^{hi} cells also produced *Tcf7*^{-} progeny, which in turn represented a terminally differentiated

cytolytic population. The stemness of *Tcf7*hi cells was in part epigenetically regulated, as previously discussed (**Fig. 34B**).
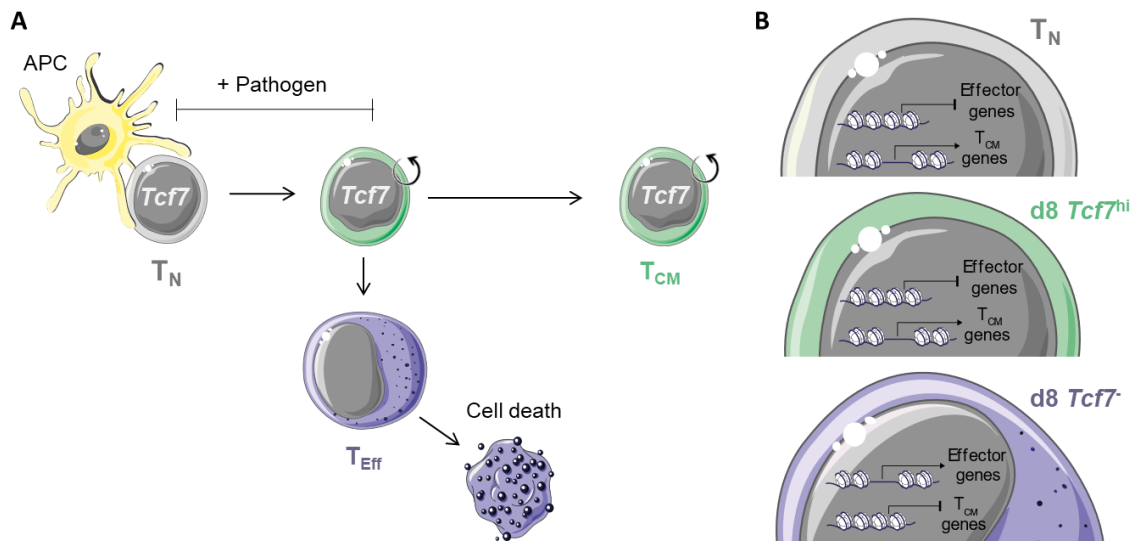

FIGURE 34: Proposed model for memory CD8+ T cell differentiation.
(**A**) Activation of T$_N$ (*Tcf7*hi) drives the formation of *Tcf7*hi stem-like cells that can give rise to *Tcf7*- cytolytic effector cells (T$_{Eff}$). In this model, cells that perform T$_{CM}$ functions co-exist with cytolytic effector cells at the peak of the immune response. Following pathogen clearance, *Tcf7*- T$_{Eff}$ cells die, while *Tcf7*hi stem-like cells survive and self-renew, maintaining the central memory T cell pool. (**B**) Similar to T$_N$, the chromatin of effector-stage *Tcf7*hi cells in effector-associated genes is poorly accessible, but central memory loci are assessible. This suggests that chromatin accessibility of T$_{CM}$ loci is maintained in *Tcf7* expressing cells. Conversely, this seems to be repressed upon *Tcf7* silencing, which further coincides with opening of effector-associated loci. (*This figure was created using Servier Medical Art templates*).

The findings leave open the question when effector and memory fates separate during the acute response. T$_N$ were proposed to generate effector and memory fated daughter cells via asymmetric division, as described by the bifurcative differentiation model. The stimulation of Tcf1+ T$_N$ yielded daughter cells that homogenously expressed high levels of Tcf1 (**Fig. 15D**), in agreement with published results [179, 180]. Thus, based on Tcf1 expression, the effector versus memory fate predisposition was not dictated during the first cell division. Instead, Tcf1 downregulation was only observed after >3 cell divisions. These data are consistent with the work of Danilo and colleagues, where downregulation of Tcf1 in CD8+ T cells activated via the TCR depends on cell division and the presence of inflammatory cytokines [182]. Consequently, our data are more compatible with a model in which the activation of naive CD8+ T cells gives initially rise to T$_{CM}$ cells, and further and/or stronger signaling input drives terminal effector differentiation [58, 59, 60]. Thus, the data supports the developmental model for memory CD8+ T cell differentiation, in which there is a progressive loss of *Tcf7* expression, and consequently stemness, as cells differentiate from naive & central memory cells to terminally differentiated effector cells.

In conclusion, we have shown that cells with central memory function co-exist with effector cells at the peak of an acute immune response. Further, these cells arise without transitioning through a cytotoxic stage. Such cells are defined by high expression of the transcription factor Tcf1 and represent a relatively undifferentiated quiescent subtype of antigen-primed CD8$^+$ T cells that preserve a genetic and epigenetic T$_{CM}$ program with similarity to naive cells. The discovery of this population significantly improves our understanding of the formation of immunological memory.

Role of Tcf1 in the control of stem cell properties of effector-phase *Tcf7*^{hi} CD8$^+$ T cells

Functionally, the stemness of effector-phase *Tcf7*^{hi} CD8$^+$ T cells depended on the expression of Tcf1 protein. The absence of Tcf1 modestly reduced the generation of *Tcf7*^{hi} effector-stage cells and promoted their aberrant differentiation. This correlated with poor expansion of Tcf1-deficient *Tcf7*^{hi} effector-phase cells, and an almost complete lack of self-renewal in response to antigen re-challenge. Thus, Tcf1 expression ensured the stemness of *Tcf7*^{hi} effector-phase cells. However, whether the loss of stemness was the cause or the consequence of increased differentiation was not clear.

In the absence of Tcf1, d8 *Tcf7*^{hi} cells upregulated a distinct IL-2/STAT5 signature, which is known to drive terminal differentiation [89, 97]. However, enforced expression of IL2rα did not impact the differentiation or self-renewal potential of Wt *Tcf7*^{hi} effector-phase cells. Thus, while high IL2rα expression marks cells that will terminally differentiate [88, 89], it was not sufficient to reduce stemness of Wt *Tcf7*^{hi} cells. It is however possible that these cells did not see IL-2 and consequently phosphorylation of STAT5 and activation of Blimp1 (*Prdm1*) did not occur. Future experiments enforcing the expression of *Prdm1*, which was also upregulated in the absence of Tcf1, would perhaps be a more direct way to assess the importance of differentiation for the loss of stemness.

Tcf1-dependent adult stem cell genes

Recent studies suggest that epigenetic silencing of T$_{CM}$ associated genes, including *Tcf7*, in effector cells is required for efficient effector differentiation [81, 82, 100]. However, the relevance of this T$_{CM}$ gene signature for central memory function (i.e. stemness) is unclear. Indeed, only a few genes mediating stemness of CD8$^+$ T cells have been defined, and it was not clear whether these depended on Tcf1.

Interestingly, absence of Tcf1 in effector-phase *Tcf7*hi cells did not impact the expression of a previously reported T$_{CM}$ signature [207] or a recently proposed stem cell-like memory signature [210]. It did also not affect the expression of genes known to impact T$_{CM}$ formation or function, including *Bcl6*, *Foxo1*, *Id3*, *Myb*, and *STAT3*. This suggested that Tcf1 was not a master transcriptional regulator of known T$_{CM}$ transcription factors. Rather we found that Tcf1 drives a transcriptional program that shares some elements in common with hematopoietic stem cells (HSC) or adult tissue stem cells referred to as "adult stem cell genes".

Indeed, we identified a set of 8 conserved adult stem cell genes that were expressed in a Tcf1-dependent fashion by *Tcf7*hi CD8+ T cells. Individual knockdown of 6 of these genes revealed that they controlled distinct aspects of *Tcf7*hi CD8+ T cells. While all 6 genes were needed for the initial generation of *Tcf7*hi effector-phase cells, *Klf4*, *Elovl6*, *Plxdc2* and *Smad1* were further needed to ensure normal recall expansion and self-renewal capacity. In addition, *Elovl6* and *Smad1* knockdown increased the differentiation of *Tcf7*hi CD8+ T cells. As expected, downregulation of *Tcf7* had the strongest effects and impacted all the above aspects of the generation and function of *Tcf7*hi CD8+ T cells. Thus, Tcf1 ensured the expression of genes that are shared among distinct types of adult stem cells and that were responsible for preserving the stemness of CD8+ T cells.

The role of these Tcf1-dependent adult stem cell genes in CD8+ T cells has not been studied before. Potential roles can be deduced from their importance in other situations. The transcription factor Klf4 plays an important role in restraining the differentiation of embryonic stem cells during embryonic development [243, 244]. Additionally, together with Oct4, Sox2 and c-Myc, Klf4 is able to reprogram differentiated cells to pluripotent stem cells [245]. Kit is expressed by germ cells, hematopoietic stem cells, and early hematopoietic progenitors and, upon binding of stem cell factor, ensures their survival, proliferation, differentiation, and migration [246]. Plxdc2 is a transmembrane receptor that binds to the stem cell niche factor PEDF (Pigment Epithelium-Derived Factor) [247]. This factor was shown to upregulate Notch signaling in neural stem cells, promoting their stemness [248]. Smad1 is a nuclear effector of the BMP (bone morphogenetic proteins) signaling pathway [249]. The BMP2/4 – Smad1 signaling pathway regulates the proliferation, survival and differentiation of early T-cell progenitors in the thymus [250]. Further, *Cyp4v3* and *Elovl6*, are involved in fatty acid biosynthesis, suggesting that metabolic regulation might play a role in the control of CD8+ T cell stemness. Clearly, further studies are required to elucidate how these genes control CD8+ T cell stemness.

An additional important aspect is how the expression of these genes is regulated during a CD8+ T cell response. Only 2/8 adult stem cell genes are bound by Tcf1, based on our re-analysis of Tcf1 ChIPseq data derived from naive CD8+ T cells. This suggested that the

expression of most adult stem cell genes does not depend directly on Tcf1 transcriptional regulation in naive cells. However, it will be necessary to address whether the same is true in effector-stage *Tcf7*hi cells. Interestingly, our ATACseq data revealed that the accessibility of most of the adult stem cell genes was increased in *Tcf7*hi cells compared to *Tcf7*- effector cells. This suggested that stemness of *Tcf7*hi effector-phase cells is epigenetically regulated, i.e. epigenetic silencing of adult stem cell genes is somehow prevented in *Tcf7*hi effector-phase cells. It will be important to determine how epigenetic silencing of these genes is mediated in *Tcf7*- cells or conversely, how it is prevented in *Tcf7*hi effector-phase cells.

Finally, in this study we established that stemness was a property of rare effector-phase CD8+ T cells and was thus not acquired late after pathogen clearance. However, whether the stemness was maintained from T_N cells or whether it needed to be acquired early following activation was less clear. Interestingly only 2/8 adult stem cell genes were induced during the primary response (*Kit* and *Plxdc2*). Most genes (6/8) were expressed at equivalent levels (or lower) in d8 *Tcf7*hi cells compared to T_N cells (**Fig. 30**). Thus, the data suggested that an important part of the CD8+ T cell stemness program was preserved, rather than induced, during the primary immune response to acute infection.

Role of Tcf1 in the CD8+ T cell response to chronic infection and cancer

As previously mentioned, CD8+ T cell differentiation in response to persistent infections or cancer differs significantly from the response to acute resolved infection. The former was thought to preclude the formation of memory CD8+ T cells. However, stem-like Tcf1+ PD-1+ CD8+ T cells that sustain the immune response to chronic infection and cancer were recently identified [145, 189, 192, 193]. Similar to the acutely responding *Tcf7*hi cells identified in this study, Tcf1+ PD-1+ CD8+ T cells have the capacity to self-renew and yield more differentiated progeny. Indeed, they are thought to continuously produce terminally differentiated (exhausted) Tcf1- PD-1+ CD8+ T cells that have cytolytic potential. While there are significant phenotypic and functional differences, the data favors a conserved CD8+ T cell differentiation scheme in which differentiated CD8+ T cells responding to acute or chronic stimuli arise from undifferentiated antigen-experienced cells. It will be of considerable interest to determine whether the stemness of Tcf1+ PD-1+ CD8+ T cells present in chronic infection and cancer depends on the same or different adult stem cell genes.

Possible applications

In LCMV infected mice, central memory CD8^{+} T cells have been shown to mediate superior viral control, as compared to T_{EM} [37]. In addition, T_{CM} cells primed via APC vaccination in mice also conferred increased protection to influenza virus infection [251]. Thus, protection against infection correlates with the presence of T_{CM} cells and their generation is a major goal for vaccinations [4, 12]. Here we identified a stem-like *Tcf7*^{hi} CD8^{+} T population at the acute phase of the primary immune response to viral infections. Moreover, we showed that similar cells could be detected early upon vaccination (**Fig. 33**). Importantly the number of these cells generated by vaccination was considerably lower compared to natural infection. It also remains to be determined whether these cells are functionally comparable to the ones generated during infection or whether the early presence/abundance of these cells correlates with protection from re-infection at later time points. If so, we propose that the detection of stem-like CD8^{+} T cells during early stages of the primary response will accelerate the quality control and the optimization of new T cell vaccine regimens that aim at generating or maintaining central memory CD8^{+} T cells.

References

1. Janeway, C.A., Jr. & Medzhitov, R. Innate immune recognition. *Annu Rev Immunol* **20**, 197-216 (2002).
2. Beutler, B. Inferences, questions and possibilities in Toll-like receptor signalling. *Nature* **430**, 257-263 (2004).
3. Murphy, K. *Janeway's Immunobiology*, vol. 8. Garland Science: New York, 2012.
4. Zanetti, M. & Franchini, G. T cell memory and protective immunity by vaccination: is more better? *Trends Immunol* **27**, 511-517 (2006).
5. Trapani, J.A. & Smyth, M.J. Functional significance of the perforin/granzyme cell death pathway. *Nat Rev Immunol* **2**, 735-747 (2002).
6. Jiang, T. *et al.* Tumor neoantigens: from basic research to clinical applications. *J Hematol Oncol* **12**, 93 (2019).
7. Schumacher, T.N. & Schreiber, R.D. Neoantigens in cancer immunotherapy. *Science* **348**, 69-74 (2015).
8. Zinkernagel, R.M. *et al.* On immunological memory. *Annu Rev Immunol* **14**, 333-367 (1996).
9. Ahmed, R. & Gray, D. Immunological memory and protective immunity: Understanding their relation. *Science* **272**, 54-60 (1996).
10. Jin, X. *et al.* Dramatic rise in plasma viremia after CD8(+) T cell depletion in simian immunodeficiency virus-infected macaques. *J Exp Med* **189**, 991-998 (1999).
11. Hegde, P.S., Karanikas, V. & Evers, S. The Where, the When, and the How of Immune Monitoring for Cancer Immunotherapies in the Era of Checkpoint Inhibition. *Clin Cancer Res* **22**, 1865-1874 (2016).
12. Seder, R.A., Darrah, P.A. & Roederer, M. T-cell quality in memory and protection: implications for vaccine design. *Nat Rev Immunol* **8**, 247-258 (2008).
13. Kaech, S., Wherry, E. & Ahmed, R. Effector and memory T-cell differentiation: Implications for vaccine development. *Nature Reviews Immunology* **2**, 251-262 (2002).
14. Forster, R. *et al.* CCR7 coordinates the primary immune response by establishing functional microenvironments in secondary lymphoid organs. *Cell* **99**, 23-33 (1999).
15. Blattman, J.N. *et al.* Estimating the precursor frequency of naive antigen-specific CD8 T cells. *J Exp Med* **195**, 657-664 (2002).
16. Badovinac, V.P., Haring, J.S. & Harty, J.T. Initial TCR-transgenic precursor frequency dictates critical aspects of the CD8 T cell response to infection. *Immunity* **26**, 827-841 (2007).
17. Mescher, M.F. *et al.* Signals required for programming effector and memory development by CD8+ T cells. *Immunol Rev* **211**, 81-92 (2006).
18. Brehm, M.A., Daniels, K.A. & Welsh, R.M. Rapid production of TNF-alpha following TCR engagement of naive CD8 T cells. *J Immunol* **175**, 5043-5049 (2005).
19. Tau, G.Z., Cowan, S.N., Weisburg, J., Braunstein, N.S. & Rothman, P.B. Regulation of IFN-gamma signaling is essential for the cytotoxic activity of CD8(+) T cells. *J Immunol* **167**, 5574-5582 (2001).
20. Kaech, S. & Ahmed, R. Memory CD8(+) T cell differentiation: initial antigen encounter triggers a developmental program in naive cells. *Nature Immunology* **2**, 415-422 (2001).
21. JAMIESON, B. & AHMED, R. T-CELL MEMORY - LONG-TERM PERSISTENCE OF VIRUS-SPECIFIC CYTO-TOXIC T-CELLS. *Journal of Experimental Medicine* **169**, 1993-2005 (1989).
22. Murali-Krishna, K. *et al.* Persistence of memory CD8 T cells in MHC class I-deficient mice. *Science* **286**, 1377-1381 (1999).
23. Schluns, K., Kieper, W., Jameson, S. & Lefrancois, L. Interleukin-7 mediates the homeostasis of naive and memory CD8 T cells in vivo. *Nature Immunology* **1**, 426-432 (2000).
24. Tan, J. *et al.* Interleukin (IL)-15 and IL-7 jointly regulate homeostatic proliferation of memory phenotype CD8(+) cells but are not required for memory phenotype CD4(+) cells. *Journal of Experimental Medicine* **195**, 1523-1532 (2002).

25. Berard, M., Brandt, K., Paus, S. & Tough, D. IL-15 promotes the survival of naive and memory phenotype CD8(+) T cells. *Journal of Immunology* **170**, 5018-5026 (2003).

26. Leignadier, J., Hardy, M., Cloutier, M., Rooney, J. & Labrecque, N. Memory T-lymphocyte survival does not require T-cell receptor expression. *Proceedings of the National Academy of Sciences of the United States of America* **105**, 20440-20445 (2008).

27. Prlic, M., Williams, M. & Bevan, M. Requirements for CD8 T-cell priming, memory generation and maintenance. *Current Opinion in Immunology* **19**, 315-319 (2007).

28. Sallusto, F., Lenig, D., Forster, R., Lipp, M. & Lanzavecchia, A. Two subsets of memory T lymphocytes with distinct homing potentials and effector functions. *Nature* **401**, 708-712 (1999).

29. Wherry, E.J. *et al.* Lineage relationship and protective immunity of memory CD8 T cell subsets. *Nat Immunol* **4**, 225-234 (2003).

30. Gebhardt, T. *et al.* Memory T cells in nonlymphoid tissue that provide enhanced local immunity during infection with herpes simplex virus. *Nat Immunol* **10**, 524-530 (2009).

31. Gebhardt, T. *et al.* Different patterns of peripheral migration by memory CD4+ and CD8+ T cells. *Nature* **477**, 216-219 (2011).

32. Steinert, E.M. *et al.* Quantifying Memory CD8 T Cells Reveals Regionalization of Immunosurveillance. *Cell* **161**, 737-749 (2015).

33. Sheridan, B.S. & Lefrançois, L. Regional and mucosal memory T cells. *Nat Immunol* **12**, 485-491 (2011).

34. Jiang, X. *et al.* Skin infection generates non-migratory memory CD8+ T(RM) cells providing global skin immunity. *Nature* **483**, 227-231 (2012).

35. Teijaro, J.R. *et al.* Cutting edge: Tissue-retentive lung memory CD4 T cells mediate optimal protection to respiratory virus infection. *J Immunol* **187**, 5510-5514 (2011).

36. Wherry, E.J. & Ahmed, R. Memory CD8 T-cell differentiation during viral infection. *J Virol* **78**, 5535-5545 (2004).

37. Wherry, E.J. *et al.* Lineage relationship and protective immunity of memory CD8 T cell subsets. *Nat Immunol* **4**, 225-234 (2003).

38. Graef, P. *et al.* Serial transfer of single-cell-derived immunocompetence reveals stemness of CD8(+) central memory T cells. *Immunity* **41**, 116-126 (2014).

39. Sallusto, F., Geginat, J. & Lanzavecchia, A. Central memory and effector memory T cell subsets: function, generation, and maintenance. *Annu Rev Immunol* **22**, 745-763 (2004).

40. Wu, T. *et al.* Lung-resident memory CD8 T cells (TRM) are indispensable for optimal cross-protection against pulmonary virus infection. *J Leukoc Biol* **95**, 215-224 (2014).

41. Appay, V. *et al.* Memory CD8+ T cells vary in differentiation phenotype in different persistent virus infections. *Nat Med* **8**, 379-385 (2002).

42. Stemberger, C. *et al.* Stem cell-like plasticity of naive and distinct memory CD8+ T cell subsets. *Semin Immunol* **21**, 62-68 (2009).

43. Zhang, Y., Joe, G., Hexner, E., Zhu, J. & Emerson, S.G. Host-reactive CD8+ memory stem cells in graft-versus-host disease. *Nat Med* **11**, 1299-1305 (2005).

44. Gattinoni, L. *et al.* Wnt signaling arrests effector T cell differentiation and generates CD8+ memory stem cells. *Nat Med* **15**, 808-813 (2009).

45. Gattinoni, L. *et al.* A human memory T cell subset with stem cell-like properties. *Nat Med* **17**, 1290-1297 (2011).

46. Lugli, E. *et al.* Identification, isolation and in vitro expansion of human and nonhuman primate T stem cell memory cells. *Nat Protoc* **8**, 33-42 (2013).

47. Lugli, E. *et al.* Superior T memory stem cell persistence supports long-lived T cell memory. *J Clin Invest* **123**, 594-599 (2013).

48. Cieri, N. *et al.* IL-7 and IL-15 instruct the generation of human memory stem T cells from naive precursors. *Blood* **121**, 573-584 (2013).

49. Fuertes Marraco, S.A. *et al.* Long-lasting stem cell-like memory CD8+ T cells with a naïve-like profile upon yellow fever vaccination. *Sci Transl Med* **7**, 282ra248 (2015).

50. Gattinoni, L. Memory T cells officially join the stem cell club. *Immunity* **41**, 7-9 (2014).

51. Busch, D.H., Fräßle, S.P., Sommermeyer, D., Buchholz, V.R. & Riddell, S.R. Role of memory T cell subsets for adoptive immunotherapy. *Semin Immunol* **28**, 28-34 (2016).

52. Gerlach, C. *et al.* The Chemokine Receptor CX3CR1 Defines Three Antigen-Experienced CD8 T Cell Subsets with Distinct Roles in Immune Surveillance and Homeostasis. *Immunity* **45**, 1270-1284 (2016).

53. Klebanoff, C.A. *et al.* Central memory self/tumor-reactive CD8+ T cells confer superior antitumor immunity compared with effector memory T cells. *Proc Natl Acad Sci U S A* **102**, 9571-9576 (2005).

54. Gattinoni, L. *et al.* Acquisition of full effector function in vitro paradoxically impairs the in vivo antitumor efficacy of adoptively transferred CD8+ T cells. *J Clin Invest* **115**, 1616-1626 (2005).

55. Knochelmann, H.M. *et al.* CAR T Cells in Solid Tumors: Blueprints for Building Effective Therapies. *Front Immunol* **9** (2018).

56. Ahmed, R., Bevan, M.J., Reiner, S.L. & Fearon, D.T. The precursors of memory: models and controversies. *Nat Rev Immunol* **9**, 662-668 (2009).

57. Restifo, N.P. & Gattinoni, L. Lineage relationship of effector and memory T cells. *Curr Opin Immunol* **25**, 556-563 (2013).

58. Lanzavecchia, A. & Sallusto, F. Progressive differentiation and selection of the fittest in the immune response. *Nat Rev Immunol* **2**, 982-987 (2002).

59. Corse, E., Gottschalk, R.A. & Allison, J.P. Strength of TCR-peptide/MHC interactions and in vivo T cell responses. *J Immunol* **186**, 5039-5045 (2011).

60. Masopust, D., Kaech, S.M., Wherry, E.J. & Ahmed, R. The role of programming in memory T-cell development. *Curr Opin Immunol* **16**, 217-225 (2004).

61. Iezzi, G., Karjalainen, K. & Lanzavecchia, A. The duration of antigenic stimulation determines the fate of naive and effector T cells. *Immunity* **8**, 89-95 (1998).

62. Langenkamp, A. *et al.* T cell priming by dendritic cells: thresholds for proliferation, differentiation and death and intraclonal functional diversification. *Eur J Immunol* **32**, 2046-2054 (2002).

63. Teixeiro, E. *et al.* Different T cell receptor signals determine CD8+ memory versus effector development. *Science* **323**, 502-505 (2009).

64. Rohr, J.C., Gerlach, C., Kok, L. & Schumacher, T.N. Single cell behavior in T cell differentiation. *Trends Immunol* **35**, 170-177 (2014).

65. Stemberger, C. *et al.* A single naive CD8+ T cell precursor can develop into diverse effector and memory subsets. *Immunity* **27**, 985-997 (2007).

66. Gerlach, C. *et al.* One naive T cell, multiple fates in CD8+ T cell differentiation. *J Exp Med* **207**, 1235-1246 (2010).

67. Gerlach, C. *et al.* Heterogeneous differentiation patterns of individual CD8+ T cells. *Science* **340**, 635-639 (2013).

68. Kaech, S.M., Hemby, S., Kersh, E. & Ahmed, R. Molecular and functional profiling of memory CD8 T cell differentiation. *Cell* **111**, 837-851 (2002).

69. Kaech, S.M. *et al.* Selective expression of the interleukin 7 receptor identifies effector CD8 T cells that give rise to long-lived memory cells. *Nat Immunol* **4**, 1191-1198 (2003).

70. Kalia, V., Sarkar, S., Gourley, T.S., Rouse, B.T. & Ahmed, R. Differentiation of memory B and T cells. *Curr Opin Immunol* **18**, 255-264 (2006).

71. Lefrançois, L. & Obar, J.J. Once a killer, always a killer: from cytotoxic T cell to memory cell. *Immunol Rev* **235**, 206-218 (2010).

72. Youngblood, B., Hale, J.S. & Ahmed, R. T-cell memory differentiation: insights from transcriptional signatures and epigenetics. *Immunology* **139**, 277-284 (2013).

73.   Crauste, F. *et al.* Identification of Nascent Memory CD8 T Cells and Modeling of Their Ontogeny. *Cell Syst* **4**, 306-317.e304 (2017).

74.   Bannard, O., Kraman, M. & Fearon, D.T. Secondary replicative function of CD8+ T cells that had developed an effector phenotype. *Science* **323**, 505-509 (2009).

75.   Harrington, L.E., Janowski, K.M., Oliver, J.R., Zajac, A.J. & Weaver, C.T. Memory CD4 T cells emerge from effector T-cell progenitors. *Nature* **452**, 356-360 (2008).

76.   Yuzefpolskiy, Y., Baumann, F.M., Kalia, V. & Sarkar, S. Early CD8 T-cell memory precursors and terminal effectors exhibit equipotent in vivo degranulation. *Cell Mol Immunol* **12**, 400-408 (2015).

77.   Scott-Browne, J.P. *et al.* Dynamic Changes in Chromatin Accessibility Occur in CD8(+) T Cells Responding to Viral Infection. *Immunity* **45**, 1327-1340 (2016).

78.   Moskowitz, D.M. *et al.* Epigenomics of human CD8 T cell differentiation and aging. *Sci Immunol* **2** (2017).

79.   Abdelsamed, H.A. *et al.* Human memory CD8 T cell effector potential is epigenetically preserved during in vivo homeostasis. *J Exp Med* **214**, 1593-1606 (2017).

80.   Akondy, R.S. *et al.* Origin and differentiation of human memory CD8 T cells after vaccination. *Nature* **552**, 362-367 (2017).

81.   Youngblood, B. *et al.* Effector CD8 T cells dedifferentiate into long-lived memory cells. *Nature* **552**, 404-409 (2017).

82.   Pace, L. *et al.* The epigenetic control of stemness in CD8(+) T cell fate commitment. *Science* **359**, 177-186 (2018).

83.   Henning, A.N., Roychoudhuri, R. & Restifo, N.P. Epigenetic control of CD8(+) T cell differentiation. *Nat Rev Immunol* **18**, 340-356 (2018).

84.   Sallusto, F., Lenig, D., Förster, R., Lipp, M. & Lanzavecchia, A. Two subsets of memory T lymphocytes with distinct homing potentials and effector functions. *Nature* **401**, 708-712 (1999).

85.   Romero, P. *et al.* Four functionally distinct populations of human effector-memory CD8+ T lymphocytes. *J Immunol* **178**, 4112-4119 (2007).

86.   Manjunath, N. *et al.* Effector differentiation is not prerequisite for generation of memory cytotoxic T lymphocytes. *J Clin Invest* **108**, 871-878 (2001).

87.   Sarkar, S. *et al.* Functional and genomic profiling of effector CD8 T cell subsets with distinct memory fates. *J Exp Med* **205**, 625-640 (2008).

88.   Kalia, V. *et al.* Prolonged interleukin-2Ralpha expression on virus-specific CD8+ T cells favors terminal-effector differentiation in vivo. *Immunity* **32**, 91-103 (2010).

89.   Pipkin, M.E. *et al.* Interleukin-2 and inflammation induce distinct transcriptional programs that promote the differentiation of effector cytolytic T cells. *Immunity* **32**, 79-90 (2010).

90.   Joshi, N.S. *et al.* Inflammation directs memory precursor and short-lived effector CD8(+) T cell fates via the graded expression of T-bet transcription factor. *Immunity* **27**, 281-295 (2007).

91.   Kaech, S.M. & Cui, W. Transcriptional control of effector and memory CD8+ T cell differentiation. *Nat Rev Immunol* **12**, 749-761 (2012).

92.   Chang, J.T. *et al.* Asymmetric T lymphocyte division in the initiation of adaptive immune responses. *Science* **315**, 1687-1691 (2007).

93.   Chang, J.T. *et al.* Asymmetric proteasome segregation as a mechanism for unequal partitioning of the transcription factor T-bet during T lymphocyte division. *Immunity* **34**, 492-504 (2011).

94.   King, C.G. *et al.* T cell affinity regulates asymmetric division, effector cell differentiation, and tissue pathology. *Immunity* **37**, 709-720 (2012).

95.   Arsenio, J. *et al.* Early specification of CD8+ T lymphocyte fates during adaptive immunity revealed by single-cell gene-expression analyses. *Nat Immunol* **15**, 365-372 (2014).

96.   Kakaradov, B. *et al.* Early transcriptional and epigenetic regulation of CD8(+) T cell differentiation revealed by single-cell RNA sequencing. *Nat Immunol* **18**, 422-432 (2017).

97.   Tripathi, P. *et al.* STAT5 is critical to maintain effector CD8+ T cell responses. *J Immunol* **185**, 2116-2124 (2010).

98.   Intlekofer, A.M. *et al.* Effector and memory CD8+ T cell fate coupled by T-bet and eomesodermin. *Nat Immunol* **6**, 1236-1244 (2005).

99.   Blackledge, N.P., Rose, N.R. & Klose, R.J. Targeting Polycomb systems to regulate gene expression: modifications to a complex story. *Nat Rev Mol Cell Biol* **16**, 643-649 (2015).

100.   Gray, S.M., Amezquita, R.A., Guan, T., Kleinstein, S.H. & Kaech, S.M. Polycomb Repressive Complex 2-Mediated Chromatin Repression Guides Effector CD8(+) T Cell Terminal Differentiation and Loss of Multipotency. *Immunity* **46**, 596-608 (2017).

101.   Zhao, E. *et al.* Cancer mediates effector T cell dysfunction by targeting microRNAs and EZH2 via glycolysis restriction. *Nat Immunol* **17**, 95-103 (2016).

102.   Fearon, D.T., Manders, P. & Wagner, S.D. Arrested differentiation, the self-renewing memory lymphocyte, and vaccination. *Science* **293**, 248-250 (2001).

103.   Klebanoff, C.A., Gattinoni, L. & Restifo, N.P. CD8+ T-cell memory in tumor immunology and immunotherapy. *Immunol Rev* **211**, 214-224 (2006).

104.   Holmes, S., He, M., Xu, T. & Lee, P.P. Memory T cells have gene expression patterns intermediate between naive and effector. *Proc Natl Acad Sci U S A* **102**, 5519-5523 (2005).

105.   Buchholz, V.R. *et al.* Disparate individual fates compose robust CD8+ T cell immunity. *Science* **340**, 630-635 (2013).

106.   Cieri, N. *et al.* Generation of human memory stem T cells after haploidentical T-replete hematopoietic stem cell transplantation. *Blood* **125**, 2865-2874 (2015).

107.   Roberto, A. *et al.* Role of naive-derived T memory stem cells in T-cell reconstitution following allogeneic transplantation. *Blood* **125**, 2855-2864 (2015).

108.   Fuertes Marraco, S.A., Soneson, C., Delorenzi, M. & Speiser, D.E. Genome-wide RNA profiling of long-lasting stem cell-like memory CD8 T cells induced by Yellow Fever vaccination in humans. *Genom Data* **5**, 297-301 (2015).

109.   Crompton, J.G. *et al.* Lineage relationship of CD8(+) T cell subsets is revealed by progressive changes in the epigenetic landscape. *Cell Mol Immunol* **13**, 502-513 (2016).

110.   Chang, J.T., Wherry, E.J. & Goldrath, A.W. Molecular regulation of effector and memory T cell differentiation. *Nat Immunol* **15**, 1104-1115 (2014).

111.   Janssen, E.M. *et al.* CD4+ T cells are required for secondary expansion and memory in CD8+ T lymphocytes. *Nature* **421**, 852-856 (2003).

112.   Shedlock, D.J. & Shen, H. Requirement for CD4 T cell help in generating functional CD8 T cell memory. *Science* **300**, 337-339 (2003).

113.   Janssen, E.M. *et al.* CD4+ T-cell help controls CD8+ T-cell memory via TRAIL-mediated activation-induced cell death. *Nature* **434**, 88-93 (2005).

114.   Hamilton, S.E., Wolkers, M.C., Schoenberger, S.P. & Jameson, S.C. The generation of protective memory-like CD8+ T cells during homeostatic proliferation requires CD4+ T cells. *Nat Immunol* **7**, 475-481 (2006).

115.   Intlekofer, A.M. *et al.* Requirement for T-bet in the aberrant differentiation of unhelped memory CD8+ T cells. *J Exp Med* **204**, 2015-2021 (2007).

116.   Cannarile, M.A. *et al.* Transcriptional regulator Id2 mediates CD8+ T cell immunity. *Nat Immunol* **7**, 1317-1325 (2006).

117.   Rutishauser, R.L. *et al.* Transcriptional repressor Blimp-1 promotes CD8(+) T cell terminal differentiation and represses the acquisition of central memory T cell properties. *Immunity* **31**, 296-308 (2009).

118.   Nguyen, K.B. *et al.* Critical role for STAT4 activation by type 1 interferons in the interferon-gamma response to viral infection. *Science* **297**, 2063-2066 (2002).

119. Yang, C.Y. *et al.* The transcriptional regulators Id2 and Id3 control the formation of distinct memory CD8+ T cell subsets. *Nat Immunol* **12**, 1221-1229 (2011).

120. Ji, Y. *et al.* Repression of the DNA-binding inhibitor Id3 by Blimp-1 limits the formation of memory CD8+ T cells. *Nat Immunol* **12**, 1230-1237 (2011).

121. Ichii, H., Sakamoto, A., Kuroda, Y. & Tokuhisa, T. Bcl6 acts as an amplifier for the generation and proliferative capacity of central memory CD8+ T cells. *J Immunol* **173**, 883-891 (2004).

122. Yoshida, K. *et al.* Bcl6 controls granzyme B expression in effector CD8+ T cells. *Eur J Immunol* **36**, 3146-3156 (2006).

123. Cui, W., Liu, Y., Weinstein, J.S., Craft, J. & Kaech, S.M. An interleukin-21-interleukin-10-STAT3 pathway is critical for functional maturation of memory CD8+ T cells. *Immunity* **35**, 792-805 (2011).

124. Rao, R.R., Li, Q., Gubbels Bupp, M.R. & Shrikant, P.A. Transcription factor Foxo1 represses T-bet-mediated effector functions and promotes memory CD8(+) T cell differentiation. *Immunity* **36**, 374-387 (2012).

125. Jeannet, G. *et al.* Essential role of the Wnt pathway effector Tcf-1 for the establishment of functional CD8 T cell memory. *Proc Natl Acad Sci U S A* **107**, 9777-9782 (2010).

126. Zhao, D.M. *et al.* Constitutive activation of Wnt signaling favors generation of memory CD8 T cells. *J Immunol* **184**, 1191-1199 (2010).

127. Zhou, X. *et al.* Differentiation and persistence of memory CD8(+) T cells depend on T cell factor 1. *Immunity* **33**, 229-240 (2010).

128. Boudousquié, C. *et al.* Differences in the transduction of canonical Wnt signals demarcate effector and memory CD8 T cells with distinct recall proliferation capacity. *J Immunol* **193**, 2784-2791 (2014).

129. Zhou, X. & Xue, H.H. Cutting edge: generation of memory precursors and functional memory CD8+ T cells depends on T cell factor-1 and lymphoid enhancer-binding factor-1. *J Immunol* **189**, 2722-2726 (2012).

130. Tejera, M.M., Kim, E.H., Sullivan, J.A., Plisch, E.H. & Suresh, M. FoxO1 controls effector-to-memory transition and maintenance of functional CD8 T cell memory. *J Immunol* **191**, 187-199 (2013).

131. Hess Michelini, R., Doedens, A.L., Goldrath, A.W. & Hedrick, S.M. Differentiation of CD8 memory T cells depends on Foxo1. *J Exp Med* **210**, 1189-1200 (2013).

132. Kim, M.V., Ouyang, W., Liao, W., Zhang, M.Q. & Li, M.O. The transcription factor Foxo1 controls central-memory CD8+ T cell responses to infection. *Immunity* **39**, 286-297 (2013).

133. Hedrick, S.M., Hess Michelini, R., Doedens, A.L., Goldrath, A.W. & Stone, E.L. FOXO transcription factors throughout T cell biology. *Nat Rev Immunol* **12**, 649-661 (2012).

134. Zhang, L. *et al.* Mammalian Target of Rapamycin Complex 2 Controls CD8 T Cell Memory Differentiation in a Foxo1-Dependent Manner. *Cell Rep* **14**, 1206-1217 (2016).

135. Araki, K. *et al.* mTOR regulates memory CD8 T-cell differentiation. *Nature* **460**, 108-112 (2009).

136. Rao, R.R., Li, Q., Odunsi, K. & Shrikant, P.A. The mTOR kinase determines effector versus memory CD8+ T cell fate by regulating the expression of transcription factors T-bet and Eomesodermin. *Immunity* **32**, 67-78 (2010).

137. Scholz, G. *et al.* Modulation of mTOR Signalling Triggers the Formation of Stem Cell-like Memory T Cells. *EBioMedicine* **4**, 50-61 (2016).

138. Delpoux, A., Lai, C.Y., Hedrick, S.M. & Doedens, A.L. FOXO1 opposition of CD8(+) T cell effector programming confers early memory properties and phenotypic diversity. *Proc Natl Acad Sci U S A* **114**, E8865-E8874 (2017).

139. Jeevan-Raj, B. *et al.* The Transcription Factor Tcf1 Contributes to Normal NK Cell Development and Function by Limiting the Expression of Granzymes. *Cell Rep* **20**, 613-626 (2017).

140. Xing, S. *et al.* Tcf1 and Lef1 transcription factors establish CD8(+) T cell identity through intrinsic HDAC activity. *Nat Immunol* **17**, 695-703 (2016).

141. Xu, L. *et al.* The transcription factor TCF-1 initiates the differentiation of T(FH) cells during acute viral infection. *Nat Immunol* **16**, 991-999 (2015).

142. Wu, T. *et al.* TCF1 Is Required for the T Follicular Helper Cell Response to Viral Infection. *Cell Rep* **12**, 2099-2110 (2015).

143. Choi, Y.S. *et al.* LEF-1 and TCF-1 orchestrate T(FH) differentiation by regulating differentiation circuits upstream of the transcriptional repressor Bcl6. *Nat Immunol* **16**, 980-990 (2015).

144. Xu, L. *et al.* The Kinase mTORC1 Promotes the Generation and Suppressive Function of Follicular Regulatory T Cells. *Immunity* **47**, 538-551.e535 (2017).

145. Wu, T. *et al.* The TCF1-Bcl6 axis counteracts type I interferon to repress exhaustion and maintain T cell stemness. *Sci Immunol* **1** (2016).

146. Gautam, S. *et al.* The transcription factor c-Myb regulates CD8(+) T cell stemness and antitumor immunity. *Nat Immunol* **20**, 337-349 (2019).

147. van de Wetering, M. *et al.* The human T cell transcription factor-1 gene. Structure, localization, and promoter characterization. *J Biol Chem* **267**, 8530-8536 (1992).

148. van Beest, M. *et al.* Sequence-specific high mobility group box factors recognize 10-12-base pair minor groove motifs. *J Biol Chem* **275**, 27266-27273 (2000).

149. Hoppler, S. & Kavanagh, C.L. Wnt signalling: variety at the core. *J Cell Sci* **120**, 385-393 (2007).

150. Logan, C.Y. & Nusse, R. The Wnt signaling pathway in development and disease. *Annu Rev Cell Dev Biol* **20**, 781-810 (2004).

151. Staal, F.J., Luis, T.C. & Tiemessen, M.M. WNT signalling in the immune system: WNT is spreading its wings. *Nat Rev Immunol* **8**, 581-593 (2008).

152. Polakis, P. The many ways of Wnt in cancer. *Curr Opin Genet Dev* **17**, 45-51 (2007).

153. Daniels, D.L. & Weis, W.I. Beta-catenin directly displaces Groucho/TLE repressors from Tcf/Lef in Wnt-mediated transcription activation. *Nat Struct Mol Biol* **12**, 364-371 (2005).

154. Chen, G. & Courey, A.J. Groucho/TLE family proteins and transcriptional repression. *Gene* **249**, 1-16 (2000).

155. Gullicksrud, J.A., Shan, Q. & Xue, H. Tcf1 at the crossroads of CD4 + and CD8 + T cell identity. *Frontiers in Biology* **12**, 83 – 93 (2017).

156. Arce, L., Yokoyama, N.N. & Waterman, M.L. Diversity of LEF/TCF action in development and disease. *Oncogene* **25**, 7492-7504 (2006).

157. Aberle, H., Bauer, A., Stappert, J., Kispert, A. & Kemler, R. beta-catenin is a target for the ubiquitin-proteasome pathway. *Embo j* **16**, 3797-3804 (1997).

158. Roose, J. *et al.* The Xenopus Wnt effector XTcf-3 interacts with Groucho-related transcriptional repressors. *Nature* **395**, 608-612 (1998).

159. Zeng, X. *et al.* Initiation of Wnt signaling: control of Wnt coreceptor Lrp6 phosphorylation/activation via frizzled, dishevelled and axin functions. *Development* **135**, 367-375 (2008).

160. Zeng, X. *et al.* A dual-kinase mechanism for Wnt co-receptor phosphorylation and activation. *Nature* **438**, 873-877 (2005).

161. Staal, F.J., van Noort, M., Strous, G.J. & Clevers, H.C. Wnt signals are transmitted through N-terminally dephosphorylated beta-catenin. *EMBO Rep* **3**, 63-68 (2002).

162. Kikuchi, A., Kishida, S. & Yamamoto, H. Regulation of Wnt signaling by protein-protein interaction and post-translational modifications. *Exp Mol Med* **38**, 1-10 (2006).

163. Verbeek, S. *et al.* An HMG-box-containing T-cell factor required for thymocyte differentiation. *Nature* **374**, 70-74 (1995).

164. Ioannidis, V., Beermann, F., Clevers, H. & Held, W. The beta-catenin--TCF-1 pathway ensures CD4(+)CD8(+) thymocyte survival. *Nat Immunol* **2**, 691-697 (2001).

165. Yu, Q., Sharma, A. & Sen, J.M. TCF1 and beta-catenin regulate T cell development and function. *Immunol Res* **47**, 45-55 (2010).

166.   Germar, K. *et al.* T-cell factor 1 is a gatekeeper for T-cell specification in response to Notch signaling. *Proc Natl Acad Sci U S A* **108**, 20060-20065 (2011).

167.   Weber, B.N. *et al.* A critical role for TCF-1 in T-lineage specification and differentiation. *Nature* **476**, 63-68 (2011).

168.   Johnson, J.L. *et al.* Lineage-Determining Transcription Factor TCF-1 Initiates the Epigenetic Identity of T Cells. *Immunity* **48**, 243-257.e210 (2018).

169.   Steinke, F.C. *et al.* TCF-1 and LEF-1 act upstream of Th-POK to promote the CD4(+) T cell fate and interact with Runx3 to silence Cd4 in CD8(+) T cells. *Nat Immunol* **15**, 646-656 (2014).

170.   Zhu, J., Yamane, H. & Paul, W.E. Differentiation of effector CD4 T cell populations (*). *Annu Rev Immunol* **28**, 445-489 (2010).

171.   Zhu, J., Yamane, H., Cote-Sierra, J., Guo, L. & Paul, W.E. GATA-3 promotes Th2 responses through three different mechanisms: induction of Th2 cytokine production, selective growth of Th2 cells and inhibition of Th1 cell-specific factors. *Cell Res* **16**, 3-10 (2006).

172.   Crotty, S. T follicular helper cell differentiation, function, and roles in disease. *Immunity* **41**, 529-542 (2014).

173.   Yu, Q. *et al.* T cell factor 1 initiates the T helper type 2 fate by inducing the transcription factor GATA-3 and repressing interferon-gamma. *Nat Immunol* **10**, 992-999 (2009).

174.   Gullicksrud, J.A. *et al.* Differential Requirements for Tcf1 Long Isoforms in CD8(+) and CD4(+) T Cell Responses to Acute Viral Infection. *J Immunol* **199**, 911-919 (2017).

175.   van Loosdregt, J. & Coffer, P.J. The Role of WNT Signaling in Mature T Cells: T Cell Factor Is Coming Home. *J Immunol* **201**, 2193-2200 (2018).

176.   Tiemessen, M.M. *et al.* T Cell factor 1 represses CD8+ effector T cell formation and function. *J Immunol* **193**, 5480-5487 (2014).

177.   Jeannet, G. *et al.* Essential role of the Wnt pathway effector Tcf-1 for the establishment of functional CD8 T cell memory. *Proc Natl Acad Sci U S A* **107**, 9777-9782 (2010).

178.   Willinger, T. *et al.* Human naive CD8 T cells down-regulate expression of the WNT pathway transcription factors lymphoid enhancer binding factor 1 and transcription factor 7 (T cell factor-1) following antigen encounter in vitro and in vivo. *J Immunol* **176**, 1439-1446 (2006).

179.   Lin, W.H. *et al.* Asymmetric PI3K Signaling Driving Developmental and Regenerative Cell Fate Bifurcation. *Cell Rep* **13**, 2203-2218 (2015).

180.   Lin, W.W. *et al.* CD8(+) T Lymphocyte Self-Renewal during Effector Cell Determination. *Cell Rep* **17**, 1773-1782 (2016).

181.   Kratchmarov, R., Magun, A.M. & Reiner, S.L. TCF1 expression marks self-renewing human CD8(+) T cells. *Blood Adv* **2**, 1685-1690 (2018).

182.   Danilo, M., Chennupati, V., Silva, J.G., Siegert, S. & Held, W. Suppression of Tcf1 by Inflammatory Cytokines Facilitates Effector CD8 T Cell Differentiation. *Cell Rep* **22**, 2107-2117 (2018).

183.   Kuchroo, V.K., Anderson, A.C. & Petrovas, C. Coinhibitory receptors and CD8 T cell exhaustion in chronic infections. *Curr Opin HIV AIDS* **9**, 439-445 (2014).

184.   Wherry, E.J. *et al.* Molecular signature of CD8+ T cell exhaustion during chronic viral infection. *Immunity* **27**, 670-684 (2007).

185.   McLane, L.M., Abdel-Hakeem, M.S. & Wherry, E.J. CD8 T Cell Exhaustion During Chronic Viral Infection and Cancer. *Annu Rev Immunol* **37**, 457-495 (2019).

186.   Doering, T.A. *et al.* Network analysis reveals centrally connected genes and pathways involved in CD8+ T cell exhaustion versus memory. *Immunity* **37**, 1130-1144 (2012).

187.   Wherry, E.J., Barber, D.L., Kaech, S.M., Blattman, J.N. & Ahmed, R. Antigen-independent memory CD8 T cells do not develop during chronic viral infection. *Proc Natl Acad Sci U S A* **101**, 16004-16009 (2004).

188.   Barber, D.L. *et al.* Restoring function in exhausted CD8 T cells during chronic viral infection. *Nature* **439**, 682-687 (2006).

189.   Utzschneider, D.T. *et al.* T Cell Factor 1-Expressing Memory-like CD8(+) T Cells Sustain the Immune Response to Chronic Viral Infections. *Immunity* **45**, 415-427 (2016).

190.   Im, S.J. *et al.* Defining CD8+ T cells that provide the proliferative burst after PD-1 therapy. *Nature* **537**, 417-421 (2016).

191.   Chen, Z. *et al.* TCF-1-Centered Transcriptional Network Drives an Effector versus Exhausted CD8 T Cell-Fate Decision. *Immunity* **51**, 840-855.e845 (2019).

192.   Siddiqui, I. *et al.* Intratumoral Tcf1(+)PD-1(+)CD8(+) T Cells with Stem-like Properties Promote Tumor Control in Response to Vaccination and Checkpoint Blockade Immunotherapy. *Immunity* **50**, 195-211 e110 (2019).

193.   Miller, B.C. *et al.* Subsets of exhausted CD8(+) T cells differentially mediate tumor control and respond to checkpoint blockade. *Nat Immunol* **20**, 326-336 (2019).

194.   Sade-Feldman, M. *et al.* Defining T Cell States Associated with Response to Checkpoint Immunotherapy in Melanoma. *Cell* **175**, 998-1013.e1020 (2018).

195.   Siddiqui, I. *et al.* Intratumoral Tcf1(+)PD-1(+)CD8(+) T Cells with Stem-like Properties Promote Tumor Control in Response to Vaccination and Checkpoint Blockade Immunotherapy. *Immunity* **50**, 195-211.e110 (2019).

196.   Klebanoff, C.A. *et al.* Inhibition of AKT signaling uncouples T cell differentiation from expansion for receptor-engineered adoptive immunotherapy. *JCI Insight* **2** (2017).

197.   Zhou, J. *et al.* Telomere length of transferred lymphocytes correlates with in vivo persistence and tumor regression in melanoma patients receiving cell transfer therapy. *J Immunol* **175**, 7046-7052 (2005).

198.   Pircher, H. *et al.* T cell tolerance to Mlsa encoded antigens in T cell receptor Vb8.1 transgenic mice. *EMBO J.* **8**, 719-727 (1989).

199.   Dillon, S.R., Jameson, S.C. & Fink, P.J. V beta 5+ T cell receptors skew toward OVA+H-2Kb recognition. *J Immunol* **152**, 1790-1801 (1994).

200.   Battegay, M. *et al.* Quantification of lymphocytic choriomeningitis virus with an immunological focus assay in 24- or 96-well plates. *J Virol Methods* **33**, 191-198 (1991).

201.   Martin, M.T. *et al.* Predictive model of rat reproductive toxicity from ToxCast high throughput screening. *Biology of reproduction* **85**, 327-339 (2011).

202.   Dobin, A. *et al.* STAR: ultrafast universal RNA-seq aligner. *Bioinformatics* **29**, 15-21 (2013).

203.   Anders, S., Pyl, P.T. & Huber, W. HTSeq--a Python framework to work with high-throughput sequencing data. *Bioinformatics* **31**, 166-169 (2015).

204.   Wang, L., Wang, S. & Li, W. RSeQC: quality control of RNA-seq experiments. *Bioinformatics* **28**, 2184-2185 (2012).

205.   Robinson, M.D., McCarthy, D.J. & Smyth, G.K. edgeR: a Bioconductor package for differential expression analysis of digital gene expression data. *Bioinformatics* **26**, 139-140 (2010).

206.   Ritchie, M.E. *et al.* limma powers differential expression analyses for RNA-sequencing and microarray studies. *Nucleic Acids Res* **43**, e47 (2015).

207.   Mackay, L.K. *et al.* Hobit and Blimp1 instruct a universal transcriptional program of tissue residency in lymphocytes. *Science (New York, N Y)* **352**, 459-463 (2016).

208.   Benjamini, Y. & Hochberg, Y. Controlling the false discovery rate: a practical and powerful approach to multiple testing. *Journal of the Royal Statistical Society* **Series B 57** 289–300 (1995).

209.   Durinck, S., Spellman, P.T., Birney, E. & Huber, W. Mapping identifiers for the integration of genomic datasets with the R/Bioconductor package biomaRt. *Nat Protoc* **4**, 1184-1191 (2009).

210.   Ivanova, N.B. *et al.* A stem cell molecular signature. *Science (New York, N Y)* **298**, 601-604 (2002).

211.   Wong, D.J. *et al.* Module map of stem cell genes guides creation of epithelial cancer stem cells. *Cell stem cell* **2**, 333-344 (2008).

212.   Subramanian, A. *et al.* Gene set enrichment analysis: a knowledge-based approach for interpreting genome-wide expression profiles. *Proc Natl Acad Sci U S A* **102**, 15545-15550 (2005).

213. Liberzon, A. *et al.* The Molecular Signatures Database (MSigDB) hallmark gene set collection. *Cell Syst* **1**, 417-425 (2015).

214. Buenrostro, J.D., Wu, B., Chang, H.Y. & Greenleaf, W.J. ATAC-seq: A Method for Assaying Chromatin Accessibility Genome-Wide. *Curr Protoc Mol Biol* **109**, 21 29 21-29 (2015).

215. Li, H. *et al.* The Sequence Alignment/Map format and SAMtools. *Bioinformatics* **25**, 2078-2079 (2009).

216. Zhang, Y. *et al.* Model-based analysis of ChIP-Seq (MACS). *Genome biology* **9**, R137 (2008).

217. Ramirez, F., Dundar, F., Diehl, S., Gruning, B.A. & Manke, T. deepTools: a flexible platform for exploring deep-sequencing data. *Nucleic Acids Res* **42**, W187-191 (2014).

218. Gu, Z., Eils, R. & Schlesner, M. Complex heatmaps reveal patterns and correlations in multidimensional genomic data. *Bioinformatics* **32**, 2847-2849 (2016).

219. Robinson, J.T. *et al.* Integrative genomics viewer. *Nat Biotechnol* **29**, 24-26 (2011).

220. Veiga-Fernandes, H., Walter, U., Bourgeois, C., McLean, A. & Rocha, B. Response of naive and memory CD8(+) T cells to antigen stimulation in vivo. *Nature Immunology* **1**, 47-53 (2000).

221. Williams, M., Holmes, B., Sun, J. & Bevan, M. Developing and maintaining protective CD8(+) memory T cells. *Immunological Reviews* **211**, 146-153 (2006).

222. Lecoeur, H., Fevrier, M., Garcia, S., Riviere, Y. & Gougeon, M.L. A novel flow cytometric assay for quantitation and multiparametric characterization of cell-mediated cytotoxicity. *J Immunol Methods* **253**, 177-187 (2001).

223. den Haan, J.M., Mebius, R.E. & Kraal, G. Stromal cells of the mouse spleen. *Front Immunol* **3**, 201 (2012).

224. Lize, M., Klimke, A. & Dobbelstein, M. MicroRNA-449 in cell fate determination. *Cell Cycle* **10**, 2874-2882 (2011).

225. Simons, B.D. & Clevers, H. Strategies for homeostatic stem cell self-renewal in adult tissues. *Cell* **145**, 851-862 (2011).

226. Tanchot, C., Rosado, M.M., Agenes, F., Freitas, A.A. & Rocha, B. Lymphocyte homeostasis. *Semin Immunol* **9**, 331-337 (1997).

227. Li, Q., Eppolito, C., Odunsi, K. & Shrikant, P.A. IL-12-programmed long-term CD8+ T cell responses require STAT4. *J Immunol* **177**, 7618-7625 (2006).

228. Johnston, R.J., Choi, Y.S., Diamond, J.A., Yang, J.A. & Crotty, S. STAT5 is a potent negative regulator of TFH cell differentiation. *J Exp Med* **209**, 243-250 (2012).

229. Nurieva, R.I. *et al.* STAT5 protein negatively regulates T follicular helper (Tfh) cell generation and function. *J Biol Chem* **287**, 11234-11239 (2012).

230. Janas, M.L., Groves, P., Kienzle, N. & Kelso, A. IL-2 regulates perforin and granzyme gene expression in CD8+ T cells independently of its effects on survival and proliferation. *J Immunol* **175**, 8003-8010 (2005).

231. Verbeek, S. *et al.* An HMG-box-containing T-cell factor required for thymocyte differentiation. *Nature* **374**, 70-74 (1995).

232. Xing, S. *et al.* Tcf1 and Lef1 transcription factors establish CD8 T cell identity through intrinsic HDAC activity. *Nature immunology* **17**, 695-703 (2016).

233. Jadhav, R.R. *et al.* Epigenetic signature of PD-1+ TCF1+ CD8 T cells that act as resource cells during chronic viral infection and respond to PD-1 blockade. *Proc Natl Acad Sci U S A* **116**, 14113-14118 (2019).

234. Brown, F.D. & Turley, S.J. Fibroblastic Reticular Cells: Organization and Regulation of the T Lymphocyte Life Cycle1. *J Immunol* **194**, 1389-1394 (2015).

235. Beura, L.K. *et al.* Intravital mucosal imaging of CD8 + resident memory T cells shows tissue-autonomous recall responses that amplify secondary memory. *Nature Immunology* **19**, 173 (2018).

236. Obar, J.J. & Lefrançois, L. Early signals during CD8 T cell priming regulate the generation of central memory cells. *J Immunol* **185**, 263-272 (2010).

237. Jung, T.M., Gallatin, W.M., Weissman, I.L. & Dailey, M.O. Down-regulation of homing receptors after T cell activation. *J Immunol* **141**, 4110-4117 (1988).

238. Yang, S., Liu, F., Wang, Q.J., Rosenberg, S.A. & Morgan, R.A. The shedding of CD62L (L-selectin) regulates the acquisition of lytic activity in human tumor reactive T lymphocytes. *PLoS One* **6**, e22560 (2011).

239. Wirth, T.C., Badovinac, V.P., Zhao, L., Dailey, M.O. & Harty, J.T. Differentiation of central memory CD8 T cells is independent of CD62L-mediated trafficking to lymph nodes. *J Immunol* **182**, 6195-6206 (2009).

240. Bachmann, M.F. *et al.* Long-lived memory CD8+ T cells are programmed by prolonged antigen exposure and low levels of cellular activation. *Eur J Immunol* **36**, 842-854 (2006).

241. Hand, T.W., Morre, M. & Kaech, S.M. Expression of IL-7 receptor alpha is necessary but not sufficient for the formation of memory CD8 T cells during viral infection. *Proc Natl Acad Sci U S A* **104**, 11730-11735 (2007).

242. Bachmann, M.F., Wolint, P., Schwarz, K., Jäger, P. & Oxenius, A. Functional properties and lineage relationship of CD8+ T cell subsets identified by expression of IL-7 receptor alpha and CD62L. *J Immunol* **175**, 4686-4696 (2005).

243. Ghaleb, A.M. & Yang, V.W. Krüppel-like factor 4 (KLF4): What we currently know. *Gene* **611**, 27-37 (2017).

244. Bialkowska, A.B., Yang, V.W. & Mallipattu, S.K. Kruppel-like factors in mammalian stem cells and development. *Development* **144**, 737-754 (2017).

245. Takahashi, K. & Yamanaka, S. Induction of pluripotent stem cells from mouse embryonic and adult fibroblast cultures by defined factors. *Cell* **126**, 663-676 (2006).

246. Lennartsson, J. & Ronnstrand, L. Stem cell factor receptor/c-Kit: from basic science to clinical implications. *Physiol Rev* **92**, 1619-1649 (2012).

247. Cheng, G. *et al.* Identification of PLXDC1 and PLXDC2 as the transmembrane receptors for the multifunctional factor PEDF. *Elife* **3**, e05401 (2014).

248. Fitchev, P., Chung, C., Plunkett, B.A., Brendler, C.B. & Crawford, S.E. PEDF & stem cells: niche vs. nurture. *Curr Drug Deliv* **11**, 552-560 (2014).

249. Miyazono, K., Maeda, S. & Imamura, T. BMP receptor signaling: transcriptional targets, regulation of signals, and signaling cross-talk. *Cytokine Growth Factor Rev* **16**, 251-263 (2005).

250. Hager-Theodorides, A.L. *et al.* Bone morphogenetic protein 2/4 signaling regulates early thymocyte differentiation. *J Immunol* **169**, 5496-5504 (2002).

251. Castiglioni, P., Gerloni, M. & Zanetti, M. Genetically programmed B lymphocytes are highly efficient in inducing anti-virus protective immunity mediated by central memory CD8 T cells. *Vaccine* **23**, 699-708 (2004).